THE ELECTROCHEMICAL FORMATION OF SEMICONDUCTOR CHALCOGENIDES

by

PAULINE NICOLE HOWELL

(Under the Direction of John Lewellen Stickney)

ABSTRACT

Electrochemical atomic layer deposition (E-ALD) is a technique that has been developed and advanced by the Stickney group. This method uses individual solutions at room temperature to deposit thin films layer-by-layer. Many materials have been grown and can be grown using this method. E-ALD is well suited for semiconductor materials due to its ability to achieve high-quality films and its ability to control the stoichiometry of the resulting film. The quality of a semiconductor material when assembled into a device, such as a solar cell, is crucial in the efficiency of said device. This dissertation details the development and investigation of multiple chalcogenide semiconductor systems. Cyclic voltammetry (CV) studies of each element are first studied to understand their electrochemistry and aid in developing a successful E-ALD program. A typical E-ALD cycle involves first depositing one element from an aqueous solution onto a chosen substrate. Ideally, a surface limited reaction such as underpotential deposition (UPD) will be used to deposit one monolayer or less of material at a time. Afterward, the second element is introduced and then deposited on top of the other to form a binary compound. This cycle can be repeated as necessary to achieve the desired film thickness. The effect of solution pHs, potentials for deposition, and deposition duration were some of the parameters investigated to optimize the resulting thin film.

The semiconductors investigated in this work are SnSe, GeSe, and SbSe. The chalcogen group is made up of the following elements: oxygen, sulfur, selenium, tellurium, and polonium. The chalcogens have multiple oxidation states, complicating their electrochemical deposition. In the case of selenium, CVs show that it can undergo both oxidative and reductive stripping in acidic solution. When forming the aforementioned materials, different challenges arose based on each elements individual electrochemistry. Film characterization was achieved mainly by XRD, SEM/EDS, EPMA, and Raman spectroscopy.

INDEX WORDS: Electrodeposition, Electrochemical Atomic Layer Deposition (E-ALD), underpotential deposition (UPD), semiconductor, thin film, chalcogenides, SnSe, GeSe, SbSe, cyclic voltammetry (CV), SEM, XRD, Raman spectroscopy

THE ELECTROCHEMICAL FORMATION OF SEMICONDUCTOR CHALCOGENIDES

by

PAULINE NICOLE HOWELL

B.S., Wofford College, 2015

A Dissertation Submitted to the Graduate Faculty of The University of Georgia in Partial Fulfillment of the Requirements for the Degree

DOCTOR OF PHILOSOPHY

ATHENS, GEORGIA

2020

THE ELECTROCHEMICAL FORMATION OF SEMICONDUCTOR CHALCOGENIDES

by

PAULINE NICOLE HOWELL

Major Professor:	John Lewellen Stickney
Committee:	Jon Amster
	Ramaraja Ramasamy

Electronic Version Approved:

Ron Walcott
Interim Dean of the Graduate School
The University of Georgia
May 2020

DEDICATION

I would like to dedicate this work to my family, my friends, and most importantly my fiancé. Your constant support allowed me to believe in myself when I didn't think I could. You pulled me out of the basement when I needed it and were my accountability buddy when I needed to go back in but didn't want to. Your love, reassurance, and confidence in me as a person and as a scientist allowed me to put those same feelings into my work and my life. You reminded me of who I was and who I could be whenever I momentarily lost that, reminding me to enjoy all of the moments especially the good ones.

Thank you to all of the friends near and far who have encouraged me these past five years. Without you, my graduate experience wouldn't have been nearly as gratifying. To my family, thank you for all of your love and support. I'd especially like to thank my mother who answered probably a thousand phone calls from the basement, listening to my ramblings about science and life whenever I needed it. Your constant belief in me inspired me to always believe in myself.

ACKNOWLEDGMENTS

It is impossible to say how grateful I am to my P.I. and mentor, Dr. John Stickney. My graduate school experience has been out of the ordinary and at times unconventional however at no point have I ever felt anything but supported by you. You pushed me to become a stronger researcher and opened up the world of electrochemistry to me. I am thankful for having a boss who was willing to discuss science and life whenever I wanted. You taught me how to learn from failure gracefully and helped me think about the way I answered questions. Your guidance taught me that it's okay to not always know the answer and to be confident in myself when I did. It is through your supervision and direction that I have become the scientist I am.

I am also so thankful for my previous group members. Everyone took the time to help me learn in the beginning and provided me the tools needed to be self-sufficient. I'd like to thank Nhi, whose diligence as a researcher showed me the type of graduate student I wanted to be. Your guidance and work ethic guided me to who I am now. I especially want to thank Peter, who helped keep me sane when it was just he and I in the basement. You allowed for a constant back and forth repertoire of scientific discourse and played the devil's advocate, allowing for many perspectives to be observed that I wouldn't have been able to on my own. Without you, I would not have been nearly as successful and I will always appreciate having you as a lab partner.

TABLE OF CONTENTS

Page

CHAPTER 1

INTRODUCTION AND LITERATURE REVIEW

1.1 PHOTOVOLTAICS AND PHOTOELECTROCHEMICAL CELLS

Transitioning from fossil fuels to renewable resources is a task that seems impossible because of the complex energy system currently in place. Though already ongoing, much research still needs to take place for renewable resources to cover the world's increasing energy demands. The global energy demand is over 15 terawatts per year and rises at an average rate of 2.1%. [1] Fossil fuels dominate as the main source of this energy. The use of fossil fuels every second equates to 1066 barrels of oil, 108,000 cubic meters of natural gas, and 250 tons of coal. These resources are limited and have many negative environmental effects. Regardless of the side effects, fossil fuels are currently the most efficient and least expensive source of energy. Renewable resources make up less than 10% of the energy supply. [1] Renewable energy sectors grow more and more each year. There has been considerable growth in the last decade in the use of renewable energy for electricity. [1] China has promoted this growth greatly because of how they implemented renewable energy options throughout their country.[1] 20% of its energy demands are presently being met with renewable energy. One source of this energy has been photovoltaic (PV) devices. The photovoltaic industry has grown by a 10-fold in China. This has helped influence a 7-fold drop in price for photovoltaics over the past decade. [1]

Substantial research is underway to improve the efficiency and cost of PVs to make them a viable alternative long-term. Photovoltaics have the potential to satisfy much of the energy demands in theory. Aspects that make them practical for long-term applications include their

scalability, up-front investment with possibly decades of energy return, and little to no maintenance after installment.[1] Some qualities needed for PVs to succeed are low-cost, high efficiency, reasonable size, and composition of sustainable materials. Over 90% of commercial solar cells today are based on the research done at Bell's Laboratories in the 1950s.[1] Si-based cells dominate the PV industry. Thin film solar cells with semiconducting materials are a minority of current PV technology but offer lower cost due to needing less material to produce the devices and having the ability to surpass the efficiencies of bulk semiconductor cells.[1]

Photoelectrochemical (PEC) cells work very similar to PVs and are another option for renewable energy.[2] Figure 1.1 shows an example of a PV cell and PEC cell. Both devices exploit incident light to create electron-hole pairs as energy sources. The main difference between a PV cell and PEC is that a PV is a completely solid-state device whereas a PEC cell has an electrolyte phase. In PEC devices, the energy harnessed from incident light drives oxidation and reduction reactions to split water and output energy as H_2.[2] Multi-junction cells utilize multiple p-n junctions to absorb more wavelengths of light, thus increasing the possible energy gathered.[3] The efficiency of these cells heavily depends on the quality of the film.

PEC cells work by the irradiation of a semiconductor with light that has energy equal to or greater than the energy required to promote an electron from the valence band to the conduction band, leaving a hole in the valence band.[1] That energy is referred to as the band gap. The electrons and holes can migrate to the surface of the semiconductor and drive the reduction and oxidation reactions to split water. As seen in figure 1.2, this process has four basic steps: light absorption by the semiconductor, charge carrier separation, migration to the surface of the semiconductor, reaction of holes and electrons with water. The efficiency of each step has its own solar-to-hydrogen (STH) efficiency. This is defined as a ratio of H_2 output energy to input

energy of the incident light.[1] Many factors are involved in material choice for PEC cells because of the needs that must be met. The material must be stable in water under the illumination of light without deteriorating. It also must have a band gap that is large enough to provide the energy required to split water but small enough that it absorbs as much of the solar spectrum as possible. For scale-up, materials should also be cheap and non-toxic. Because of these demands, many PEC cells are composed of two or more materials that have different band gaps and thus absorb more of the solar spectrum. When the two materials are connected, it creates a junction. There are multiple types of junctions including p-n junctions, Schottky contacts, and Ohmic contacts,

The efficiency of a single junction cell is completely reliant on the band gap of the semiconductor used in the device.[3] If the photon energy hitting the junction is greater than the band gap, then excess energy is lost as heat. However, if the photon energy is not greater than the band gap, then it will not absorb the photon and none of the energy is captured. This phenomenon limits single-junction cells to a maximum efficiency to 30% based off calculations by Shockley and Queisser.[1] The multi-junction cell addresses this issue by using multiple materials with varying band gaps to absorb more of the solar spectrum.[3] Different energies of light are absorbed by the different materials and this creates a higher likelihood that incident light will fit the requirements for absorption. The materials are layered highest band gap material to lowest band gap material to distribute energy properly. Figure 1.3.A shows this distribution of energy through a cell composed of varying band gap materials. Another way to form a multi-junction cell is seen in figure 1.3.B. This example uses layers of the same sub-cell with increasing thickness. This improves power conversion via enhanced light absorption.

1.2 ELECTROCHEMICAL ATOMIC LAYER DEPOSITION

Rapid growth in device technology has created a need for methods to deposit semiconductor materials with control at the atomic level.[6] Chemical vapor deposition (CVD) is one technique by which these materials can be grown. In CVD experiments, a heated substrate is exposed to a volatile precursor gas to produce a deposit through a chemical reaction.[7] The duration of exposure largely determines the thickness and many side reactions can occur during this time, leading to volatile by-products.[6-8] Atomic layer deposition (ALD) is similar to CVD in that it is a gas phase technique. However, ALD makes use of self-limiting reactions to grow thin films layer by layer.[8,9] This allows control of the composition and quality of the film throughout the deposition process. To perform an ALD experiment a vacuum system and gaseous precursors are required as well as monitoring the pressure, temperature, flow rates, etc.[8]

Electrochemical atomic layer deposition (E-ALD) utilizes the same principles as ALD in that surface limited reactions are used to grow thin films. However, the growth process occurs in the solution phase. This process was pioneered by the Stickney group over thirty years ago. Research has focused on the development and optimization of binary compounds as well as ternary and quaternary compounds.[10-17] E-ALD utilizes underpotential deposition (UPD) to facilitate surface limited growth. UPD occurs before the potential at which the element would deposit on itself allowing for a maximum of one atomic monolayer of material to deposit. In this case, a monolayer corresponds to one surface atom for every substrate atom. UPD is not possible for every element and varies element to element because of their unique chemistry. E-ALD uses a deposition cycle where one element is introduced and deposited, a blank solution rinses out the first element, and then the second desired element is introduced and deposited. This cycle is repeated until the desired thickness is achieved. The electrochemistry of the individual elements

should be studied first to determine the appropriate potentials for UPD. Because UPD is a surface limited technique, the thickness of the film should be linear with increasing cycles.

1.3 CYCLIC VOLTAMMETRY AND FLOW CELLS

Cyclic voltammetry (CV) is an electrochemical method that helps determine the identity of oxidation and reduction features of an element in solution. This process is achieved by using a sweeping potential over a period of time while recording the resulting current. Typically, negative current indicates the reduction of a species onto the substrate. Positive current indicates the oxidation of material off of the surface. When first investigating a material, window openings of the solution are done to find where surface limited and bulk deposition occurs. A window opening involves using a constant starting potential and sequential experiments where the potential is scanned to increasingly negative values. Window openings can also be done with a constant negative limit and changing the upper limit. By changing the lower potential limit, changes in reduction and oxidation peaks observed can help identify the process and species involved. Correlation between the reductive features and resulting oxidative peaks allows for bulk and surface limited peaks to be identified. After peak identification, further experiments will be done where an element is deposited at a potential of interest for a period of time and then oxidatively stripped off of the substrate. This can be done in the precursor solution as well as a blank solution. A blank solution is made up of the same electrolytes and any buffers as the elemental precursor solution. Using a blank solution allows the stability of the element to be seen when there are not any precursor ions present. The oxidative stripping curves can be integrated to make estimations of the amount of material deposited. By using the size of the polycrystalline gold substrate and the number of electrons involved in the deposition, the coverage in monolayers can be calculated. In every CVs presented, the electrode surface was kept at 2.1 cm^2.

Conversion between charge and monolayer was used to quantify the compound growth rate. A monolayer is defined as one adsorbate per Au substrate atom, which is about 1.2×10^{15} atoms per cm^2. This is a simple way of studying the first few layers of material.

Identification of electrochemical phenomena like UPD can be hard to do in typical electrochemical setups. Electrodeposition usually occurs in a closed system with either 2 or 3 electrodes. CVs can be done in the precursor solution but to perform sequential studies in other solutions would require physically moving the substrate to another bath, exposing the surface to air. This limits the type of experiments that can be performed without introducing error and makes the performance of E-ALD near impossible. Thus, an electrochemical flow cell has been developed in the Stickney lab over many years to facilitate reproducible and controllable electrodeposition. Figure 1.4 shows the experimental setup currently used. This system allows the use of multiple solution bottles without any manual switching. These bottles contain the elemental precursor solutions and blank solutions used for electrochemical experiments as well as a sulfuric solution used for cleaning the substrate. The solutions are purged with nitrogen to remove any oxygen. The solutions are pumped through a valve block and into the flow cell with a peristatic pump. The valve block allows only the designated solution to flow into the flow cell and is controlled by a computer program. After the solution flows through the flow cell it is collected in a waste bottle. Potential control of the cell is also controlled by the computer program allowing complete control over the processes that occur on the substrate.

The flow cell is a 3 electrode setup between two pieces of Plexiglas as shown in figure 1.5. The auxiliary electrode is an S-shaped gold wire that is inlaid into the top piece of Plexiglas. This maximizes the surface area of the electrode, allows for visibility into the cell, and is more stable than other materials such as ITO. The reference electrode is an Ag/AgCl electrode, purchased

from Basi. The reference electrode sits inside a cavity on the top piece of Plexiglas. The working electrode is the substrate of choice. Typically, polycrystalline Au slides are used to do preliminary studies. Copper tape is attached to the substrate to allow for electrical connection. The slide is held between the two pieces of Plexiglas with the aid of an inert gasket. The gasket limits the exposed surface area of the substrate to 2.1 cm^2. All four corners of the top and bottom Plexiglas are screwed together, sandwiching the substrate and closing off the cell to outside exposure. Solutions can be freely flown through the cell using the computer program. This setup helps facilitate the ability to perform E-ALD and in-depth CV studies with great reproducibility.

1.4 THIN FILM CHARACTERIZATION

Once an E-ALD cycle has been developed for a material, characterization of the thin film is necessary to evaluate the actual makeup and purity. Basic things to identify include the stoichiometry, the morphology, the thickness, and the chemical identity of the sample. Methods used to do as such include X-ray diffraction (XRD), Raman spectroscopy, scanning electron microscopy (SEM) coupled with energy-dispersive X-ray spectroscopy (EDS), electron probe microanalysis (EPMA), and ellipsometry. Depending on the properties of the material, supplementary testing such as ovonic threshold or photoelectric effects may be examined.

The very first thing to notice is general color and homogeneity to the eye. Different materials will exhibit various colors based off of band gap ad thickness. Looking at the thin film using an optical microscope will also help see if major macroscopic issues are present. Ideally, the material is grown layer by layer, ensuring a smooth sample. If the E-ALD cycle is not optimal, Volmer-Weber growth may happen. This means that multiple nucleation sites are present and growth happens outwards from the sites leading to uneven islands of deposition. Evidence of this type of growth can be seen using SEM. SEM is a great tool for viewing the surface of the thin

film at the nanoscale. It is important to image multiple areas on the sample to confirm homogeneity. The sample thickness can also be determined by breaking the sample and taking side-view imaging. Ellipsometry is an alternate method for determining the thickness of the sample.

The SEM has an EDS attached which allows for the elemental composition to be analyzed. The selection of the excitation energy is chosen based on the materials in the sample. Lower excitation energies will penetrate less of the film and give more surface related data. EPMA is another method that can give elemental composition. EPMA may be preferable if the excitation energies of two desired elements are too close together for accurate identification. Though EDS and EPMA give compositional information, they cannot give chemical composition. X-ray diffraction helps identify the chemical compounds present. During XRD, an X-ray source hits the sample at various angles and the reflected X-rays are recorded. The pattern and intensity of the spectrum can be compared to a library of knowns to identify present crystalline compounds. XRD works on the principle that the sample is infinitely thick. Typical thin films made using E-ALD are between 20-50 nm. Grazing angle XRD uses a smaller incident angle to bypass the need for thicker films and allows more surface information to be observed. Another method for chemical identification is Raman spectroscopy. Raman spectroscopy works by using a laser source with a specific wavelength to excite Raman modes of the material. Observed peaks can be compared to a library and used to identify what compounds are present.

References:

1. Armaroli, N; Balzani, V. Solar Electricity and Solar Fuels: Status and Perspectives in the Context of the Energy Transition. *Chem. Eur. J*. **2016**, *22*, 32 – 57
2. Archer, M. Photovoltaics and photoelectrochemistry: similarities and differences. *Physica E.* **2002,** *22,* 61-64.
3. Friedman, D.J. Progress and challenges for next-generation high-efficiency multijunction solar cells. *Curr. Opin. Solid State Mater. Sci.* **2010**, *14,* 131-138.
4. Stickney, J. Semiconductors, Electrochemical Atomic Layer Deposition (E-ALD). *Encyclopedia of Applied Electrochemistry.* Springer, New York, 2014, pp 1947-1953.
5. Wick, R; Tilley, D. Photovoltaic and Photoelectrochemical Solar Energy Conversion with Cu_2O. *J. Phys. Chem.* **2015**, *119,* 26243-26257.
6. Johnson, R. W.; Hultqvist, A.; Bent, S. F. A Brief Review of Atomic Layer Deposition: from Fundamentals to Applications. *Materials Today* **2014**, *17* (5), 236–246.
7. Crutchley, R. J. CVD and ALD Precursor Design and Application. *Coordination Chemistry Reviews* **2013**, *257* (23-24), 3153.
8. Abegunde, O.O.; Akinlab, E.T.; Oladijo, O.P.; Akinlabi1, S.; Ude, A.U. Overview of thin film deposition techniques. *AIMS Material Science* **2019**, *6*(2), 174-199.
9. George, S. M. Atomic Layer Deposition: An Overview. *Chemical Reviews* **2010**, *110* (1), 111–131.
10. Gregory, B. W.; Stickney, J. L. Electrochemical Atomic Layer Epitaxy (ECALE). *Journal of Electroanalytical Chemistry* **1991**, 300, 543561.

11. Villegas, I.; Stickney, J. L. Preliminary Studies of GaAs Deposition on Au(100), (110), and (111) Surfaces by Electrochemical Atomic Layer Epitaxy. *Journal of the Electrochemical Society* **1992**, 139, 686694.

12. Colletti, L. P.; Teklay, D.; Stickney, J. L. Thin-Layer Electrochemical Studies of the Oxidative Underpotential Deposition of Sulfur and Its Application to the Electrochemical Atomic Layer Epitaxy Deposition of Cds. *Journal of Electroanalytical Chemistry* **1994**, 369, 145152.

13. Colletti, L. P.; Stickney, J. L. Optimization of the growth of CdTe thin films formed by electrochemical atomic layer epitaxy in an automated deposition system. *Journal of the Electrochemical Society* **1998**, 145, 35943602.

14. Venkatasamy, V.; Jayaraju, N.; Cox, S. M.; Thambidurai, C.; Mathe, M.; Stickney, J. L. Deposition of HgTe by electrochemical atomic layer epitaxy (EC-ALE). *Journal of Electroanalytical Chemistry* **2006**, 589, 195202.

15. Venkatasamy, V.; Jayaraju, N.; Cox, S. M.; Thambidurai, C.; Stickney, J. L. Studies of Hg((1-x))Cd(x)Te formation by electrochemical atomic layer deposition and investigations into bandgap engineering. *Journal of the Electrochemical Society* **2007**, 154, H720H725.

16. Kim, J. Y.; Stickney, J. L. Ultrahigh vacuum surface studies of the electrochemical atomic layer deposition of indium telluride on n-type GaAs(100). *Journal of Physical Chemistry C* **2008**, 112, 59665971.

17. Gebregziabiher, D. K.; Kim, Y. G.; Thambidurai, C.; Ivanova, V.; Haumesser, P. H.; Stickney, J. L. Electrochemical atomic layer deposition of copper nanofilms on ruthenium. *Journal of Crystal Growth* **2010**, 312, 12711276

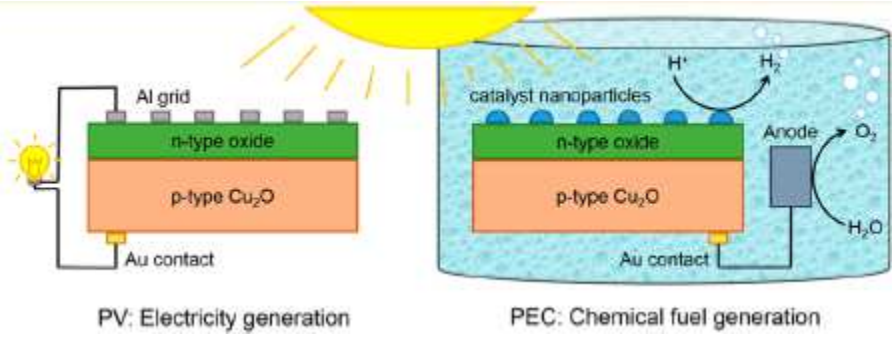

Figure 1.1 Comparison between a PV and PEC cell setup. [5]

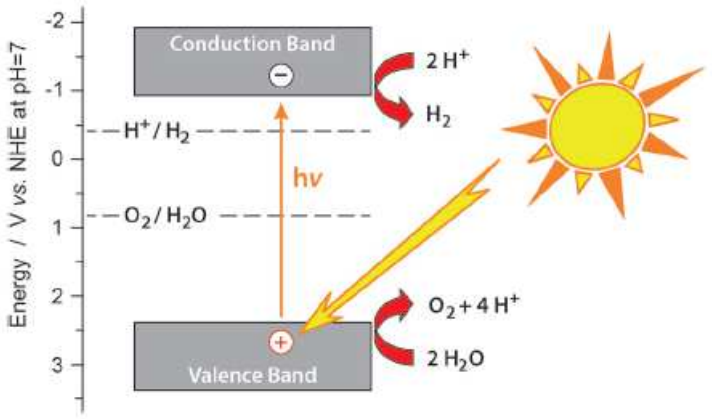

Figure 1.2 Energy band gap diagram for the energy required to split H_2O in a PEC cell. [1]

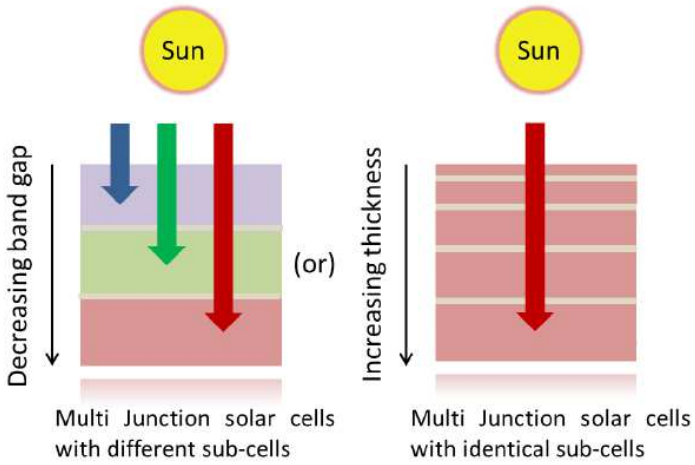

Figure 1.3 Structures for two multi-junction solar cells. Left showing a stacked solar cell comprised of different types of sub-cells (1.3.A) and right depicting a stacked solar cell comprised of identical sub-cells of differing thicknesses (1.3.B).

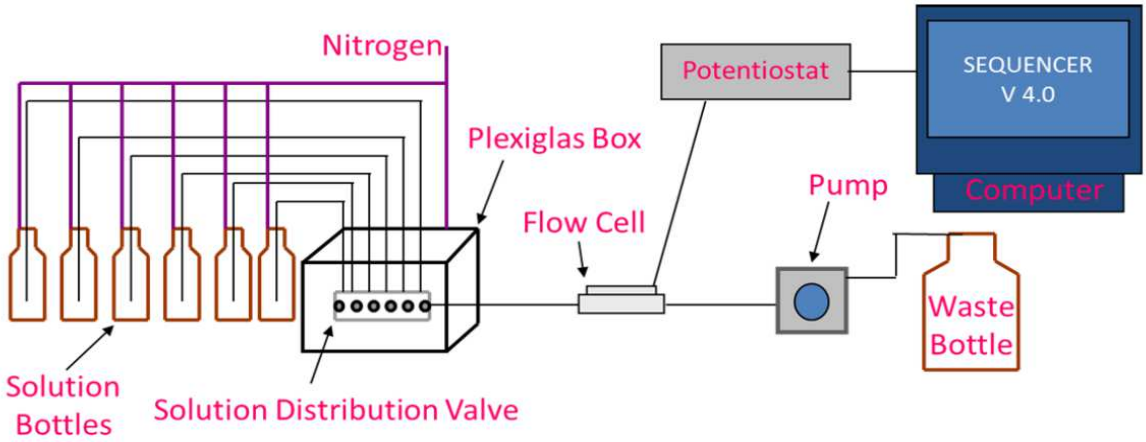

Figure 1.4 Schematic of the experimental setup used for E-ALD. Solution bottles are housed and purged with nitrogen. These bottles are connected to a solution distribution valve. From the valve, a line runs to the flow cell and then to a pump. A waste bottle collects used solutions. A potentiostat is connected to the setup and a computer so that potential and flow can be controlled by a computer program, Sequencer 4.

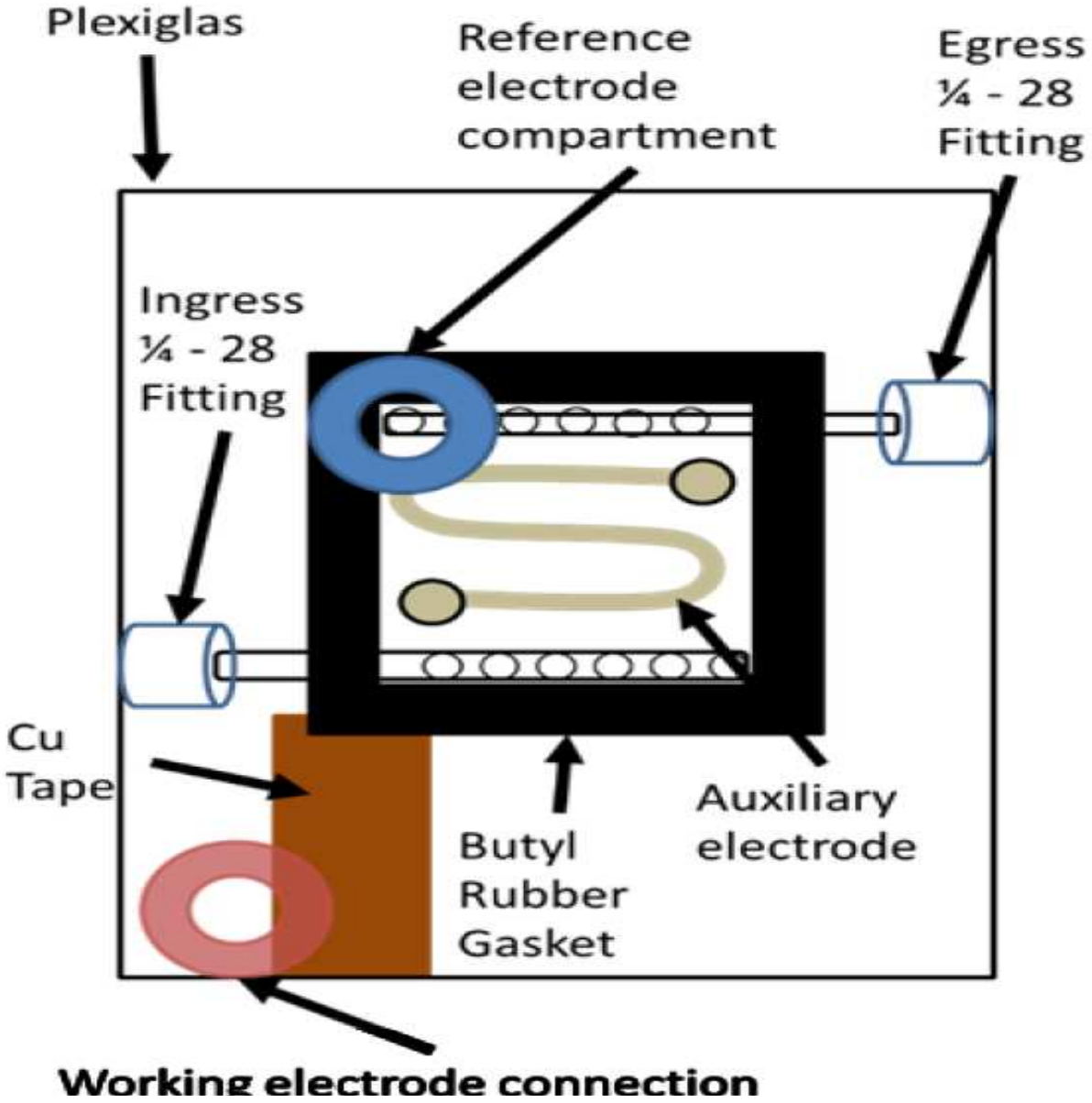

Figure 1.5 Schematic for the as-used three-electrode setup in the flow cell. The sides of the cell are made of an inert Plexiglas. The working electrode is the selected substrate and is electrically connected with Cu tape. Inlaid Au wire sits in the top piece of Plexiglas and serves as the auxiliary electrode. The reference electrode is a Ag/AgCl electrode. The solution flows in through the ingress holes and across the surface of the substrate to the outlet holes.

CHAPTER 2

GERMANIUM SELENIDE[1]

[1] Howell, P.; Sisk, P.; Stickney, J. To be submitted to the ECS Journal

2.1 ABSTRACT

Ge and Se electrochemistry was investigated to find suitable deposition parameters to develop and E-ALD program for GeSe. Initial studies were performed using pH 9 solutions of Ge and Se with perchloric acid as the electrolyte and sodium tetraborate as a buffer. Ge has been studied by past group members and was known to deposit best at pH 9. However, CV studies showed that Se was not able to deposit at pH 9. Multiple solutions between pH 1.6 and 9 were investigated for both Ge and Se to find complimentary deposition regions. Three scenarios were heavily researched to develop an E-ALD cycle: pH 9 Ge and pH 9 Se, pH 9 Ge and pH 3 Se, and pH 3 Ge and pH 3 Se. Each element's stability was investigated in both pH 3 blank and pH 9 blank to ensure that switching pH would not ruin the previously deposited element. Both the pH 9 Ge/pH 3 Se and pH 3Ge/pH 3 Se systems showed the ability to grow multiple monolayers of GeSe with close to 1:1 stoichiometry.

2.2 INTRODUCTION

GeSe is a 2D chalcogenide semiconductor with a narrow band gap and ovonic threshold switching capacity.[1,2] These properties make it a material of interest for memory devices and lithium-ion batteries.[2,3] Germanium selenide can exist as GeSe or $GeSe_2$ however $GeSe_2$ has not been greatly documented in the literature. GeSe has been synthesized using methods such as chemical vapor deposition, atomic layer deposition, and melt quenching.[1,4] As far as is known by the author, GeSe thin films have not been formed using electrodeposition. The authors group has deposited GeTe using E-ALD.[5] The similarities in the cyclic voltammetry of Se and Te suggest

that similar approaches should be taken when attempting to deposit GeSe. Previous work has also been done by Stickney group members studying the electrodeposition of Ge and $Ge_xSb_yTe_z$.[5-7] Results from that work suggest that pH 9 is the ideal pH for Ge solutions. Se solutions at pHs 1.6, 3, 5, 7, and 9 were made and studied to find a solution with suitable deposition potentials to pH 9 Ge. Se typically shows regions where UPD, bulk deposition, and reductive stripping occur. One issue is finding a potential range where Ge will deposit without reductively stripping the previously deposited Se. Another phenomenon that may occur is that Ge will not be able to be deposited without reductively stripping away the Se. This matter was seen with the formation of GeTe.[5,7] In work done by previous group member Liang, this occurrence was manipulated to form multiple layers of Ge, which is usually self-limited.[7] Tellurium deposition potentials and reductive stripping are at a more negative potential than seen in Se. This presumably makes the formation of GeSe harder than GeTe. One of the methods to combat this issue is the inclusion of a third element that will protect the Se that has been deposited. Sb was added to GeTe to form $Ge_xSb_yTe_z$ and combat Te reductive stripping.[5] Similar approaches will be made to form $Ge_xSb_ySe_z$.

Electrochemical atomic layer deposition (E-ALD) is an ideal method for depositing a material like GeSe in a low cost, easy way. E-ALD allows for each the needs of each individual to be tailored through the use of specific solutions when paired with a flow cell system. This process was pioneered by the Stickney group over thirty years ago. Research has focused on the development and optimization of binary compounds. [8-15] E-ALD employs underpotential deposition (UPD) to limit growth to one monolayer or less. UPD occurs before the potential at which the element would deposit on itself allowing for a maximum of one atomic monolayer of material to deposit. UPD varies for every element. The E-ALD cycle should be developed so that

as one element is deposited, the previously deposited element is still stable. This will be especially important when dealing with Se.

Selenium is one of the chalcogen elements and has unique electrochemical features. It exhibits multiple oxidation states and can be both oxidatively and reductively stripped.[16] The oxidation states of selenium are as follows: selenite (+4), selenate (+6), elemental Se (0), and selenide (-2).[17] Reductive stripping occurs due to the ability of Se^0 to convert to Se^{2-}. The Pourbaix diagram of Se can help in identifying which selenium state is present is solution.[18] As seen in the Pourbaix diagram, pH has a huge effect on the present states and the deposition regions of the solution. The majority of research on Se electrochemistry has been done in acidic media though theoretically Se should be stable in basic conditions as well.[16-18] Selenium electrochemistry has been heavily researched in the Stickney group.[19-22] Based off of this research, it is known that selenium exhibits multiple surface limited deposition regions, bulk deposition, and reductive stripping. Scanning tunneling microscopy (STM) shows that multiple Se structures can be present in less than a monolayer of coverage, including the formation of Se_8 ring structures.[19-22] This is something that should be thought about when developing an E-ALD cycle. The first layer of material on the surface is critical in the formation of the subsequent layers. Control over the growth of GeSe is imperative for it properly function as an ovonic threshold switching (OTS) selector.

2.3 EXPERIMENTAL

Multiple solutions of Se and Ge were used in these experiments. The Ge solution was studied at pH 1.6, 3, and 9. The solutions used for initial studies were made with 0.2 mM GeO_2 (Alfa Æsar 99.999% pure). The electrolyte in these solutions was 0.1 M $HClO_4$ (GFS Chemicals,

Inc.). The pH 9 Ge solution also had a buffer of 50mM $Na_2B_4O_7 \cdot 10H_2O$ (Alfa Æsar 99+%). pH 3 and pH 9 Ge solutions were adjusted to the desired pH using NaOH (Fisher Chemical). Additional pH 3 and pH 9 Ge solutions were made with 5 mM GeO_2. Se solutions were made using 0.2 mM SeO_2 (Alfa Æsar 99.999% pure). pH 1.6, pH 3, pH 5, pH 7, and pH 9 solutions were used. These solutions all had 0.1 M $HClO_4$. pH adjusting was done with NaOH on pH 3, pH 5, pH 7, and pH 9 solutions. A buffer of 50mM $Na_2B_4O_7 \cdot 10H_2O$ was used in pH 5, pH 7, and pH 9 solutions. Blank solutions of each pH consisted of the same solution makeup except without the Se or Ge precursors.

The solution bottles used to store and connect solutions to the electrochemical flow cell were first cleaned by soaking them in a Nochromix (Godax Labratories) bath for a minimum of one hour. They were then rinsed sufficiently with 18 MΩ water (Millipore Advantage 10). All solutions are purged with N_2 gas to remove any oxygen for at least one hour before the experiments. The electrochemical flow cell (Electrochemical ALD L.C.) has a three-electrode setup. The auxiliary electrode is an inlaid Au wire in the shape of an "S." The reference electrode was Ag/AgCl in 3 M NaCl (Bioanalytical Systems, Inc.). When not in use the reference electrode was stored in a supersaturated NaCl solution. The working electrode is the substrate that will be deposited on. All experiements in this chapter use polycrystalline Au (Evaporated Metal Films) as the substrate. The polycrystalline Au is comprised of 100 nm of Au on top of 5 nm Ti on a glass slide, with the Ti used as an adhesion layer. The resulting working area of the cell is 2.2 cm^2. The Au slides are cleaned before putting them into the cell. This process includes rinsing the slide with acetone (Fisher Chemical), then rinsing with nanopure water, and drying it in N_2 gas. Next, the slide soaks in concentrated nitric acid (JT Baker) for at least 30 seconds. An

additional rinse with nanopure water and N_2 drying precedes the immediate placement of the slide inside the cell.

The slide is additionally cleaned electrochemically before starting experimentation. A 0.1 M H_2SO_4 (Fisher Chemical) solution is used to clean the slide. This solution is flown into the cell at open circuit potential (OCP) and then a cleaning program is used to oxidize and reduce contaminants off the Au surface. The cleaning program pulses the potential to -200 mV and 1400 mV multiple times and then performs two CVs between -200 mV and 1400 mV. These potentials are chosen based on the electrochemistry of Au in sulfuric acid. This method has been recognized in the Stickney group as a sufficient method of cleaning prior to experimentation. Depending on the type of experiment performed, Au slides can sometimes be reused by simply employing a electrochemical cleaning cycle after the experiment.

Solutions flow through a valve block (Neptune Research & Development, Inc.) before entering the flow cell. The valve block allows for multiple solutions to be flown through the cell without contamination or manual solution switching. The solution flow and potential control are automated using an in-house Labview program, Sequencer, that previous group members developed. The potentiostat (Electrochemical ALD L.C.) allows potential control of the cell at any given time.

For surface characterization, an SEM (FE-SEM Thermo Fisher Teneo) was used at both 5 keV and 10 keV accelerating voltages. For more surface related information and to limit the burning of certain films, 5 keV was selected. 10 keV allows for deeper penetration of the thin film and higher imaging quality. The EDS detector (150mm Oxford $XMax^N$) was used for elemental analysis. Raman Spectroscopy (DXR Raman Microscope, Thermo Scientific) was

used for structural identification. A 780 nm Laser source was chosen to evaluate the germanium selenide films because that was a suitable source for its Raman active modes.

2.4 RESULTS AND DISCUSSION

2.4.1 HISTORY AND CYCLIC VOLTAMMETRY OF GERMANIUM

Germanium has been comprehensively studied in the Stickney group over many years. The first investigations were done by Liang in 2007.[6] Initial research focused on the aqueous deposition of Ge from different pH solutions.[23] Figure 2.1 shows the cyclic voltammetry of solutions between pH 1.21 and 12.93. From this figure, it is evident that Ge can electrodeposit at a variety of pHs however the maximum deposition is possible at more basic conditions. Figure 2.2 highlights the maximum coverages that can be achieved at each potential with the maximum deposition of Ge occurring with the pH 9.32 solution. The CVs of the different pHs in figure 2.1 show the effect of pH on the deposition regions in each solution. As the pH becomes more basic the range for reduction shifts negatively. This is an expected outcome related to the Nernst equation and ideally the position should shift around negative 60 mV for each 1 pH unit shift.

These first studies briefly investigated the pH effects using CVs but focused on researching pH 4.72 Ge solutions using CVs and STM.[6] The STM images show the, as described, “moire” pattern on the surface and later investigations by Ledina identify this as the beginnings of germanene formation.[23,24] One of the issues with investigating Ge at this pH is that H_2 formation is occurring near the same potentials used for deposition. This made it incredibly hard to use STM reproducibly. By changing the pH to a more basic value of 9.0, the H_2 formation is pushed to a more negative potential. This allowed for a more detailed investigation of germanene formation to be done.[25,26] The research published by Bui indicates that at pH 9, one

full monolayer of germanene is formed by -0.9 V to -1.0 V. This is important to note for binary compound formation because germanene is a self-limiting material that can poison the surface from further growth. Before it was known that germanene was forming on the surface, research in our group struggled to understand why a maximum of 3.5 MLs could be formed.[23,7] This is due to the 8-ring honeycomb structure it forms and the conductivity that it loses with increasing coverage.

When starting the investigations into Ge electrochemistry, the first solution studied was pH 9 Ge. CVs were done in pH 9 Ge solutions to ensure that slight variations in electrolyte makeup did not change results in comparison to previous research. Research of Ge was previously done using Na_2SO_4 as the electrolyte. Figure 2.3 shows a window opening of CVs for Ge at pH 9 in a 0.1 M perchloric acid electrolyte with a sodium tetraborate buffer. This figure shows a series of CVs with the same positive starting point of 0.5 V. The potential was then scanned to increasingly more negative points to determine where surface limited and bulk regimes occurred. Window openings can be done this way or with a constant negative potential and varying upper potential limits.

The first reductive feature in figure 2.3 is observed after -600 mV. This is where UPD Ge is depositing. This identification is possible because to respective oxidative curves do not grow with increasing potential scans. If the reductive curve is indicative of bulk, the resulting oxidative curve will continue to grow as the potential increases to more negative potentials. In figure 2.3, the green scan to -1000 mV shows the maximum negative potential where surface limited Ge characteristics prevail. There are two oxidative peaks observed in the positive scan. The first peak is centered around -800 mV and the second is at -150 mV. Based on STM work in previous research the corresponding features are Ge on the Au surface for the -150 mV peak and

the beginning formations of germanene for the -800 mV peak.[25] The germanene formed at this point is not very well ordered or fully connected making it easily oxidized off the surface. This is why it oxidizes at a more negative potential than the other features.

Once the potential is scanned to a more negative potential, like -1100 mV in the light blue scan of figure 2.3, the -800 mV peak begins to disappear and the formation of the -400 mV peaks starts forming. The -400 peak corresponds to the oxidation of bulk germanium or germanene off of the surface. The -800 mV begins to disappear because the poorly ordered initial germanene has begun to be incorporated into larger, better-formed sheets. As the potential is shifted to a more negative potential such as -1400 mV in the purple scan of figure 2.3, the -800 mV peak has completely disappeared and a large -400 mV peak can be observed. The -150 mV peak will always be present regardless of the -400 mV peak because it is the Ge on Au and does not correspond to germanene.

In this research, two other pHs were investigated: pH 1.6 and pH 3. CVs of the three pHs can be seen in figure 2.4. As with Liang's research seen in figure 2.1, figure 2.4 shows a shift to more negative potentials for all reductive and oxidative features when the pH is increased. Whereas the previous focus of research centered on determining the deposition mechanisms Ge, this research was concerned with combining Ge deposition with that of Se. For an E-ALD cycle to be successful, maximum Ge deposition is not a requirement and other pHs may be more viable for a GeSe binary compound. Based on this desire, pH 3 was explored due to this range being a favorable place for Se deposition. A window opening of pH 3 Ge can be seen in figure 2.5.

The reductive features of Ge at pH 3 seen in figure 2.5 are very different from that of pH 9 shown in figure 2.3. In pH 3 Ge, as the potential is scanned negatively, a large reductive

current starts around -500 mV. This made it hard to identify where either surface limited or bulk reductive peaks were occurring. This type of reduction can be indicative of H_2 formation however visible bubbles were not observed in the cell at this time and did not impede the Ge deposition to the author's knowledge. As the scans were reversed to positive potentials, three peaks can be observed. As Ge trends at pH 3 were not well investigated previously in the group, it was necessary to identify these peaks. This was done was by first depositing the Ge at pH 9, then stripping the resulting deposit in both pH 9 blank solutions and pH 3 blank solutions. This allowed for the same experiment to be done where the deposited Ge would be known while seeing how the oxidative peaks changed with pH change. Figure 2.6 shows the CVs of Ge deposited at potentials between -900 mV and -975 mV in both pH 9 and pH 3 blanks and figure 2.7 shows the same experiment for Ge deposited between -1000 mV and -1050 mV.

Figure 2.6 shows the placement of the disorganized germanene peak and Ge on Au peak for pH 9 at -800 mV and -150 mV respectively. When looking at the corresponding scans stripped in pH 3 blank, the Ge on Au peak comes in at around -150 mV like in pH 9. However, the disorganized germanene peaks are now a set of triplet peaks between -400 mV and -600 mV. The further separation and identity of the individual peaks were not possible using CVs. The use of the STM would make identifying these individual peaks a possibility. Figure 2.7 shows the deposition of pH 9 Ge at bulk regions between -1000 mV and -1050 mV. It is obvious that the germanene at pH 3 also comes in between the disorganized germanene and surface Ge peaks, centered around -250 mV. With more aggressive Ge deposition potentials, the disorganized Ge peaks also disappeared in pH 3, though not pictured in this figure. Based on these experiments, the location of disorganized germanene is between -400 mV and -600 mV at pH 3, bulk

germanene oxidizes at -250 mV in pH 3, and Ge on Au is stripped off of the substrate at -150 mV.

2.4.2 CYCLIC VOLTAMMETRY AND HISTORY OF SELENIUM

Selenium is another element that has been deeply studied by the Stickney group throughout the years. Initial studies were done by Lister et al in the mid-1990s using Auger, LEED, and STM to investigate the electrochemical formation of Se on pristine Au.[19-22] This research focused on finding out the atomic coverages and structures of subatomic layer amounts of Se deposited on different crystalline faces of Au. They used an acidic pH to deposit Se and noticed multiple surface coverages. The coverages observed were 1/4 coverage (2X2), followed by a (2X$\sqrt{10}$) at 1/3 coverage, and then a *c*(2X2) at 1/2 coverage. The structures correspond to the way the unit cell is organized on the Au surface. Depending on the second element desired in a binary compound formation, one structure may be more favorable than another. An additional structure with 0.7 ML coverage was observed with a Se_8 ring structure.[19] Figure 2.8 shows the proposed structures in relation to Au (100).

The reason the lower surface coverages of Se was studied so carefully is due to the very complex electrochemistry of Se. At acidic pHs, Se electrochemistry has multiple surface limited deposition regimes, bulk deposition, and reductive stripping. Like Ge, Se electrochemistry was investigated at multiple pHs to ensure proper selection of pH for the eventual design of a GeSe E-ALD program. Figure 2.9 shows Se CVs for pH 1.6 through pH 9. The pH 1.6 and pH 3 both show similar peaks with a shift due to the change in pH. However, pH 5, 7, and 9 show degradation in the peaks that appear. A blank solution scan has been included in this figure so that peaks corresponding to Au oxidation or reduction can be observed. The peaks related to Au

oxidation occur at the farthest positive locations in each scan and Au reduction is the reductive feature seen between 250 mV and 1000 mV for the different pHs. Tracking the change in Au peak location helps in identifying where the respective Se peaks should occur.

Figure 2.10 shows a window opening of a pH 3 Se solution. If scanning negatively from 500 mV, the first reductive features present are that of surface limited Se. These peaks occur between 250 mV and -100 mV. Selenium does not have standard UPD and instead has multiple surface limited coverages that can be reproducibly achieved as described previously. Continuing with the negative scan, there is a plateau in the current and it is in this region where bulk Se can be grown. At -430 mV, a sharp negative peak is observed that signifies reductive stripping. Here, the Se^0 that has been reduced onto the surface can be converted into Se^{-2}. This is a characteristic that is special to the chalcogen elements. Studies showed that only bulk Se can be reduced at this potential though. If the potential is further scanned negatively a second reductive stripping feature occurs where the surface limited Se is finally reduced off of the surface. By continuing the scan further negative still, a final negative feature is observed past -1250 mV and this is due to H_2 formation. In the positive scan, bulk Se is first seen oxidatively stripping off of the Au surface at 600 mV followed by surface limited Se which strips at 750 mV. Se does not have a limit to how much bulk can be grown, unlike Ge which has a maximum of 3.5 MLs when deposited on itself.

As seen in figure 2.9, pH 1.6 Se shows all of the same reductive and oxidative features as pH 3 Se and will not be further detailed at this time. However, in the pH 5 Se solution, there is a major loss of observable peaks compared to pH 3 Se. A window opening in pH 5 Se is seen in figure 2.11. The peaks are much less pronounced at this pH in comparison to the pH 3 and pH 1.6 solutions. It is clear from the negative scans that there is some surface limited deposition

occurring between 0 mV and -500 mV. As the scan goes further negative, it seems evident that reductive stripping is occurring around -500 mV to -750 mV. After that the potential rapidly decreases, indicating H_2 formation. On the reverse scan to positive potentials, both bulk and surface limited peaks are observed for the stripping of Se off of the Au surface between 400 mV and 800 mV. The bulk oxidation peak at 500 mV is much smaller than the observed bulk peaks in the pH 1.6 and pH 3 solutions. It is possible that holding at a negative potential may grow the observed bulk peak. The Au oxidation peak at this pH is also different than in pH 1.6 and pH 3.

When looking at the pH 7 scan in figure 2.9, even more of the peaks have degraded. It is no longer easily evident where reduction of Se on or off of the surface is taking place. The oxidation of Se shows less bulk formation but still most of the surface limited Se. For pH 9 Se, almost all peaks have disappeared and barely any Se is stripped off of the surface in the oxidative scan. Figure 2.12 shows the window opening of the pH 9 solution. The dotted scan corresponds to the respective blank pH 9 solution scan on clean gold. There is a shift between the H_2 formation in the Se solution and the blank solution. The only observable reductive feature in Se begins at -750 mV. The window of deposition is very small before the H_2 formation starts and results in a very small oxidation peak at 400 mV. Even with holding at a negative potential for a longer period only a small increase in the Se oxidation peak was observed. However, with the shift in the Au oxidation peak in the Se solution compared to the blank solution it was hoped that possibly a selenate species might be oxidizing at the same potentials as the Au hence the lack of change in the 400 mV peak.

With this information, three circumstances were chosen to investigate. The first option was using the best-case scenario for Ge, pH 9, and hoping that pH 9 Se deposition would be more favorable on the Ge covered Au surface. This case will be referred to as GeSe 9/9. The

second option was using the best pH solution for each element, pH 9 Ge and pH 3 Se. The pH 3 Se was selected over pH 1.6 to lessen the pH difference between the two solutions. This case will be referred to as GeSe 9/3. The third option investigated was using pH 3 Se and pH 3 Ge. In previous group work, the maximum amount of Ge was desired and acidic Ge impeded studies like STM. However, for the GeSe E-ALD cycle to be successful here the growth per cycle can be sub-monolayer as long as the growth is linear and increases cycle to cycle making pH 3 Ge a viable option. This scenario will be referred to as GeSe 3/3.

2.4.3 SELENIUM ELECTRODEPOSITION METHODS

The chalcogen characteristics of selenium required experiments to be done to better understand the ways it could be deposited with a focus on pH 3 and pH 9 Se solutions. Previous work in the Stickney lab recognized three methods of deposition.[19-22] In case one, the selenium is deposited at a specific potential for a specified amount of time. The idea would be to deposit the desired amount and for an E-ALD cycle and that would be one monolayer of material or less. The second case begins with depositing bulk Se and then anodically stripping the excess off to leave the desired amount. The third case also starts by depositing a bulk amount of selenium. However, instead of anodically stripping the excess, the reductive stripping potential is used to cathodically strip off the excess material.

When developing an E-ALD cycle, all potential choices need to be carefully selected to ensure that previously deposited material will be stable during the repetition of cycles. Regardless of pH, Se oxidatively strips at a potential far more positive than Ge. This meant that utilizing the case two method of selenium electrodeposition would result in Ge being stripped from the surface. For this reason, only case one and case three Se electrodeposition methods were investigated. In the following experiments, a pH 3 Se solution was used to deposit Se on

the surface. To determine the amount and identity of the resulting Se this material was oxidatively stripped off of the substrate in a blank solution by performing a CV. To better understand the behavior of Se in basic conditions, both pH 3 and pH 9 blanks were used. Based on the CVs of pH 9 Se in figure 2.12, it was unclear if Se would be stable at this pH regardless of if it was first deposited using the pH 3 solution. Figure 2.13 shows the results of the case one method of Se deposition.

In figure 2.13, the Se deposition potential was held for 30 seconds when depositing pH 3 Se. For these experiments, Se was flown into the cell at open circuit potential until the cell volume had been exchanged at least three times. This allows for the deposition to be reproducible because the concentration of Se is stable. The potential was then pulsed to the listed potentials and held for 30 seconds. After deposition, a blank solution was flown into the cell for an additional 30 seconds. It is understood that during the switch to a blank solution, some Se may deposit by being at the deposition potential but this most closely resembles the way it would happen in a GeSe E-ALD cycle. After sufficient blank has been flushed through the cell, the potential is pulsed to 250 mV in pH 3 blank experiments and 0 mV in pH 9 blank experiments. A positive scan is then performed to see how much Se was deposited.

Figure 2.13.A shows the scans for pH 3 Se stripped in pH 3 blank solution. When Se was deposited at -300 mV, a bulk amount of Se was deposited. This makes sense because it is at a potential prior to reductive stripping, -430 mV. By -700 mV, the Se deposited has reduced to 0.32 MLs. At -800 mV, even less Se is deposited and the sharpness of the surface limited peak has lessened. This continues as the potential becomes increasingly negative and by -1100 mV the Se MLs are down to 0.06 MLs. It makes sense that the surface limited peak would continue to

shrink past -700 mV because that is where the secondary reductive stripping feature begins, as seen in figure 2.10.

When looking at figure 2.13.B, instead of stripping the pH 3 Se in pH 3 blank it has now been oxidized using a pH 9 blank. It was very important that sufficient rinsing time was used not only to ensure that all Se was rinsed out of the cell but also to make sure that the pH had been changed from pH 3 to pH 9. In the pH 9 blank the same trends are seen in the amount of selenium that is stripped off of the surface when compared to the data from the pH 3 blank CVs. This data proved that pH 3 Se previously deposited on Au was stable in pH 9 blank and could be stripped from the surface, even if it was not able to successfully deposit at pH 9.

Case three involved first depositing a bulk amount of Se. This was done at -250 mV for 30 seconds with the amount of Se deposited around 1.5 MLs. From that step, a blank solution was flown into the cell for 30 seconds at -250 mV. Then the potential was pulsed to a more negative potential and held for 30 seconds before oxidizing the Se off of the Au surface using a CV. Figure 2.14 shows the result of those experiments. In figure 2.14.A both solutions used were pH 3. The peak shape of Se, when reduced at -300 mV, has changed from the peak seen in figure 2.13.A. In 2.14.A, there is an additional Se surface limited peak observed at 950 mV. This peak may be a result of a different Se structure due to deposition or slight differences in the polycrystalline Au surface. The coverage is still a bulk amount of Se because it has not yet reached a reductive stripping potential. As the reductive potential is reduced negatively to -400 mV, much of the bulk Se is lost already and the remaining bulk peak oxidizes more quickly. This indicates that it has become much less stable than before. By a -700 mV reductive stripping potential, all bulk Se is gone but the surface limited peak is still stable. This remains true for -900

mV and -1100 mV. However, the peak shape becomes broader at the increasingly negative potentials. The Se coverage plateaus though which is different than observed in case one.

Figure 2.14.B shows how Se deposited from a pH 3 solution reductively strips in a pH 9 blank. When using the pH 9 blank solution to reductively strip the Se that had been deposited, different stripping potentials were used. These potentials were based on the different reductive features observed in the pH 9 Se CVs seen in figure 2.12. This experiment helped clarify regions where reductive stripping occurred. For -400 mV reduction, all of the previously deposited pH 3 Se is still present and the bulk peak retains its sharp feature. By -600 mV the bulk peak begins to reduce. In this CV there is the less stable bulk peak stripping at 300 mV along with some of the original 350 mV bulk peak stripping. It may be possible that when exchanging the pH 3 solution for the pH 9 solution some rearrangement may be occurring however it does not cause a loss of Se. By -1000 mV, all of the bulk features have disappeared and a constant Se coverage is achieved, 0.35 MLs Se. This remains true even for more negative potentials like -1200 mV. This is encouraging for the GeSe 9/3 scenario as potentials in this range may be necessary for Ge deposition.

2.4.4 pH 9 GERMANIUM AND pH 9 SELENIUM

The first layers of deposited material will determine the quality of an electrodeposited thin film. It is crucial to understand how the voltammetry of an element changes when it is on an altered Au surface. Because of this, careful examination of the first layers should be done. After determining the ranges of deposition for a single element, the second element can be introduced to the system. Based off of the electrochemistry of Ge seen in figure 2.2, deposition potentials between -800 mV and -1000 mV should be sufficient for depositing Ge. The CVs of Se at pH 9

do not show much promise for deposition, but it was hoped that Se would prefer depositing on a Ge covered Au substrate.

Figure 2.15 shows the examination of the GeSe 9/9 case. To study how Se would behave on Ge, a surface limited amount of Ge was first deposited on the Au substrate. A deposition potential of -925 mV was chosen to ensure no bulk Ge or germanene would be present and 0.33 MLs of Ge were deposited. A blank was then used to rinse Ge out of the cell. After this, Se was introduced to the cell at the listed potential and deposited at the same potential. The selenium was then rinsed out of the cell and a CV in a blank solution was done to examine the changes in Ge and Se. One of the factors that needed to be monitored was the potential for Se deposition. As seen in figure 2.15, the use of potentials above -1000 mV led to the oxidation of Ge during Se deposition. Ge on Au without exposure to Se most closely resembles the -1000 mV CV, having the presence of the -800 mV and -150 mV surface limited features and disorganized germanene. However, in the -1100 mV Se CV, the original peaks have changed shape and there is the presence of the germanene peak at -400 mV. This phenomenon will be discussed later in other GeSe cases.

The -900 mV Se deposition scan in figure 2.15 shows a more drastic loss of Ge and still no significant Se deposition. This trend continues for the -800 mV and -700 mV Se deposition attempts. Based on experimental attempts, Se deposition was still unfavorable at this basic of a condition.

2.4.5 pH 9 GERMANIUM and pH 3 SELENIUM

The second study was done using the best pH choice for maximum deposition of both Ge and Se. Based on the previous group work and research described previously in this work, the

most favorable Ge solution is pH 9 and for Se is pH 3. This is the most complex situation described because of using two considerably different pH solutions. Blanks at pH 3 and pH 9 were used to ensure that the pH of the cell was at the correct pH when a new element was introduced. Another thing to think about when developing the cycle is that the potentials where elements strip change as the pH is changed. So even though pH 9 will be used to deposit Ge, the potentials chosen for Se in the pH 3 solution need to be based on the stability of Ge at pH 3 and vice versa. The data from figures 2.6, 2.7, 2.13, and 2.14 helped determine where Se and Ge were stable at each pH. Figure 2.16 roughly summarizes the different deposition regions for Ge and Se at both pH 3 and 9. A concern that was noted with using the GeSe 9/3 system was that surface limited Se deposition occurs in a region where Ge will oxidize. This meant that utilizing case three Se deposition would not be possible.

Figure 2.17 shows CVs and coverages for pH 3 Se deposition on a pH 9 Ge covered Au surface. The oxidation of the resulting deposit was done in pH 3 blank since Se was the second element deposited. No potentials higher than -600 mV were used for Se deposition because doing so would oxidize the Ge that was first deposited. This series of experiments involved first depositing pH 9 Ge at -1000 mV after which a pH 9 blank was rinsed through the cell. 0.75 MLs of Ge was deposited during this step. Following this, a pH 3 blank was flushed through the cell for a sufficient amount of time to change the pH from pH 9 to pH 3. The pH 3 blank solution was rinsed through the cell at a potential where the Ge would be stable through pH exchange. Selenium solution was then deposited using the listed potential. When using the listed potentials for Se deposition, the Ge coverage remains close to the starting amount. As more negative Se deposition potentials were used, less Se was deposited which follows the same trends observed on a clean Au substrate (figure 2.13). The Ge peak shape changes from its original look when Se

is deposited on the surface. In the -900 mV Se deposition scan, where Se coverage is the lowest, the Ge peak retains most of its triplet shape. As more Se is deposited at the more negative potentials, the triplet peak converges and shifts to a more positive stripping potential. This indicates that the stability of the Ge has been increased. The new peak location is very close to that of germanene and it is possible that when the Se was deposited that the disorganized germanene was pushed together to form better sheets of deposit.

Figure 2.18 shows a comparison a series of CVs corresponding to observed Se and Ge peaks for different scenarios including Se on clean Au, Ge on clean Au at both surface limited coverages and bulk coverages, and Se on Ge covered Au. When surface limited Ge is deposited on clean Au, two sets of peaks are present as seen in the green scan. When Se is deposited on top of that Ge in the black scan, not only does the triplet peak corresponding to disorganized germanene disappear but also the -100 mV peak corresponding to germanium on the Au surface. This may indicate that the Se is displacing the Ge from the Au surface. It could also indicate that the Ge is no longer bonding to the Au and instead is bonding to Se to form a GeSe compound. An example of a bulk Ge CV has been included in the aqua scan to show the difference in the placement of a germanene peak found in the GeSe CV shown in black. The Se peak in the black does not change location when compared to Se on clean Au shown in the red scan. However, more Se is deposited on the Ge coated Au surface than deposits under the same conditions on a clean Au substrate. This indicates a preference in Se depositing on Ge and is favorable for depositing GeSe. Another feature that changes when Se is present is the shape of the Au oxidation peak. When Ge is deposited on Au, the peak remains the same as a clean Au surface shown in dark blue. With the presence of Se, the Au peak completely alters from a low broad peak to a sharper peak with higher current at 1350 mV. This can mean multiple things. It is

possible that a very stable Se species is on the surface or that the Au crystallinity has been altered by the Se.

Based on the data shown in figure 2.17, -700 mV was selected as the deposition potential of Se in the first cycle. -925 mV was used for the Ge potential because it allowed for a sufficient surface limited amount of Ge. Figure 2.19 shows the resulting CVs and coverages of the following step where Ge was deposited on top of the GeSe coated Au substrate. The coverage was checked between the blank exchange as well to make sure that no Ge or Se was lost when flowing pH 9 and pH 3 blank solutions. The coverage before starting this experiment was 0.19 MLs of Ge and 0.43 MLs of Se. When the second layer of Ge is deposited as shown in figure 2.19, the -800 mV and -150 mV peaks are now present again. As expected, Ge coverage increases during this step. Unfortunately, at the potentials needed to deposit Ge some of the previously deposited Se was lost when depositing the second layer of Ge. As increasingly negative Ge deposition potentials were used, more and more Se was reduced off of the surface.

Figure 2.20 shows CVs for each step in two complete E-ALD cycles. Using the listed parameters there is around 1 ML of GeSe on the Au surface after 2 cycles. Steps 1 and 2 make up the first complete cycle and steps 3 and 4 make up the second. In the first step, Ge is deposited on the surface and two different peaks are observed. When Se is deposited on the Ge-Au surface, those two peaks converge into one. This convergence happens again in the 4^{th} step when Se is deposited onto the Ge-Se-Ge surface. One issue was that Se coverage has no net gain. The amount that was stripped during the second Ge deposition is about the same that deposited afterward meaning that the Se may not grow stoichiometrically with the Ge. This indicates that during a third cycle, Ge would increase but the Se coverage would remain close to the observed

amount at the end of cycle 2. Further manipulation of potential choice is needed to evaluate whether a thin film would deposit using the GeSe 9/3 system.

2.4.6 pH 3 GERMANIUM AND pH 3 SELENIUM

In this research, pH 3 Ge and pH 3 Se solutions were used to develop an E-ALD cycle for GeSe. Based on the CVs seen in figures 2.5 and 2.10, studies were performed to evaluate where each element was stable when deposited on each other as was done in the first GeSe scenarios. Figure 2.21 shows the resulting CVs and coverages when pH 3 Se was deposited on pH 3 Ge. In these experiments, the first 0.5 MLs of Ge was deposited by pulsing to -600 mV and holding for 30 seconds. After that, a pH 3 blank solution was used to flush Ge out of the cell. Then Se was deposited for 30 seconds at the listed potentials. There is a 300 mV region where the Ge coverage remains very close to the original amount between -500 mV and -800 mV. When Se was deposited at -400 mV a significant amount of Ge was oxidized off of the surface. The CVs show similar trends as seen in the GeSe 9/3 case. When more Se is deposited on the Ge covered Au substrate, the Ge peaks are altered and become one central peak around -150 mV. There is also still a slight shift in location from what would be seen with germanene as seen when the GeSe CVs are compared to bulk Ge on Au.

Figure 2.22 shows the CVs and coverages of Ge on the GeSe coated Au. Unlike GeSe 9/3, the Se coverage remains constant even after the second layer of Ge has been deposited. Based on the data shown in figures 2.21 and 2.22 -600 mV was chosen as the deposition potential of both Se and Ge. Figure 2.23 shows two complete cycles. The amount of Ge and Se deposited in the second cycle is much less than in the first cycle because it is easier to deposit on

a clean Au surface. However, the coverages do show a net gain throughout the second cycle and are nearly a 1:1 stoichiometric ratio.

Initial thin films were made using the GeSe 3/3 system. Both the Ge and Se deposition potential were -600 mV and the previously described cycle was repeated 50 times to grow the film. Raman spectroscopy of the thin film was done using a 780 nm laser source. This data and a picture of the resulting film can be seen in figure 2.24. The sample is thickest at the inlet in comparison to the rest of the thin film. This means that further tailoring of the E-ALD cycle needs to be done to create a more uniform film. The Raman peaks observed occur at 110 cm^{-1}, 130 cm^{-1}, 190 cm^{-1}, 250 cm^{-1}, and 480 cm^{-1}. Based on literature comparisons, the 190 cm^{-1} peak is believed to correspond to GeSe. The most predominant peak at 250 cm^{-1} matches closest to amorphous selenium.[28] The 480 cm^{-1} may also correspond to Se based on the literature though the observed peak location is slightly shifted from the 480 cm^{-1} that is expected. SEM/EDS analysis of the resulting film also showed that the film was predominantly comprised of Se instead of GeSe. Readjustments to the E-ALD cycle need to be done to evaluate where the Ge deposition begins to fail.

2.5 CONCLUSION

A GeSe E-ALD cycle was successfully developed for at least 2 cycles in both the GeSe 9/3 case and the GeSe 3/3 case. Cyclic voltammetry studies confirmed the presence of both Se and Ge on a gold substrate. Based on the changes in the Ge peak shape and location observed in the CVs, some transformation happens to the structure of Ge when Se is deposited. When using the GeSe 3/3 E-ALD cycle, a thin film was deposited that exhibited mainly Se when characterized. Further studies should be done to see if Ge deposition simply stops occurring after

the first few cycles, if the Ge is being replaced by the Se deposited, or if the Ge growth is self-limited.

REFERENCES:

1. Mishra, P.; Lohani, H.; Kundu, A. K.; Patel, R.; Solanki, G. K.; Menon, K. S. R.; Sekhar, B. R. Electronic Structure of Germanium Selenide Investigated Using Ultra-Violet Photo-Electron Spectroscopy. *Semiconductor Science and Technology* **2015**, *30* (7), 075001.
2. Jeong, D. S.; Lim, H.; Park, G.-H.; Hwang, C. S.; Lee, S.; Cheong, B.-K. Threshold Resistive and Capacitive Switching Behavior in Binary Amorphous GeSe. *Journal of Applied Physics* **2012**, *111* (10), 102807.
3. Im, H. S.; Lim, Y. R.; Cho, Y. J.; Park, J.; Cha, E. H.; Kang, H. S. Germanium and Tin Selenide Nanocrystals for High-Capacity Lithium Ion Batteries: Comparative Phase Conversion of Germanium and Tin. *The Journal of Physical Chemistry C* **2014**, *118* (38), 21884–21888.
4. Sharma, P.; Rangra, V. S.; Sharma, P.; Katyal, S. C. Effect of Antimony Addition on the Optical Behaviour of Germanium Selenide Thin Films. *Journal of Physics D: Applied Physics* **2008**, *41* (22), 225307.
5. Liang, X.; Jayaraju, N.; Thambidurai, C.; Zhang, Q.; Stickney, J. L. Controlled Electrochemical Formation of Ge x Sb y Te z using Atomic Layer Deposition (ALD). *Chemistry of Materials* **2011**, *23*(7), 1742–1752.
6. Liang, X.; Jayaraju, N.; Stickney, J. L. Aqueous Ge Atomic Layer Deposition on Au. *ECS Transactions* **2007**.

7. Liang, X.; Zhang, Q.; Lay, M. D.; Stickney, J. L. Growth of Ge Nanofilms Using Electrochemical Atomic Layer Deposition, with a "Bait and Switch" Surface-Limited Reaction. *Journal of the American Chemical Society* **2011**, *133*(21), 8199–8204.
8. Gregory, B. W.; Stickney, J. L. Electrochemical Atomic Layer Epitaxy (ECALE). *Journal of Electroanalytical Chemistry* **1991**, 300, 543561.
9. Villegas, I.; Stickney, J. L. Preliminary Studies of GaAs Deposition on Au(100), (110), and (111) Surfaces by Electrochemical Atomic Layer Epitaxy. *Journal of the Electrochemical Society* **1992**, 139, 686694.
10. Colletti, L. P.; Teklay, D.; Stickney, J. L. Thin-Layer Electrochemical Studies of the Oxidative Underpotential Deposition of Sulfur and Its Application to the Electrochemical Atomic Layer Epitaxy Deposition of CdS. *Journal of Electroanalytical Chemistry* **1994**, 369, 145152.
11. Colletti, L. P.; Stickney, J. L. Optimization of the growth of CdTe thin films formed by electrochemical atomic layer epitaxy in an automated deposition system. *Journal of the Electrochemical Society* **1998**, 145, 35943602.
12. Venkatasamy, V.; Jayaraju, N.; Cox, S. M.; Thambidurai, C.; Mathe, M.; Stickney, J. L. Deposition of HgTe by electrochemical atomic layer epitaxy (EC-ALE). *Journal of Electroanalytical Chemistry* **2006**, 589, 195202.
13. Venkatasamy, V.; Jayaraju, N.; Cox, S. M.; Thambidurai, C.; Stickney, J. L. Studies of Hg((1-x))Cd(x)Te formation by electrochemical atomic layer deposition and investigations into bandgap engineering. *Journal of the Electrochemical Society* **2007**, 154, H720H725.

14. Kim, J. Y.; Stickney, J. L. Ultrahigh vacuum surface studies of the electrochemical atomic layer deposition of indium telluride on n-type GaAs(100). *Journal of Physical Chemistry C* **2008**, 112, 59665971.
15. Gebregziabiher, D. K.; Kim, Y. G.; Thambidurai, C.; Ivanova, V.; Haumesser, P. H.; Stickney, J. L. Electrochemical atomic layer deposition of copper nanofilms on ruthenium. *Journal of Crystal Growth* **2010**, *312*, 12711276.
16. Bouroushian, M. Electrochemistry of the Chalcogens. *Monographs in Electrochemistry Electrochemistry of Metal Chalcogenides* **2010**, 57–75.
17. Saji, V. S.; Lee, C.-W. Selenium Electrochemistry. *RSC Advances* **2013**, *3* (26), 10058.
18. Pourbaix, M. *Atlas of Electrochemical Equilibria in Aqueous Solutions*; Pergamon Press: Paris, 1966.
19. Lister, T. E. Electrochemical Formation of Se Atomic Layers on Au(100). *Journal of Vacuum Science & Technology B: Microelectronics and Nanometer Structures* **1995**, *13* (3), 1268.
20. Lister, T. E.; Stickney, J. L. Atomic Level Studies of Selenium Electrodeposition on Gold(111) and Gold(110). *The Journal of Physical Chemistry* **1996**, *100* (50), 19568–19576.
21. Sorenson, T. A. A Comparison of Atomic Layers Formed by Electrodeposition of Selenium and Tellurium Scanning Tunneling Microscopy Studies on Au(100) and Au(111). *Journal of The Electrochemical Society* **1999**, *146* (3), 1019.
22. Huang, B. M.; Lister, T. E.; Stickney, J. L. Se Adlattices Formed on Au(100), Studies by LEED, AES, STM and Electrochemistry. *Surface Science* **1997**, *392* (1-3), 27–43.
23. Liang, X.; Kim, Y.-G.; Gebergziabiher, D. K.; Stickney, J. L. Aqueous Electrodeposition of Ge Monolayers. *Langmuir* **2010**, 26 (4), 2877–2884.

24. Ledina, M.A.; Bui, N.; Liang, X.; Kim, Y.G.; Jung, J.; Perdue, B.; Tsang, C.; Drnec, J.; Carl`a, F.; M. P. Soriaga, M.P.; Reber, T.J.; Stickney, J.L. Electrochemical Formation of Germanene: pH 4.5 *Journal of The Electrochemical Society* **2017**, *164* (7) D469-D477.

25. Bui, N. N.; Ledina, M.; Reber, T. J.; Jung, J.; Stickney, J. L. Electrochemical Scanning Tunneling Microscopic Study of the Potential Dependence of Germanene Growth on Au(111) at pH 9.0. *ACS Nano* **2017**, 11 (9), 9481–9489.

26. Jung, J.; Bui, N. N.; Shen, S.; Reber, T. J.; Brezner, J. M.; Mubeen, S.; Stickney, J. L. In Situ Surface-Enhanced Raman Spectroscopic Studies of Electrochemically Formed Germanene. *The Journal of Physical Chemistry C* **2018**, *122* (27), 15696–15705.

27. Concepts, D. GeSe (Germanium Selenide). http://www.hqgraphene.com/GeSe.php (accessed Sept 18, 2019).

28. Selenium R060137. https://rruff.info/)/R060137 (accessed Jul 14, 2019).

CHAPTER 2. FIGURES

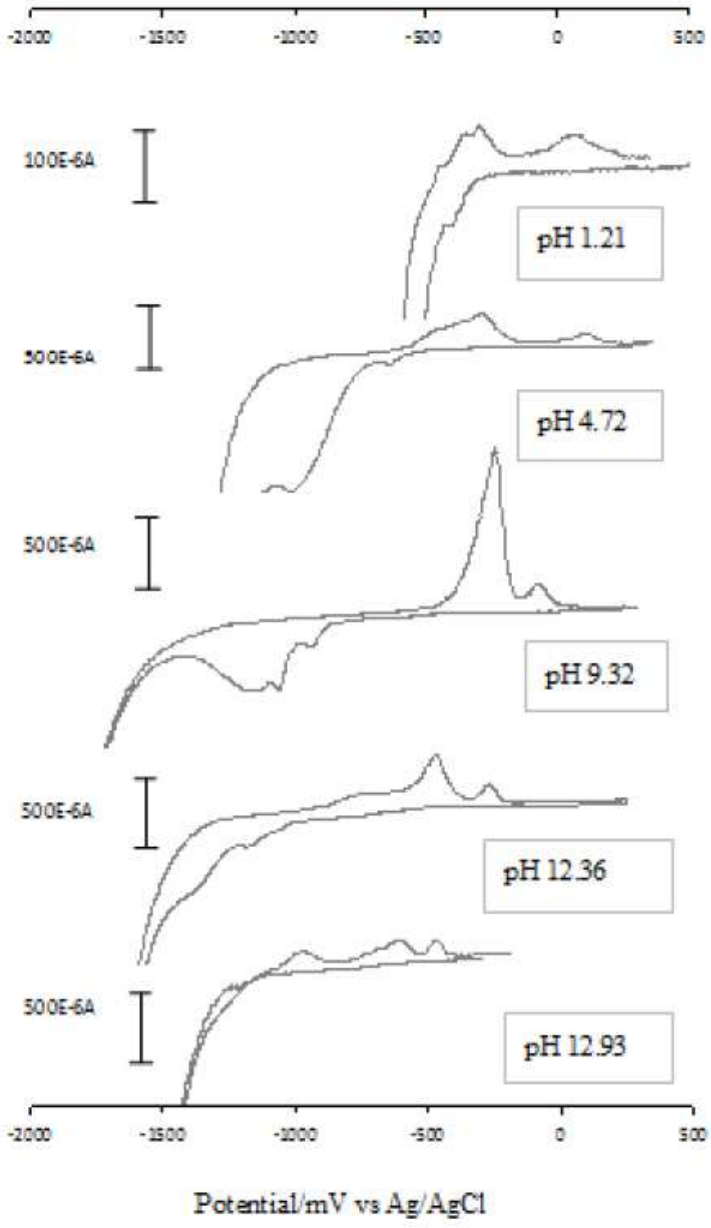

Figure 2.1 Cyclic voltammetry of germanium solutions at different pHs.[6]

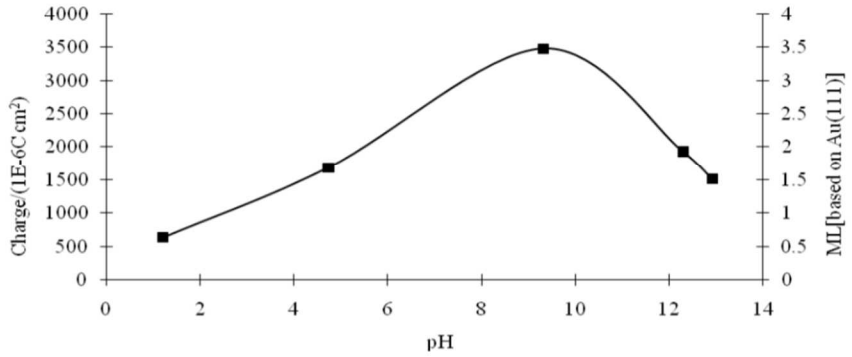

Figure 2.2 Plot of the maximum Ge able to deposit at various pH conditions. Different times for holding and deposition potentials were used based off of the requirement of Ge at said pH.[6]

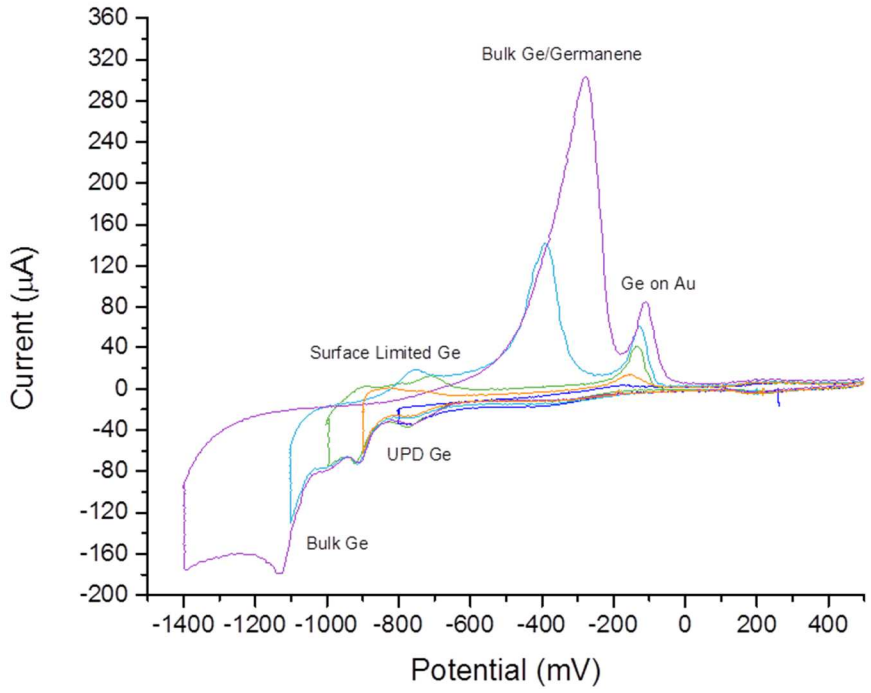

Figure 2.3 Window opening of CVs for 0.2 mM Ge solution at pH 9. Areas of interest have been labeled with the process of deposition or oxidation.

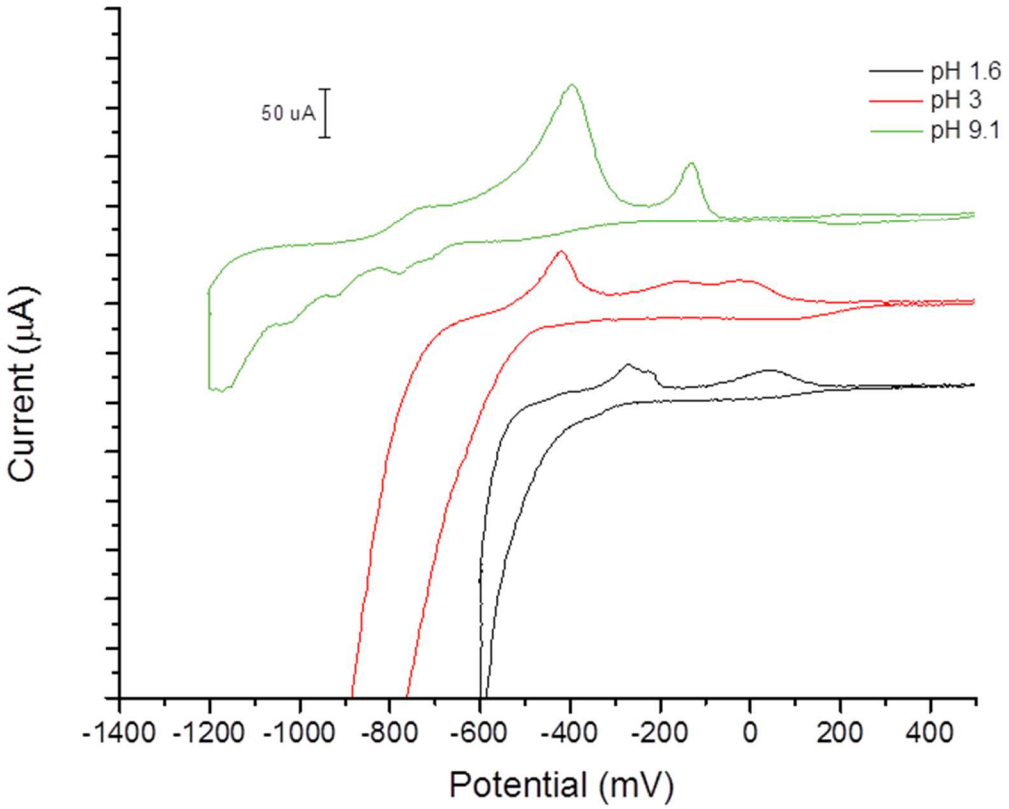

Figure 2.4 Cyclic voltammetry of 0.2 mM Ge solutions at pH 1.6, 3, and 9. A scale of 50 μA included. Each solution has a respective axis of 0 occurring in line with their positive limits.

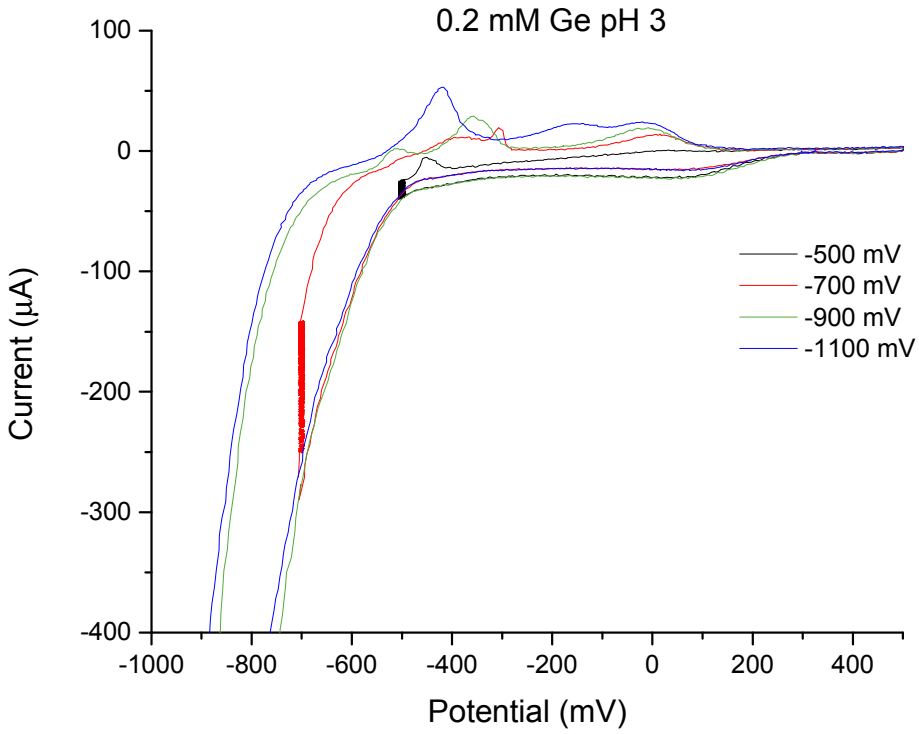

Figure 2.5 Window opening of pH 3 0.2 mM Ge CVs. Potentials were held at negative limits for 30 seconds.

A)

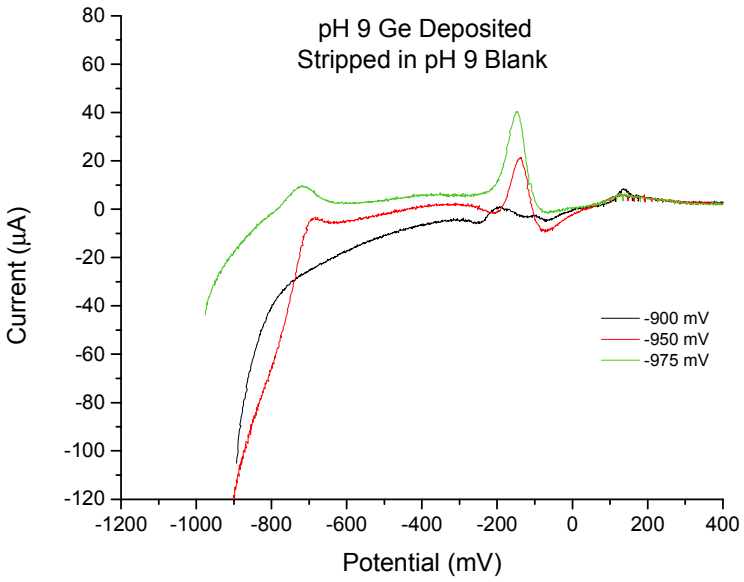

B)

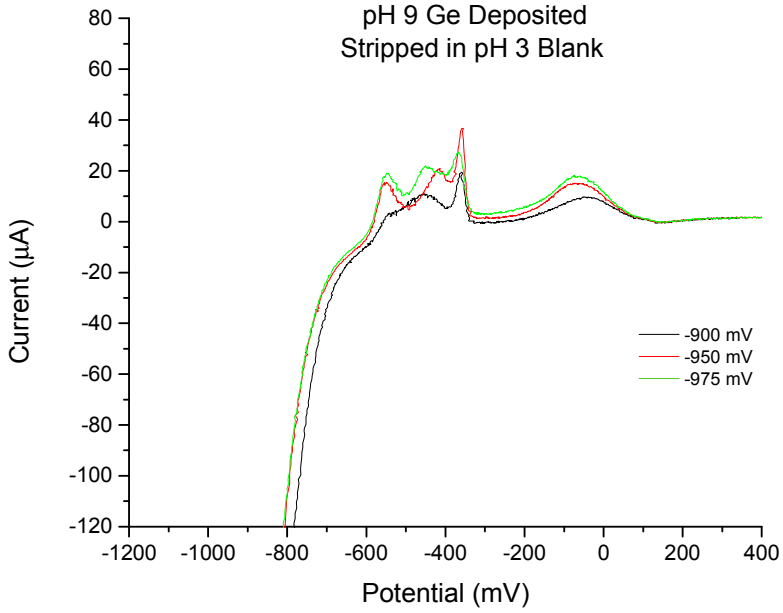

Figure 2.6 Pulse deposition of pH 9 Ge stripped in A) pH 9 blank solution and B) pH 3 solution. Ge was deposited between -900 mV and -975 mV.

A)

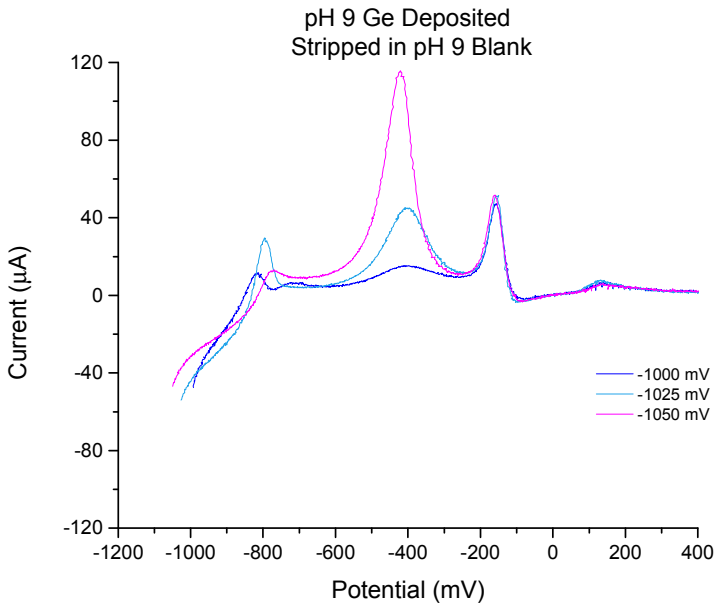

B)

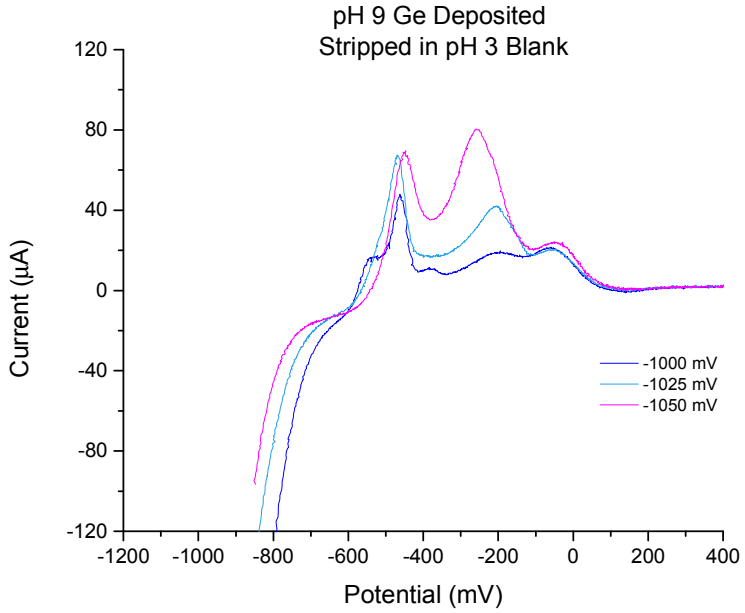

Figure 2.7 Pulse deposition of pH 9 Ge stripped in A) pH 9 blank solution and B) pH 3 solution. Ge was deposited between -1000 mV and -1050 mVs

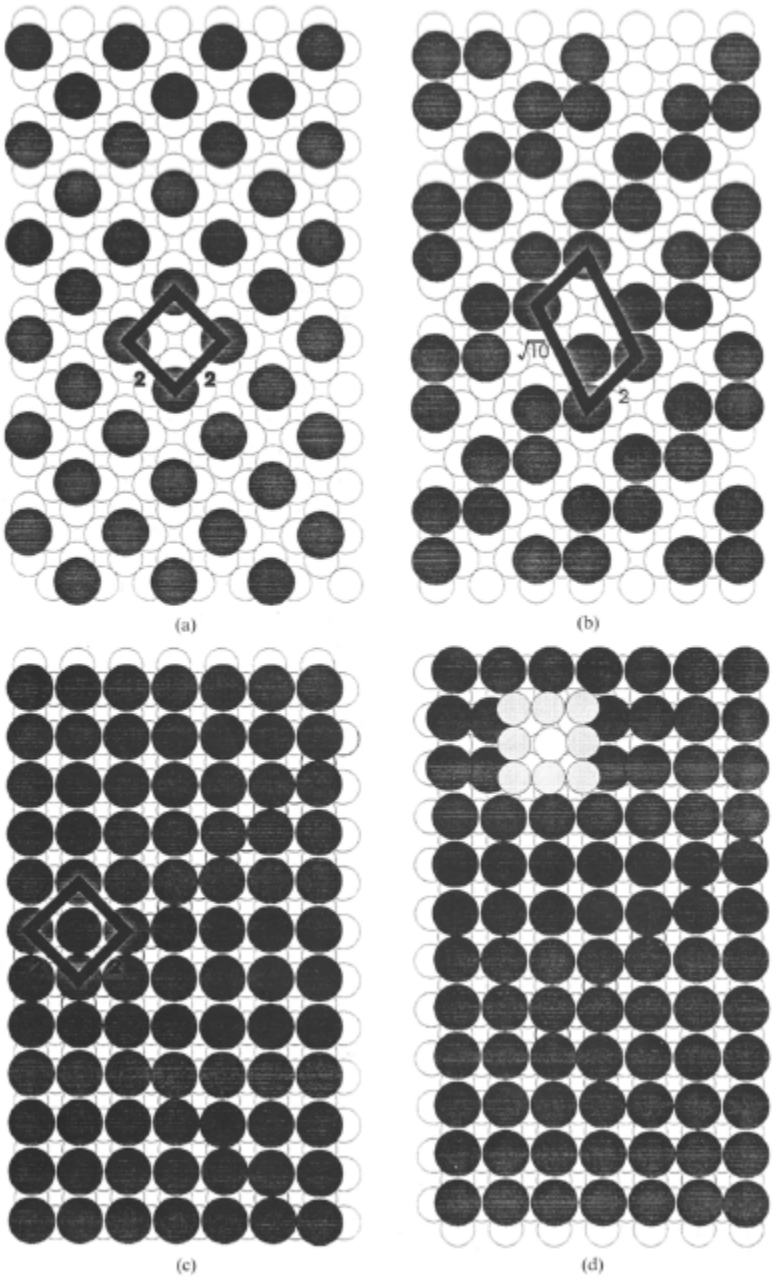

Figure 2.8 Proposed structures of Se coverages observed: A) 1/4 coverage (2X2), B) a (2X√10) at 1/3 coverage, C) a *c*(2X2) at 1/2 coverage, and D) c(2X2) surrounding a Se_8 ring with a 0.7 ML coverage.[22]

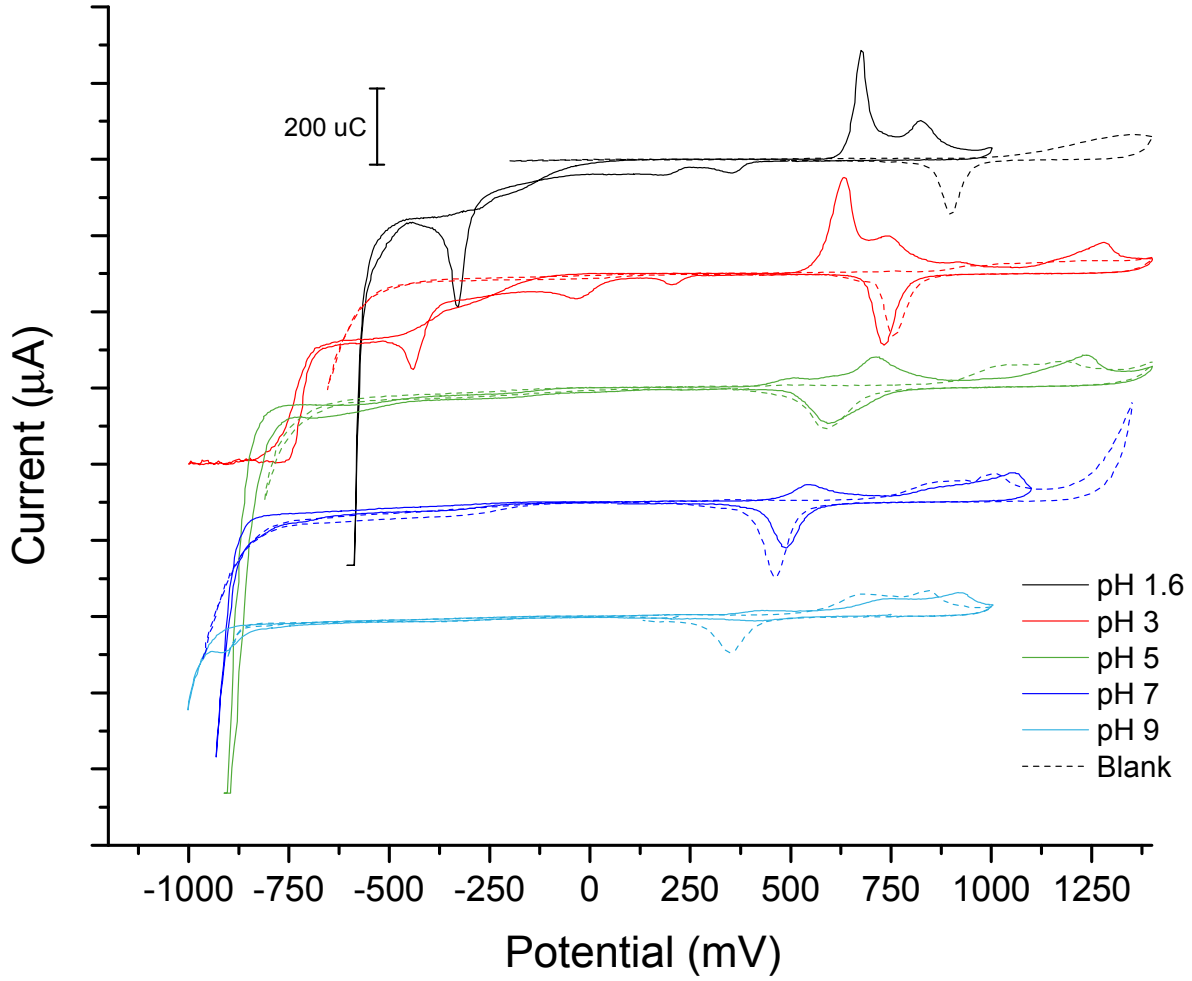

Figure 2.9 CVs of 0.2 mM Se at pH 1.6, 3, 5, 7, and 9. Blank scans at the respective pHs have been included for each pH as the dashed line for comparison of Au oxidation and reduction peaks. Solutions with a pH of 3-9 used NaOH to pH adjust. Solutions with a pH between 5and 9 have a sodium borate buffer.

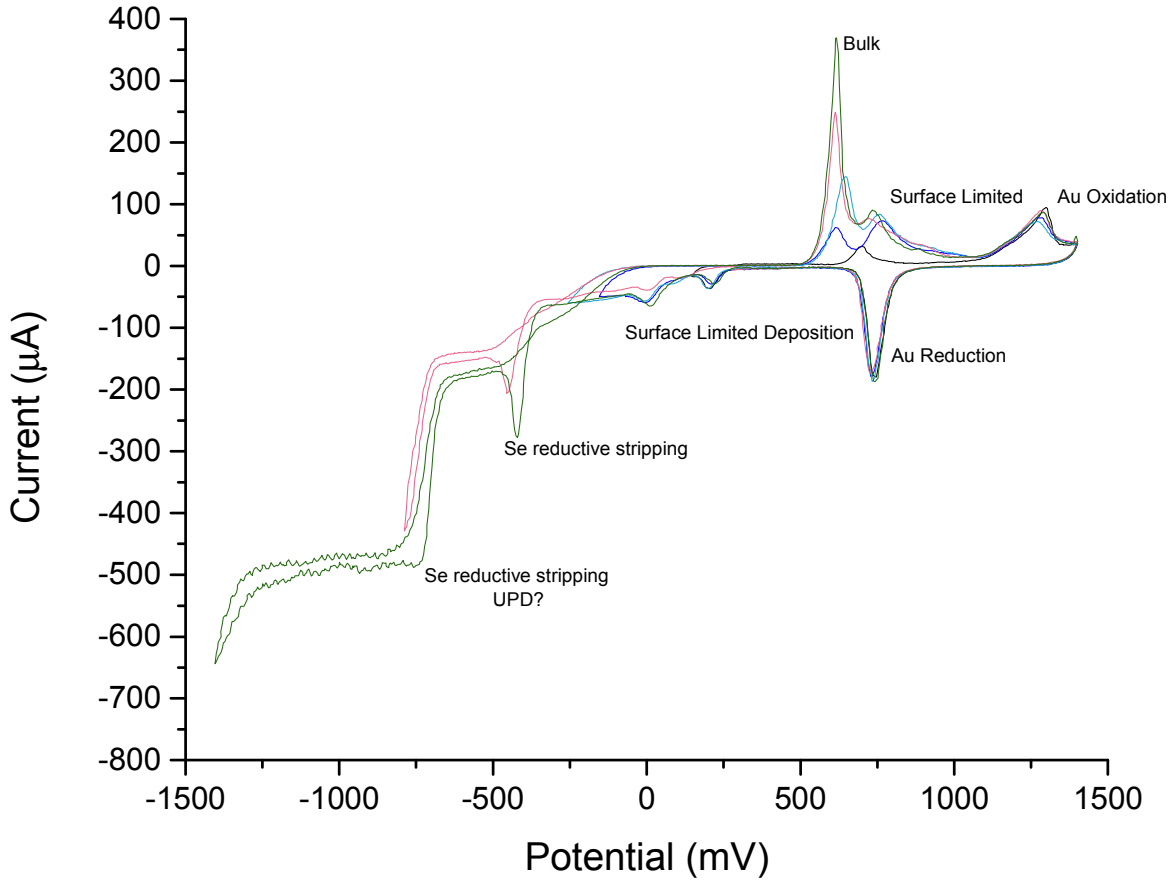

Figure 2.10 Window opening of CVs of a pH 3 0.2 mM Se solution. Areas of interest have been labeled with electrochemical processes occurring in those regions.

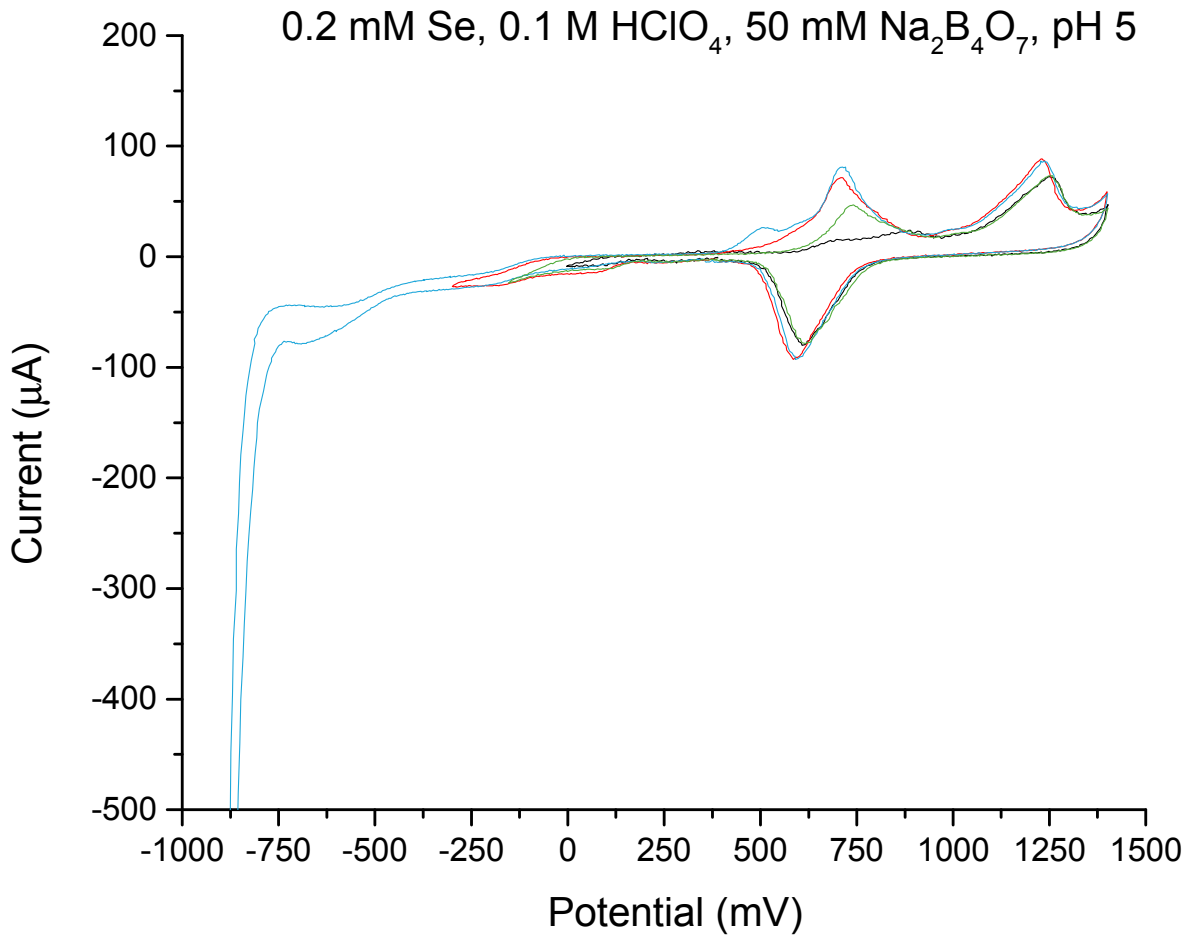

Figure 2.11 Window opening of CVs using a pH 5 0.2 mM Se solution.

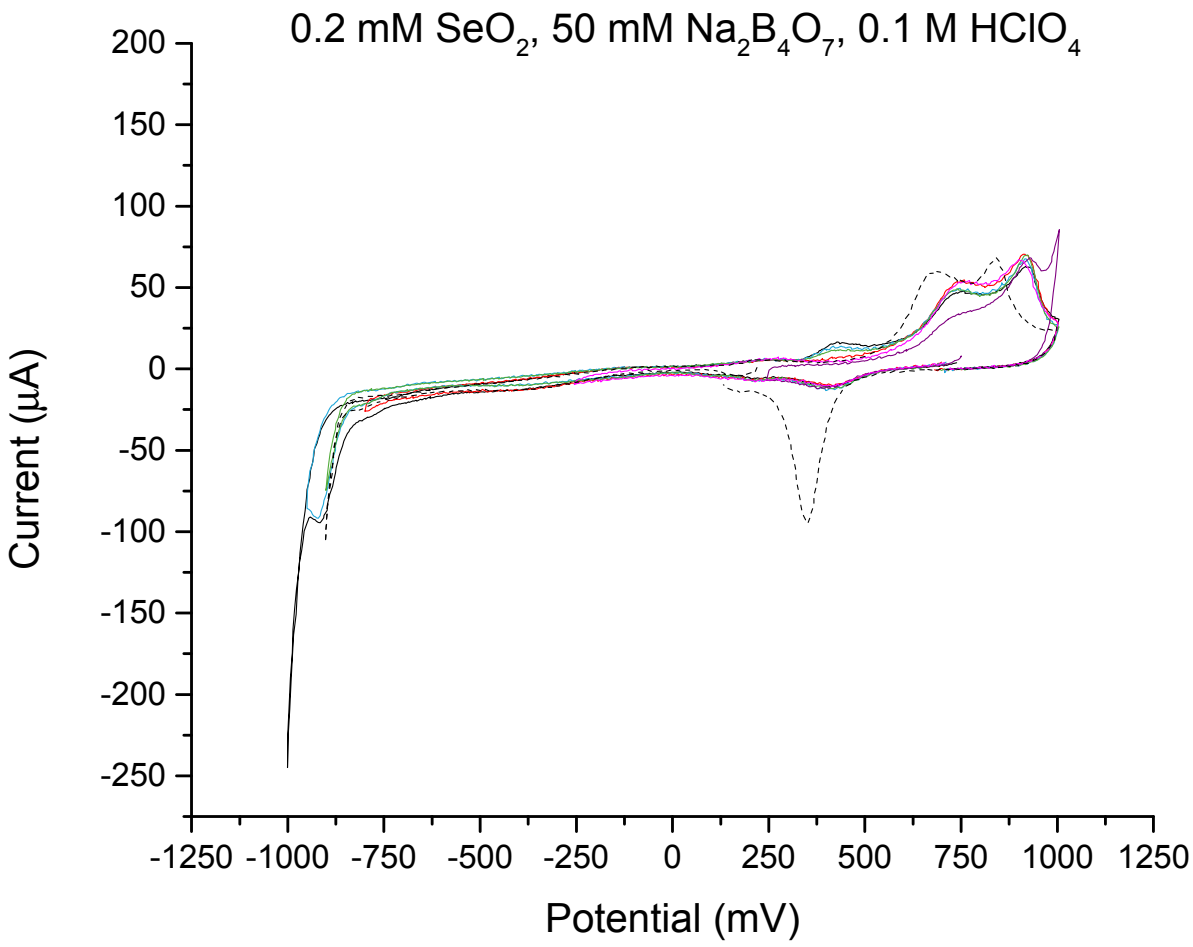

Figure 2.12 Window opening of CVs for a pH 9 0.2 mM Se solution. A blank scan of pH 9 solution has been included in the dashed scan for reference.

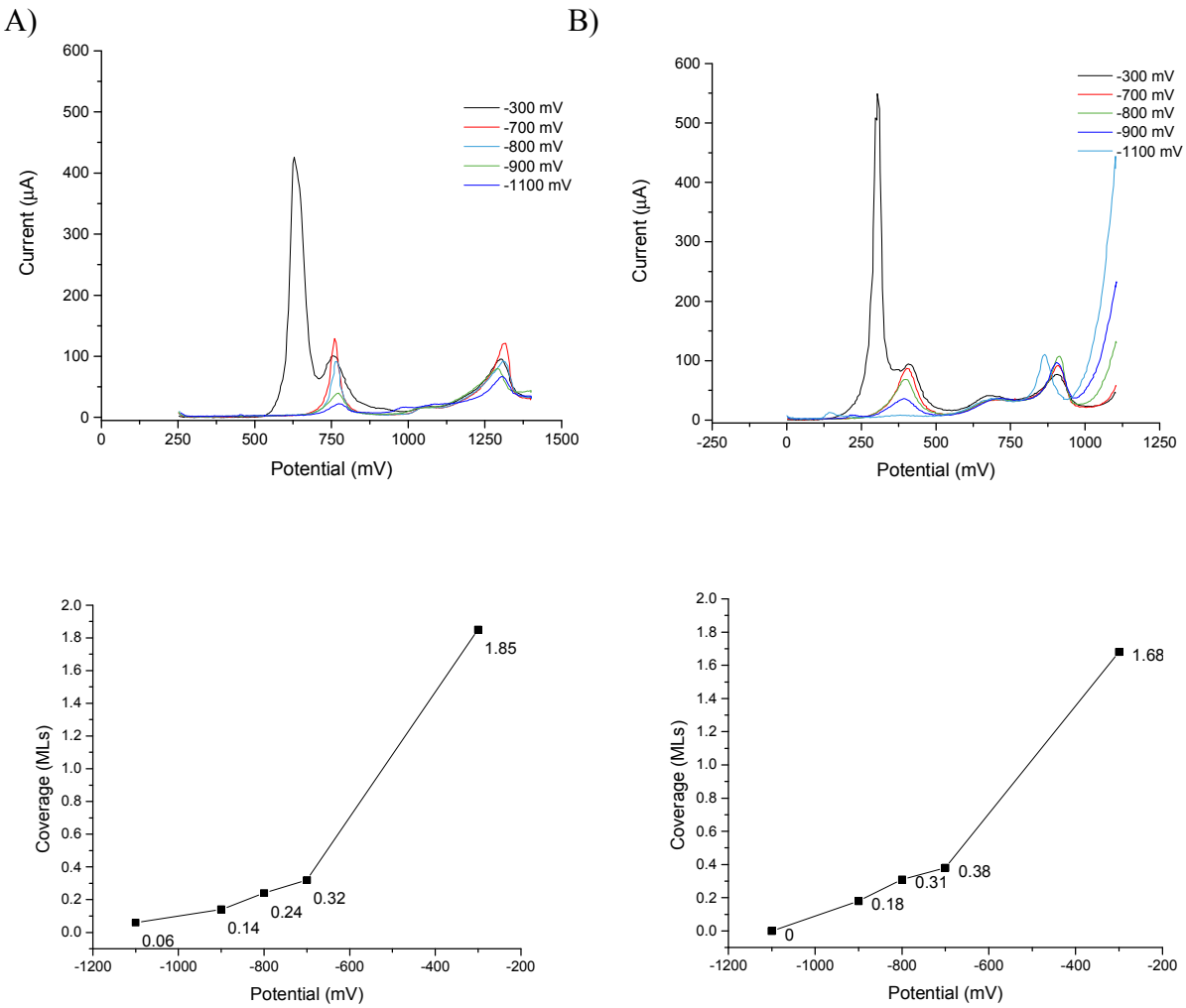

Figure 2.13 Example of Se deposition using the Case 1 method. Se was first deposited using a pH 3 solution then was stripped in a blank solution A) pH 3 B) pH 9. Coverages are reported below the CVs.

A) B)

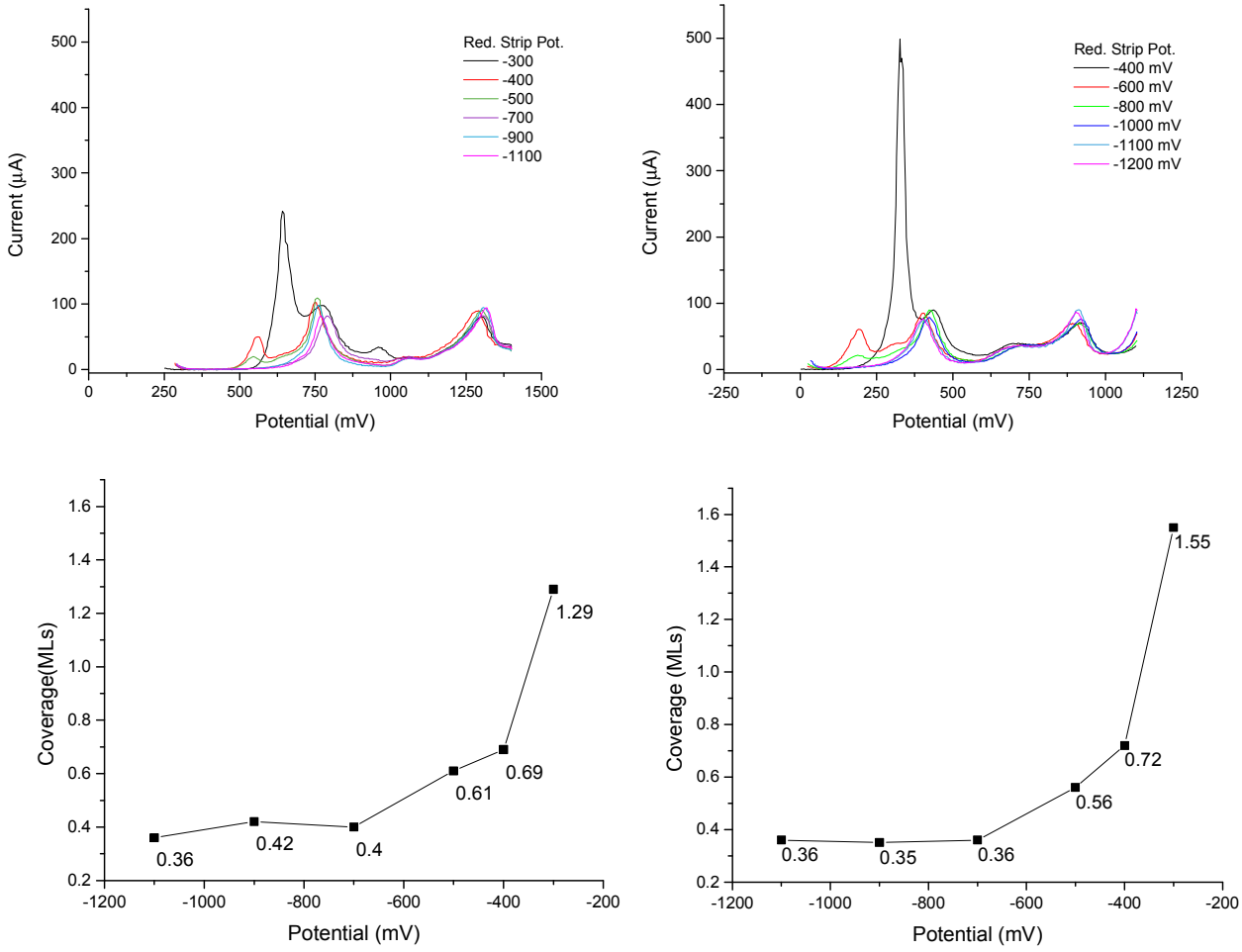

Figure 2.14 Example of Se deposition using the Case 3 method. Se was first deposited using a pH 3 solution then was stripped in a blank solution A) pH 3 B) pH 9. Coverages are reported below the CVs.

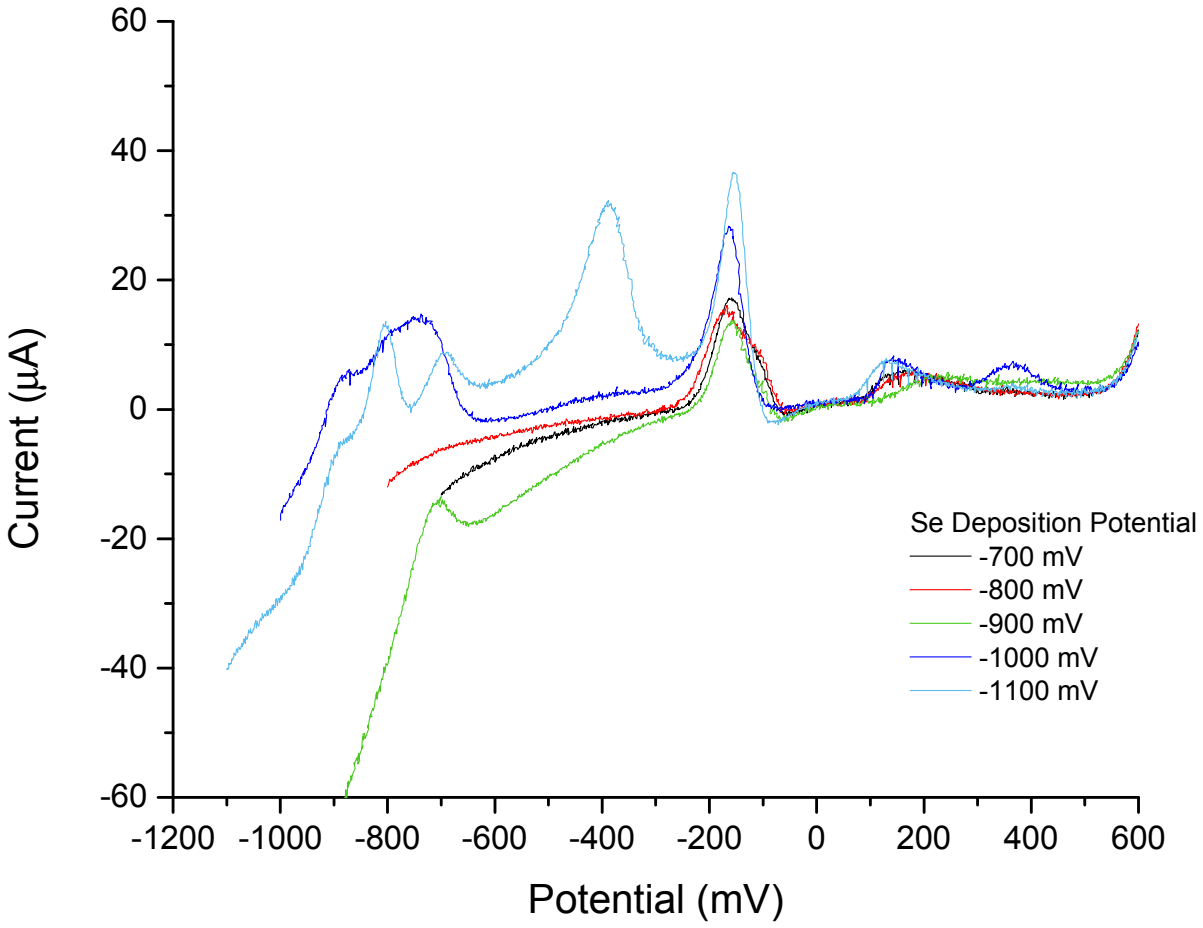

Figure 2.15 CVs showing Se deposited on Ge at pH 9. Both solutions were pH 9 and Ge was first deposited at -925 mV. After flushing the Ge solution out of the cell with a pH 9 blank solution, Se was deposited using varying potentials. Afterward, a pH 9 blank solution was rinsed through the cell and then an oxidative stripping scan was performed.

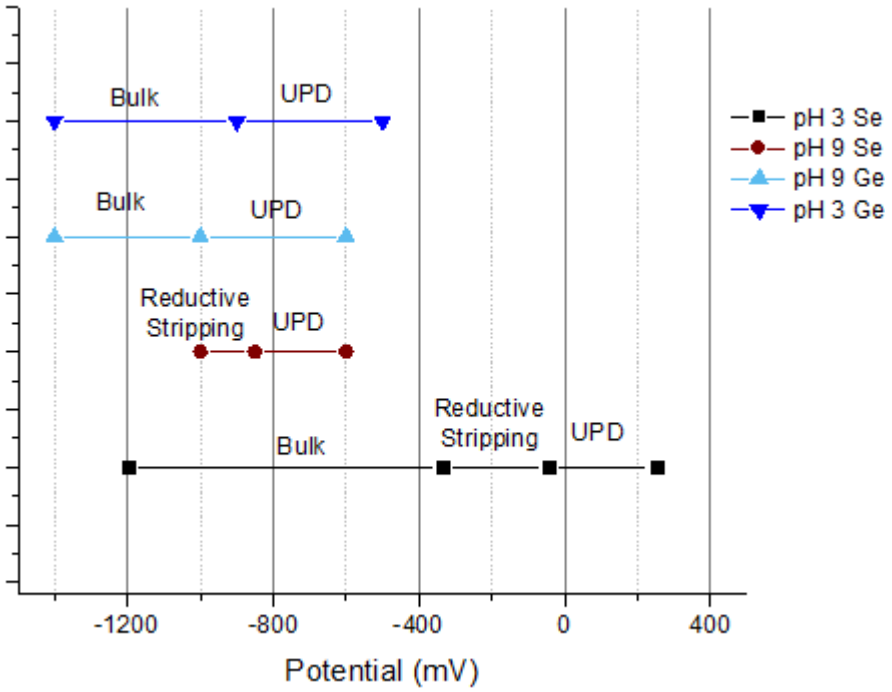

Figure 2.16 General regions where reduction occurs for Se and Ge in pH 3 and pH 9. These ranges were determined from cyclic voltammetry.

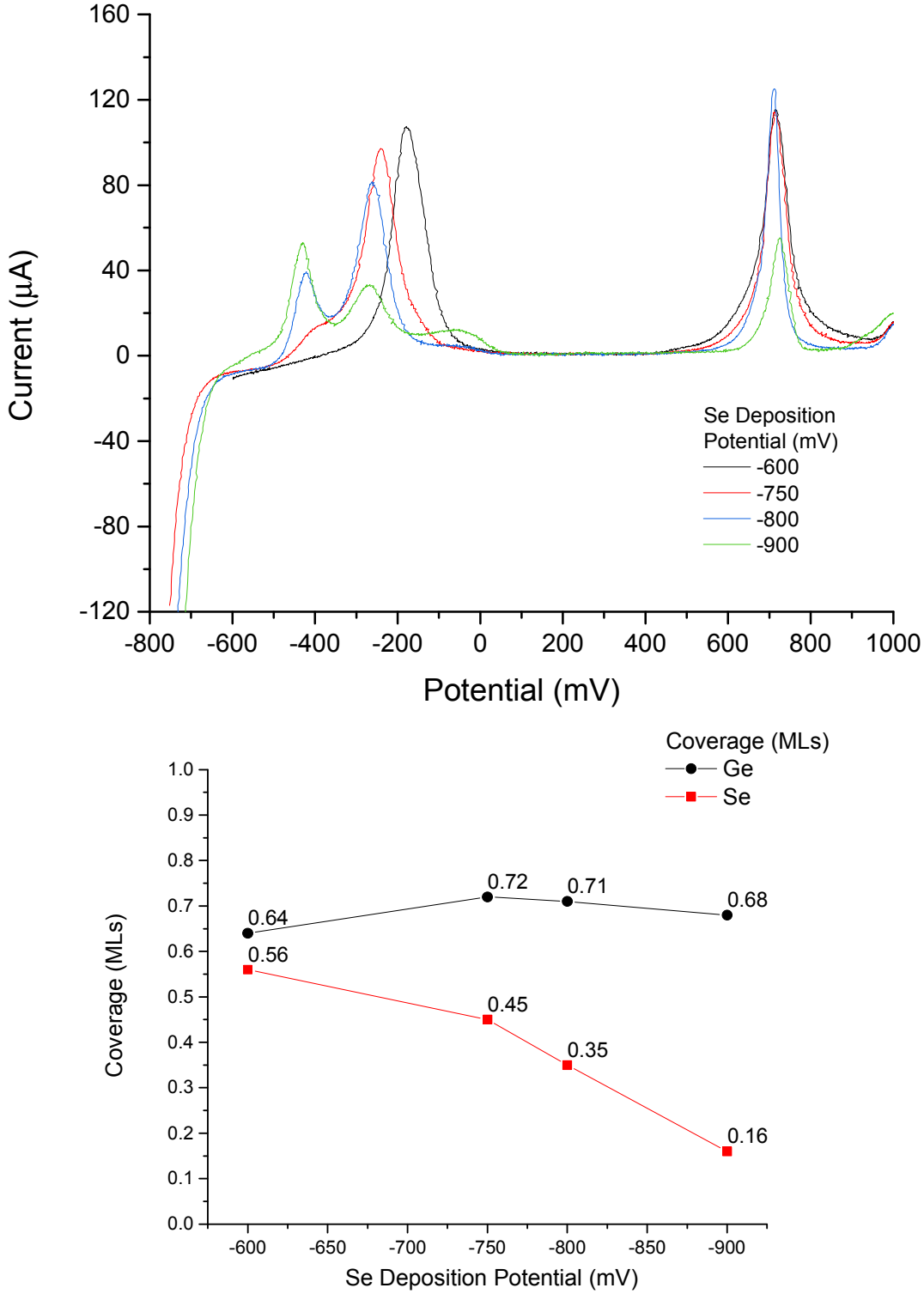

Figure 2.17 CVs of Se on a Ge-coated Au substrate. pH 9 Ge was first deposited at -1000 mV. Next, a pH 9 blank was flown through the cell followed by a pH 3 blank solution to change the pH in the cell to pH 3. pH 3 Se was deposited at different potentials and then a pH 3 blank was flown through the cell before performing an oxidative stripping scan. The top shows the resulting CVs and bottom shows the coverages of Ge and Se.

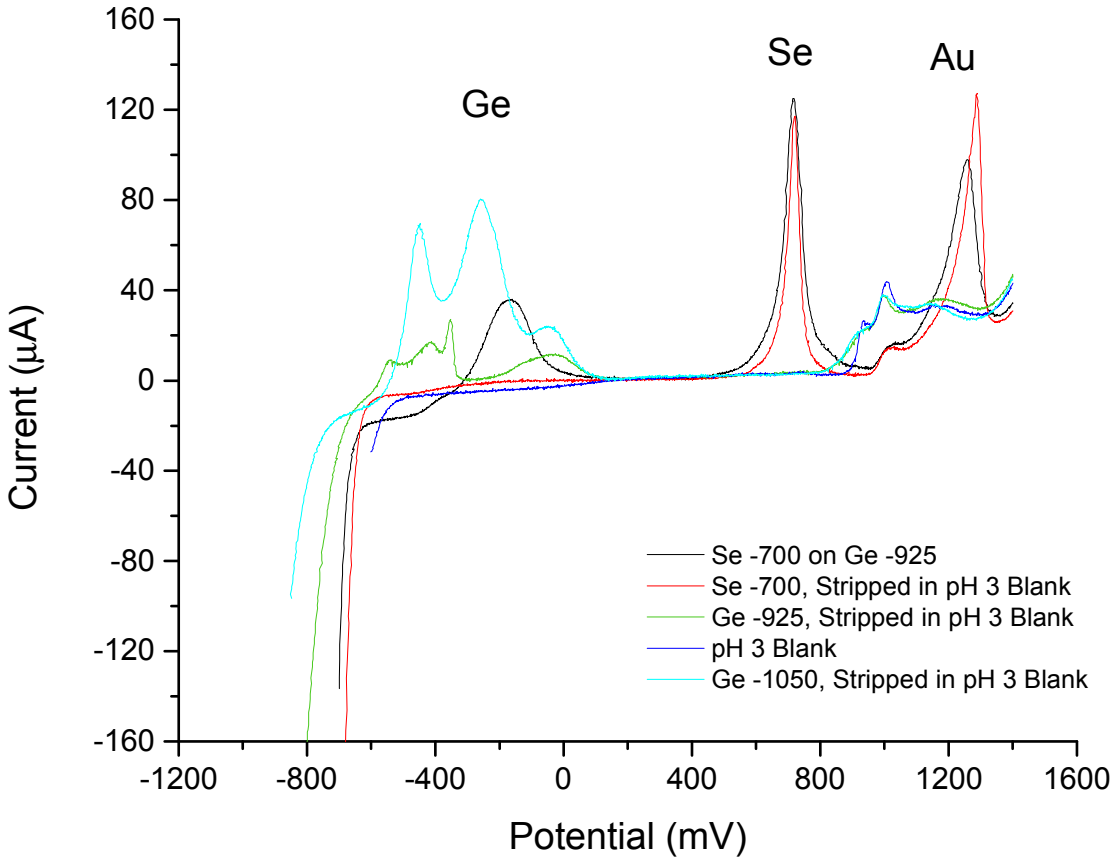

Figure 2.18 Comparison of CVs resulting from different scenarios of Se and/or Ge deposition. All scans shown are at pH 3.

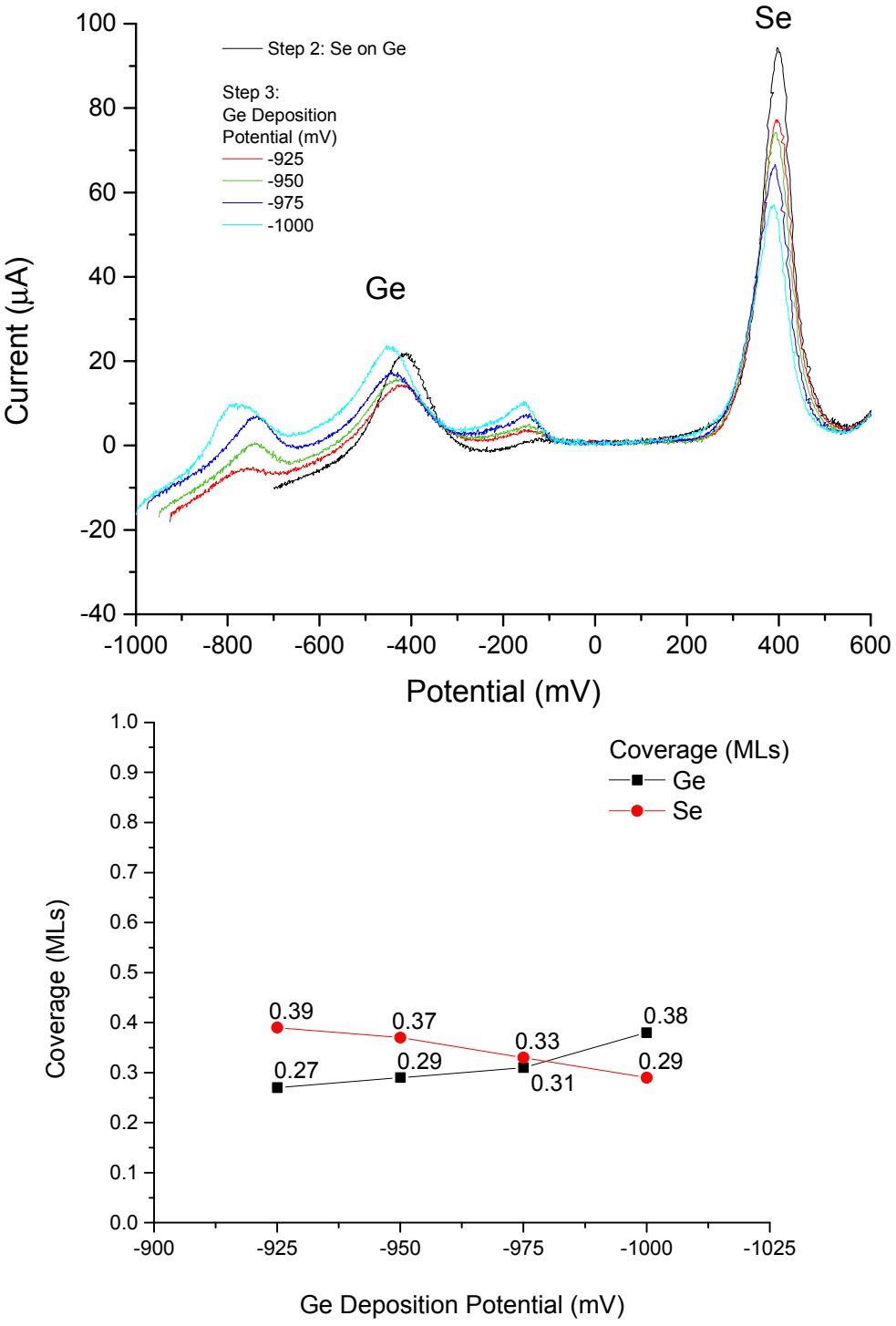

Figure 2.19 CVs (top) and coverages (bottom) showing pH 9 Ge being deposited on top of a Se-Ge covered Au substrate. pH 9 Ge was first deposited at -925 mV. Next, a pH 9 blank was flown through the cell followed by a pH 3 blank solution to change the pH in the cell to pH 3. pH 3 Se was deposited at -700 mV and then a pH 3 blank was flown through the cell. pH 9 blank was then flushed through the cell before introducing Ge and depositing it at different potentials before performing an oxidative stripping scan in pH 9 blank.

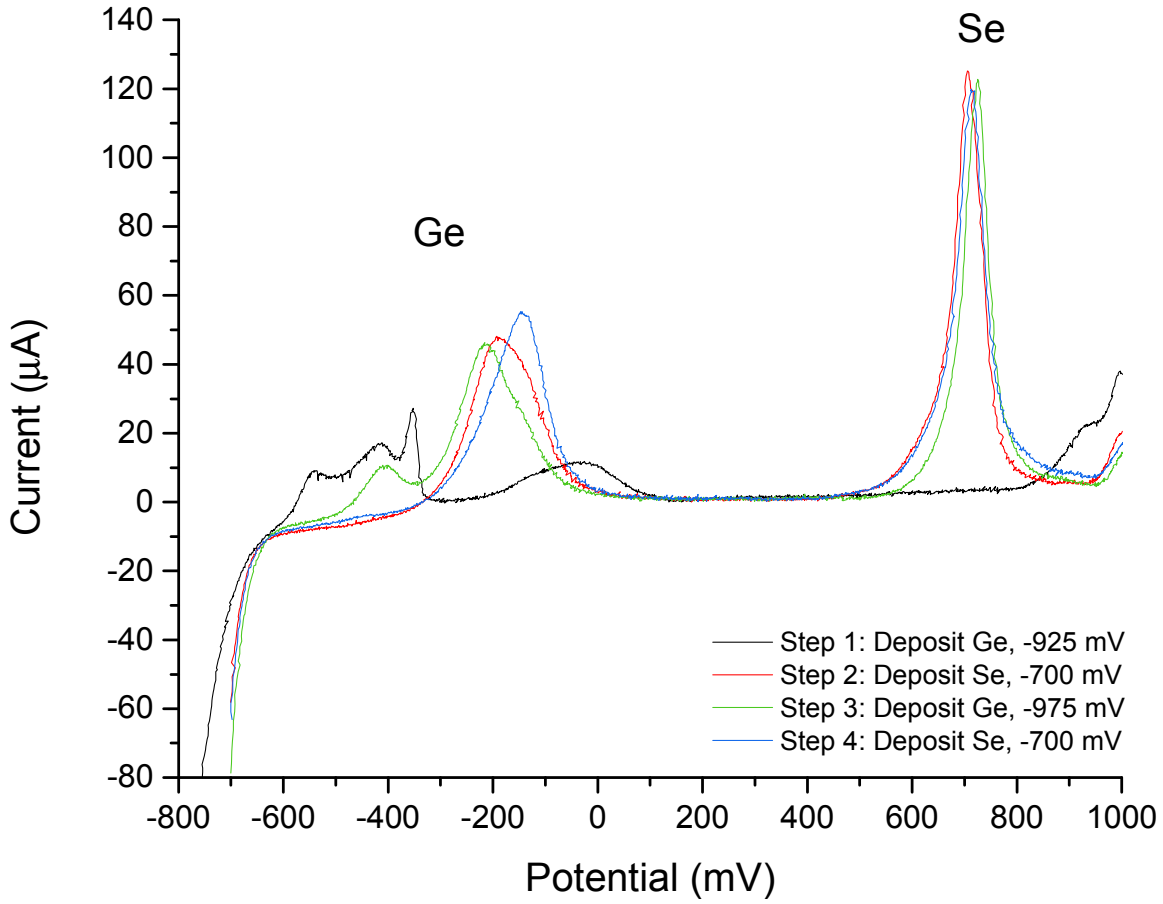

Se on Ge, 2 Cycles		
	Ge Coverage (MLs)	Se Coverage (MLs)
Step 1	0.32	n/a
Step 2	0.36	0.52
Step 3	0.47	0.42
Step 4	0.48	0.53

Figure 2.20 CVs showing the progression of Ge and Se deposition through two complete cycles of GeSe E-ALD deposition. Coverage and deposition parameters are as-listed. Steps 1 and 2 complete cycle 1. Steps 3 and 4 correspond to cycle 2. Below the CVs are the corresponding coverages of Se and Ge throughout the 2 cycles.

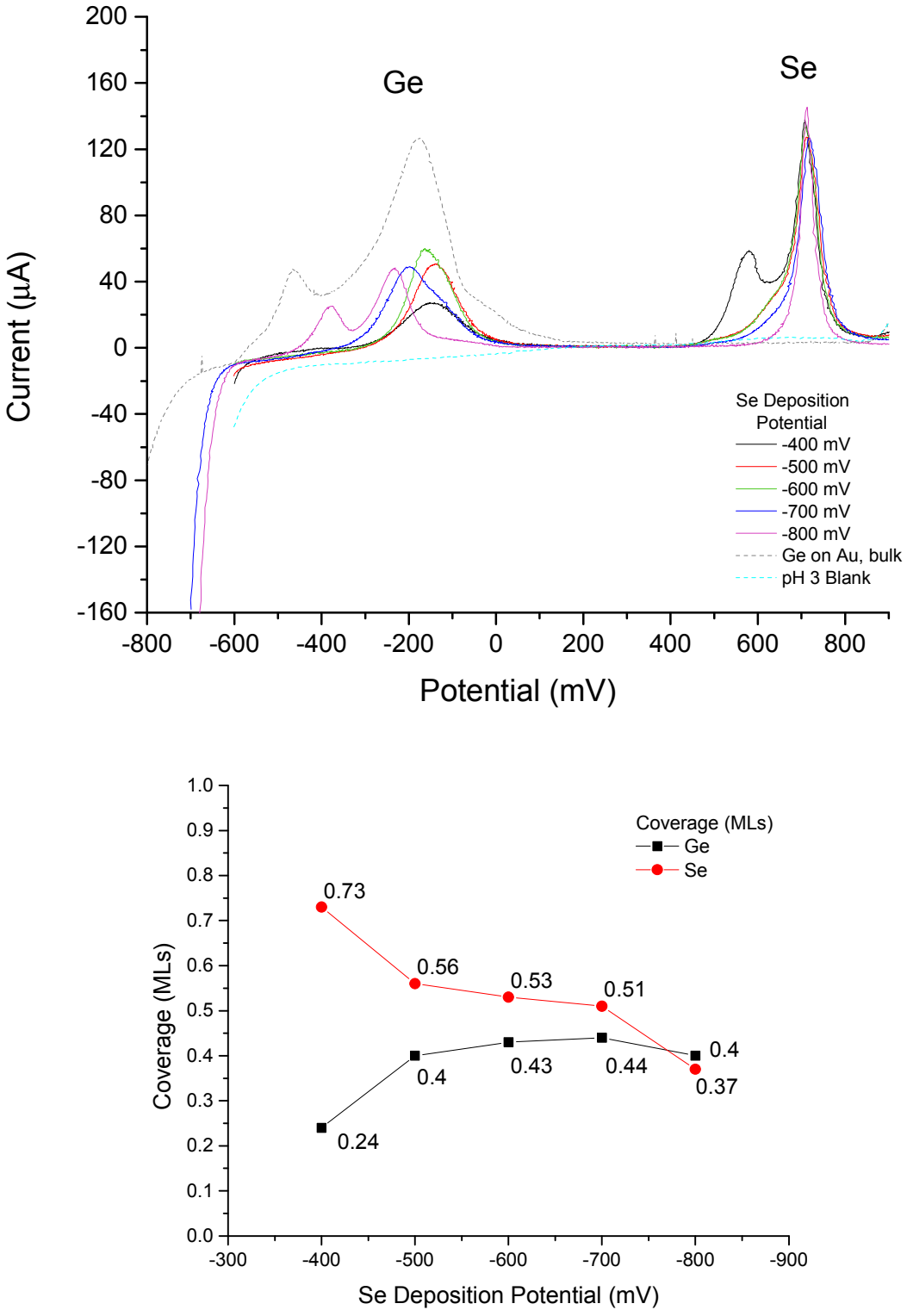

Figure 2.21 CVs of Se on a Ge-coated Au substrate. pH 3 Ge was first deposited at -600 mV. Next, the pH 3 blank solution was flown through the cell and then pH 3 Se was deposited at different potentials. A pH 3 blank was flown through the cell before performing an oxidative stripping scan. The top shows the resulting CVs and bottom shows the coverages of Ge and Se.

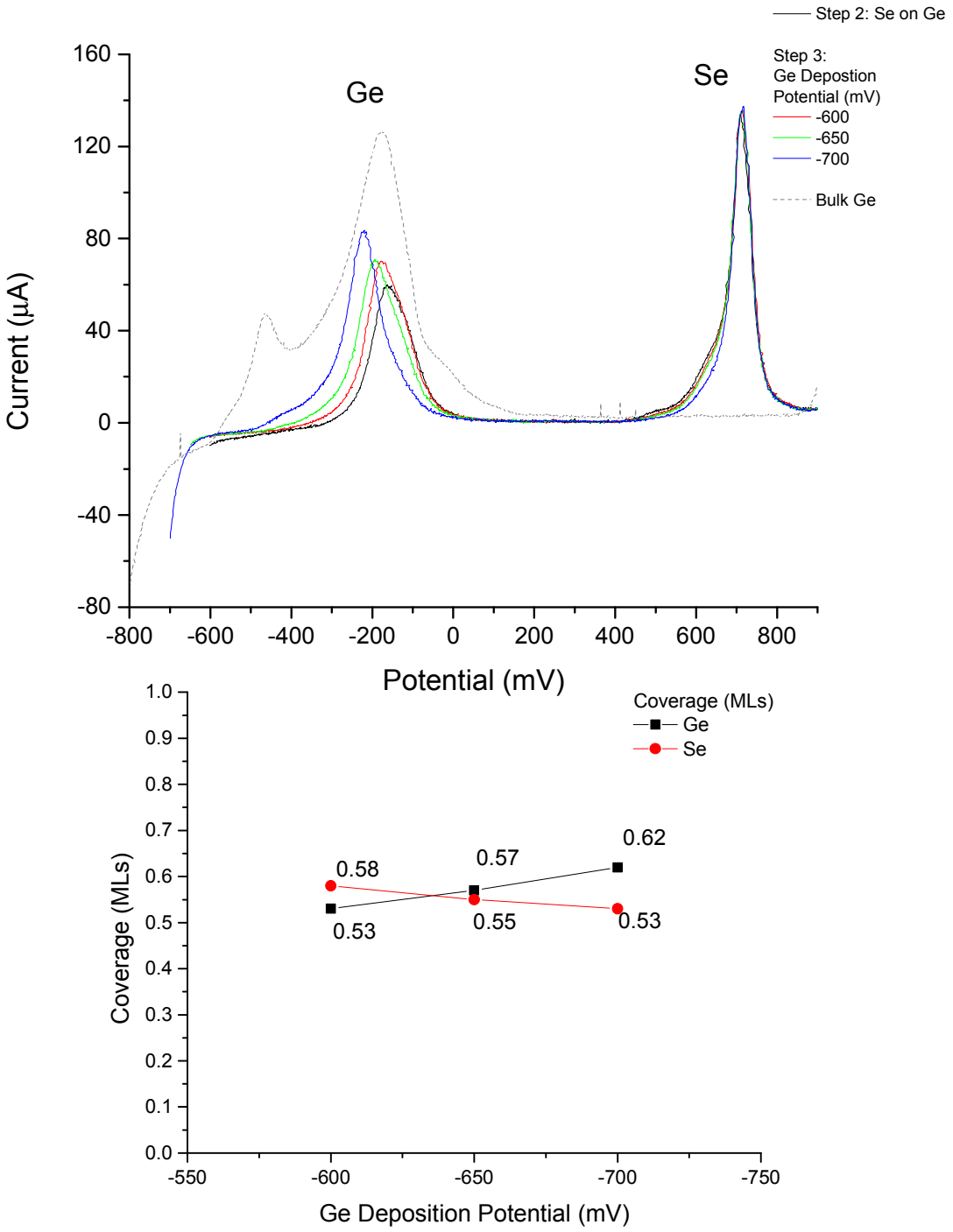

Figure 2.22 CVs (top) and coverages (bottom) showing pH 3 Ge being deposited on top of a Se-Ge covered Au substrate. pH 3 Ge was first deposited at -600 mV. Next, a pH 3 blank was flown through before pH 3 Se was deposited at -600 mV and then a pH 3 blank was flown through the cell. pH 3 blank was then flushed through the cell before introducing Ge and depositing it at different potentials before performing an oxidative stripping scan in pH 3 blank.

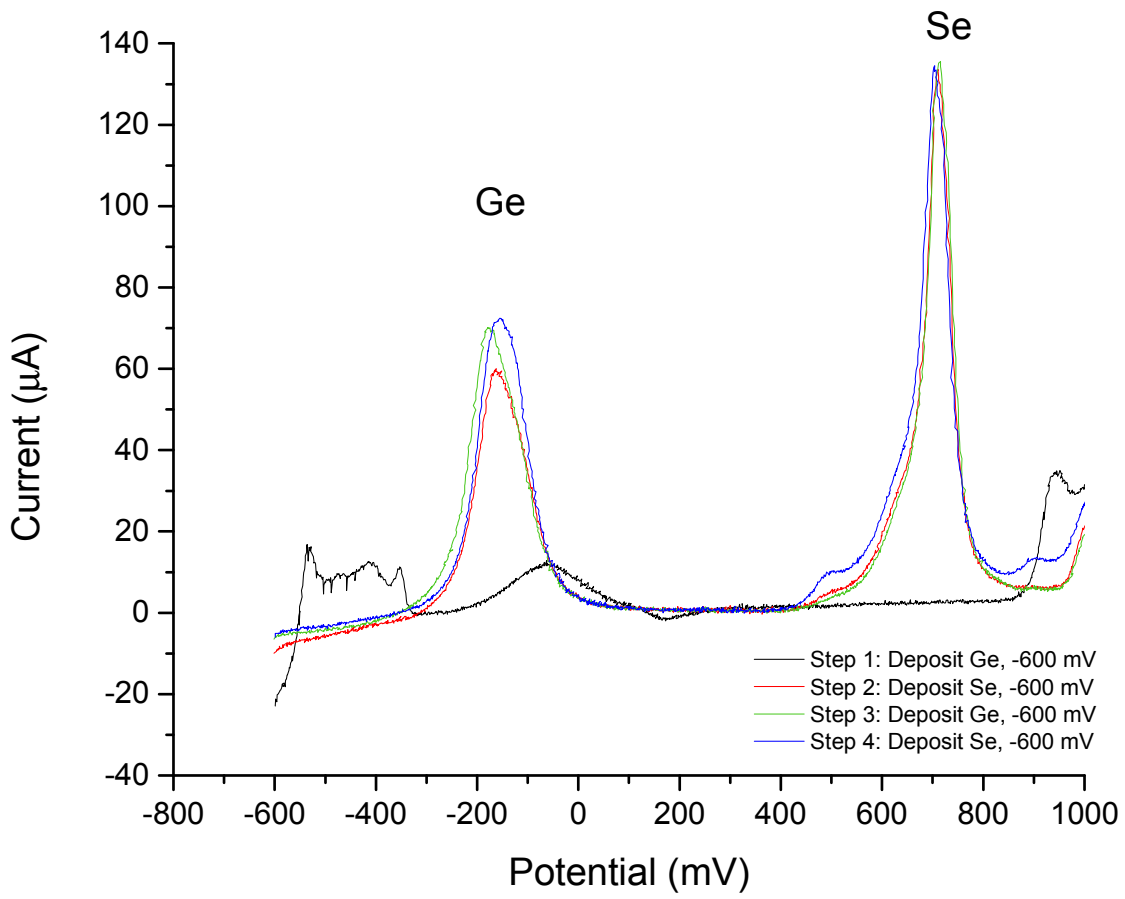

Se on Ge, 2 Cycles		
	Ge Coverage (MLs)	Se Coverage (MLs)
Step 1	0.46	n/a
Step 2	0.43	0.53
Step 3	0.53	0.58
Step 4	0.52	0.60

Figure 2.23 CVs showing the progression of Ge and Se deposition through two complete cycles of GeSe E-ALD deposition using pH 3 solutions for both precursors. Coverage and deposition parameters are as-listed.

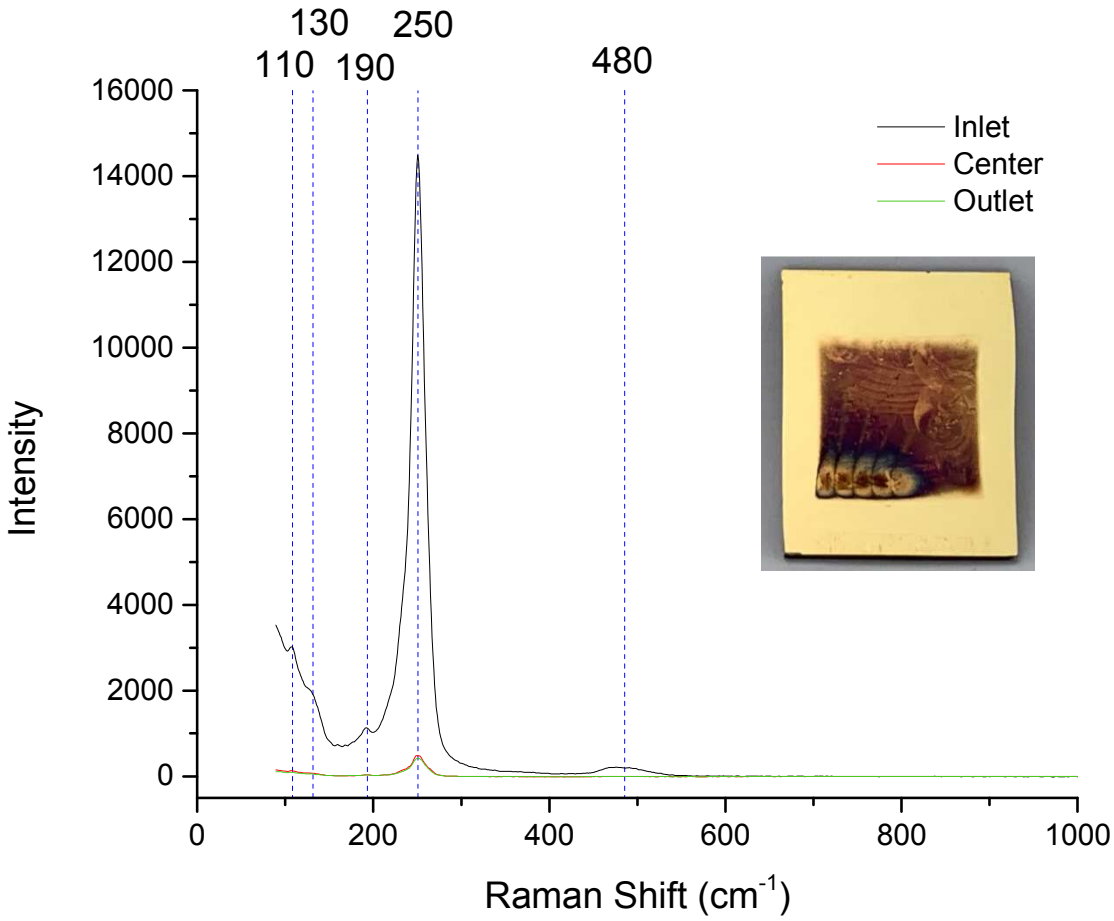

Figure 2.24 Raman spectra of a 50 cycle GeSe deposit at the inlet(bottom), center, and outlet (top) of the thin film taken with a 780 nm, laser. Notable peaks have been labeled for clarity.

CHAPTER 3

TIN SELENIDE[2]

[2] Howell, P.; Mubeen, S.; Stickney, J. To be submitted to the ECS Journal

3.1 ABSTRACT

SnSe thin films were deposited using the E-ALD method. Optimization of the thin films was achieved through examination of the cyclic voltammetry of the individual elements and investigations into the effect of each step throughout the E-ALD cycle. Choice of the parameters, such as potential at which the precursor solutions and blank solutions were introduced to the cell, showed varied resulting films. Three electrolytes were used in the experimental process. The initial electrolyte used was sulfuric acid. This was chosen based on prior Sn research done in the group. An E-ALD cycle was developed and the change in resulting thin films was examined by investigating the effect of changing Sn and Se deposition potentials systematically. Regardless of potential choice, thin films made using this electrolyte were not homogenous and exhibited the presence of both SnSe and $SnSe_2$. The second electrolyte examined was perchloric acid. The use of this electrolyte improved the solution stability of Sn and the quality of thin films. The E-ALD cycle was further optimized with this electrolyte by changing the flow rate of the solution and the concentration of Sn. Thin films still showed the presence of both SnSe and $SnSe_2$. Finally, HCl was used as the electrolyte for Sn and with this change, homogeneous SnSe thin films were made. Characterizations of the thin films were done using SEM/EDS, XRD, and Raman Spectroscopy.

3.2 INTRODUCTION

Tin selenide is an IV-VI chalcogenide semiconductor with favorable electronic and optical properties for use in devices like solar cells and lithium ion batteries.[1-3] Tin selenide

exhibits multiple phases: SnSe, $SnSe_2$, and Sn_2Se_3.[2] However, Sn_2Se_3 is not thermodynamically favored and typically only SnSe and $SnSe_2$ are experimentally achievable. Depending on the stoichiometry, characteristics including band gap and crystal structure change. SnSe is a p-type semiconductor with a band gap of 1.0 eV. These properties make SnSe an alternative to CdTe as an absorber layer in photoelectrochemical cells.[4] CdTe is the most common semiconductor absorber layer because of its ideal band gap at 1.45 eV and high absorption efficiency.[5] However, CdTe uses toxic components that are not earth-abundant and it is subject to photocorrosion in the types of electrolytes used in PEC cells. $SnSe_2$ is an n-type semiconductor with a band gap of 1.6 eV. It also has properties that make it a favorable choice in photoelectrochemical cells.

Tin selenides have been previously formed by many methods including vapor deposition, brush plating, chemical bath deposition, laser ablation, electrodeposition, as well as other techniques.[2] In 2005, Sn-Se compounds were made using an E-ALD.[6] Cyclic voltammetry and amperometric studies were done but the determination of the quality of these films was not investigated using any other characterization methods. An issue with tin selenide films is controlling the phase and many deposits exhibit both SnSe and $SnSe_2$. E-ALD is an ideal choice for making SnSe or $SnSe_2$ thin films because of its control over the deposition at a monolayer scale and the ability to design the solutions and deposition potentials. E-ALD was developed by the Stickney lab almost 30 years ago and has been used to make many materials.[7-14] Electrodeposition used in combination with the flow cell system allows the growth of a material to be monitored during deposition. Current/potential time traces are recorded during deposition and allow for the observed current to be tracked constantly. Changes in current indicate changes happening to the substrate as each element is being introduced to the cell and deposited. Analysis

of this data in conjunction with other methods of characterization of the resulting thin film allows the improvement of the film unique to E-ALD.

Another aspect unique to the E-ALD method is the ability to tailor the solution makeup to the needs of each element. Three electrolytes were investigated for SnSe deposition. First studies were done using H_2SO_4 as the electrolyte for Sn and Se solutions. The stability of the Sn solution was low and films created using this electrolyte were poor in quality. The second solution investigated was $HClO_4$. This Sn solution had longer stability than H_2SO_4 but still eventually precipitated. The third electrolyte investigated is HCl. These films show the highest homogeneity and PEC response. The Se solutions had no problems with stability regardless of electrolyte. Selenium has been heavily researched in the Stickney group and its expected characteristics were well known prior to this study.[15-18] Tin solution chemistry and electrochemistry was unknown and required trial and error in finding a suitable composition.

The tin selenide thin films have been characterized using X-ray diffraction (XRD), scanning electron microscopy with electron dispersive spectroscopy (SEM/EDS), and Raman spectroscopy. Our collaborator Dr. Mubeen completed photoelectrochemical testing. The XRD and Raman spectroscopy results aid in the differentiation of the SnSe and $SnSe_2$. SEM allows for the microscopic view of the surface of the substrate. The EDS allows for elemental identification. However, that will only identify the amount of Sn and Se present and may not be relevant if the thin films have the presence of both SnSe and $SnSe_2$. Photoelectrical testing was done to evaluate whether or not the film acted as a p/n type material and determine its stability in electrolytes.

3.3 EXPERIMENTAL

In the investigation of the SnSe system, multiple solutions were examined. The first tin solution was 0.2 mM SnO_2 (Alfa Æsar 99.996% pure) in 0.1 M H_2SO_4 (Fisher Chemical). The following experiments were done using 0.2 mM $SnCl_2 \cdot 2H_2O$ (Sigma Aldrich 99.99% pure) in 0.1 M $HClO_4$ (GFS Chemicals, Inc.). A 2 mM $SnCl_2 \cdot 2H_2O$ (Sigma Aldrich 99.99% pure) in 0.5 M $HClO_4$ (GFS Chemicals, Inc.) solution was also used. The final tin solution makeup was 2 mM $SnCl_2 \cdot 2H_2O$ (Sigma Aldrich 99.99% pure) in 0.1 M HCl (JT Baker). The tin precursor was sonicated in a 50:50 solution containing the concentrated acid of choice and water for at least 30 minutes before diluting to its final solution volume. This was done to ensure the tin dissolved. Solutions were replaced regularly due to precipitation. The pH of all tin solutions was 1.6.

The selenium solutions were first made of 0.2 mM SeO_2 (Alfa Æsar 99.999% pure) in 0.1 M H_2SO_4 (Fisher Chemical). The second makeup was of 0.2 mM SeO_2 (Alfa Æsar 99.999% pure) in 0.1 M $HClO_4$ (GFS Chemicals, Inc.). This second solution was used for experiments involving Sn in $HClO_4$ and HCl. The Se solutions showed no issues with precipitation or instability. The pH used for these solutions was also 1.6. Blank solutions used were 0.1 M H_2SO_4 (Fisher Chemical) and then 0.1 M $HClO_4$ (GFS Chemicals, Inc.).

All solutions were made with 18 MΩ water (Millipore Advantage 10) and stirred for at least an hour depending on the precursor added. The solution bottles used to store and connect solutions to the electrochemical flow cell were first cleaned by soaking them in a Nochromix (Godax Labratories) bath for a minimum of one hour. They were then rinsed sufficiently with 18 MΩ water (Millipore Advantage 10). All solutions are purged with N_2 gas to remove any oxygen for at least one hour before the experiments. The electrochemical flow cell (Electrochemical

ALD L.C.) has a three-electrode setup. The auxiliary electrode is an inlaid Au wire in the shape of an "S." The reference electrode was Ag/AgCl in 3 M NaCl (Bioanalytical Systems, Inc.). When not in use the reference electrode was stored in a supersaturated NaCl solution. The working electrode is the substrate that will be deposited on. All experiments in this chapter use polycrystalline Au (Evaporated Metal Films) as the substrate. The polycrystalline Au is comprised of 100 nm of Au on top of 5 nm Ti on a glass slide, with the Ti used as an adhesion layer. The resulting working area of the cell is 2.2 cm^2. The Au slides are cleaned before putting them into the cell. This process includes rinsing the slide with acetone (Fisher Chemical), then rinsing with nanopure water, and drying it in N_2 gas. Next, the slide soaks in concentrated nitric acid (JT Baker) for at least 30 seconds. An additional rinse with nanopure water and N_2 drying precedes the immediate placement of the slide inside the cell.

The slide is additionally cleaned electrochemically before starting experimentation. A 0.1 M H_2SO_4 (Fisher Chemical) solution is used to clean the slide. This solution is flown into the cell at open circuit potential (OCP) and then a cleaning program is used to oxidize and reduce contaminants off the Au surface. The cleaning program pulses the potential to -200 mV and 1400 mV multiple times and then performs two CVs between -200 mV and 1400 mV. These potentials are chosen based on the electrochemistry of Au in sulfuric acid. This method has been recognized in the Stickney group as a sufficient method of cleaning before experimentation. Depending on the type of experiment performed, Au slides can sometimes be reused by simply employing an electrochemical cleaning cycle after the experiment.

Solutions flow through a valve block (Neptune Research & Development, Inc.) before entering the flow cell. The valve block allows for multiple solutions to be flown through the cell without contamination or manual solution switching. The solution flow and potential control are

automated using an in-house Labview program, Sequencer, that previous group members developed. The potentiostat (Electrochemical ALD L.C.) allows potential control of the cell at any given time.

For surface characterization, an SEM (FE-SEM Thermo Fisher Teneo) was used at both 5 keV and 10 keV accelerating voltages. For more surface related information and to limit the burning of certain films, 5 keV was selected. 10 keV allows for deeper penetration of the thin film and higher imaging quality. The EDS detector (150mm Oxford $XMax^N$) was used for elemental analysis. A 532 nm Laser source was chosen to evaluate the tin selenide films because that was a suitable source for its Raman active modes. XRD (PANalytical X'PERT Pro) was utilized for crystallographic information. Typical XRD assumes infinite thickness and is typically used for powders. To optimize results taken on a thin film, diffractograms were obtained using an open Eulerian cradle at a glancing angle. The source was 1.54 Å Cu K_α radiation. Raman Spectroscopy (DXR Raman Microscope, Thermo Scientific) was also used for structural identification. A 532 nm Laser source was chosen to evaluate the tin selenide films because that was a suitable source for its Raman active modes.

3.4 RESULTS AND DISCUSSION

3.4.1 TIN SELENIDE THIN FILMS USING SULFURIC ACID ELECTROLYTE

The motivation for our group beginning research on tin selenide thin films was to eventually deposit the superlattice CZTS(e). CZTS is a quaternary semiconductor comprised of copper, zinc, tin, and either sulfur or selenium. It can be made with selenium, sulfur, or a mixture of both. The quaternary compound would be formed by first developing E-ALD cycles for the binary compounds ZnS, CuS, and SnSe. Those cycles could then be repeated in various orders to

form CZTS. Interest in CZTS has grown rapidly in the 2000s as an alternative to CIGS based devices.[19] CIGS is made from copper, indium, gallium, and selenium. Both quaternary compounds have high efficiency when incorporated into photovoltaic devices. However, CIGS requires rare and high-cost elements, indium and gallium. Replacing In and Ga with Sn and Zn allows for a cheaper and non-toxic alternative. Other group members developed the deposition sequences for ZnS and CuSe. Either SnSe or SnS needed to be researched to form CZTS using E-ALD. In comparison to metals like Ag and Cu, Sn was not a well-studied metal in the Stickney group. When comparing the knowledge base of selenium and sulfur, selenium had been much more heavily researched by the Stickney group. Thus SnSe was selected instead of SnS.

The first sets of experiments were done using sulfuric acid as the electrolyte. The purpose of electrolyte in electrodeposition is to aid in dissociating ions and transporting electric charge. Thus, the electrolyte choice and concentration can vastly change the electrochemistry and deposition of a material. A window opening of CVs for 0.2 mM Sn in 0.1 M H_2SO_4 is shown in figure 3.1. All CVs started at the same positive potential 200 mV. The potential was held at the negative turning potential for 30 seconds to allow sufficient Sn electrodeposition to take place. As the potential was scanned negatively in the Sn solution, the first reductive feature can be seen starting at -200 mV. This reduction corresponds to the underpotential deposition of Sn onto the gold substrate. As the potential is scanned to more negative potentials, the current rapidly decreases past -600 mV. The oxidative features of these CVs show peaks between -400 mV to -200 mV and 0 mV to 100 mV. The most positive peak can be identified as the UPD stripping peak because it does not grow past its maximum regardless of potential. The bulk peak is located between -400 mV and -200 mV. Two peaks are seen in the broad oxidation peak and may correspond to different structures of Sn being oxidized from the Au surface.

Figure 3.2 is a window opening of CVs for the solution of 0.2 mM Se in 0.1 M H_2SO_4. The potential did not need to be held at the turning potential because selenium electrodeposition occurs at a much faster rate than the Sn. The first reductive feature observed in the CVs occurs at 350 mV and is a surface limited feature. The second reductive feature begins near 0 mV and is the onset of bulk selenium deposition. As described in chapter 2, selenium is a chalcogen element and has the unique ability to reductively strip off of the surface. That phenomenon is observed in the CVs beginning at -350 mV. The oxidative peaks are located between 700 mV and 1000 mV. The surface limited oxidation peaks can be seen growing during the scans to potentials 300 mV, 250 mV, 200 mV, 150 mV, 100 mV, 50 mV, and 0 mV. By 0 mV, the Se surface limited oxidation peak is fully formed. Once the potential is scanned past that to -50 mV, a second oxidation peak is observed at 700 mV. As the potential is scanned to more negative potentials this 700 mV peak grows larger and the surface limited peak appears to grow as well. The growth in this peak is not due to the surface limited amount changing but instead, the current being shifted due to the bulk deposit growth.

When developing a deposition cycle for SnSe, the areas for reductive stripping of selenium needed to be avoided when depositing the Sn. Two sets of experiments were done to evaluate the quality of tin selenide films and potential choice. The effect of Sn deposition potentials on resulting thin films was examined by changing the potential between -300 mV and -400 mV. The Se potential was kept constant to avoid multiple sources of change. The Se deposition potential chosen was -100 mV. This potential ensured that sufficient Se could be deposited without oxidatively stripping Sn from the surface while also not depositing excess bulk Se. Another set of deposits was made with a constant Sn potential of -325 mV and Se deposition potentials between 0 mV and -200 mV.

The steps for the proposed SnSe E-ALD cycle are listed in figure 3.3. These parameters were chosen based on previous experiments performed and allowed for a deposit to be grown. This cycle was repeated 100 times for each of the following thin films. Figure 3.4 shows the resulting thin films deposited at varied Sn deposition potentials and SEM images taken at the inlet and outlet of the films. The thin films are all oriented so that the inlet is at the bottom and the outlet is at the top. Figure 3.5 shows the ratio of Sn:Se based on EDS elemental analysis. Figure 3.6 shows Raman spectra and figure 3.7 shows the XRD diffractograms of the thin films.

As seen in figure 3.4, vastly different thin films occur by changing the Sn deposition potential. When a -300 mV Sn deposition potential was used, a blue deposit can be seen at the inlet of the cell. The thin film thickness decreases greatly past this area. This indicates that deposition is being influenced by the solution physically hitting the substrate and increasing the thickness in that area. Similar phenomena can be seen in the other Sn deposition potentials as well. The thickness of the deposit can be roughly estimated by the color of the deposit. The blue "toes" observed at the inlet of the -300 mV sample are expected to be thicker than the light brown deposit seen at the center and outlet of the thin film. When the thin film is in the cell and being deposited a range of colors can usually be observed and indicates levels of growth.

The SEM images in figure 3.4 show that there is a difference between the growth morphologies of SnSe at the inlet when compared to the outlet for each thin film. Though the -400 mV film visually appears to be more homogeneous than the others, SEM images still show that the outlet of the thin film has significantly less material than at the inlet. The morphology observed in the SEM of the inlets of the thin films shows varied structures. The structures indicate that the thin film is not growing layer by layer as desired in an E-ALD cycle. They also

show that the potential of Sn deposition affects the resulting structures. The outlets all exhibit larger more spread out features, indicative of nucleation of growth.

EDS data was used to create a comparison of ratios of Sn:Se shown in figure 3.5. Most ratios lie around 1-2 which would be expected for a SnSe or $SnSe_2$ thin film. The -300 mV film has the closest ratios to a 1:1 SnSe film however the Raman and XRD data seen in figures 3.6 and 3.7 show that both SnSe and $SnSe_2$ are present in the film. The -350 mV film has the closest ratio to 1:2 indicating $SnSe_2$ but also shows the presence of both SnSe and $SnSe_2$ in the Raman and XRD data.

The second set of experiments was done using a constant Sn deposition potential of -325 mV while varying the Se deposition potential between 0 mV and -200 mV. Figure 3.8 shows optical pictures and SEM images of the inlet and outlet of the resulting thin films. The optical images are all oriented the same way, with the inlet at the bottom and the outlet at the top. Figure 3.9 shows the ration of Sn:Se based on elemental analysis from EDS. Figure 3.10 has the Raman spectra of the inlet and the outlet of the films. Figure 3.11 has XRD diffractograms of the tin selenide thin films.

As seen in figure 3.8, the appearance of the thin films changes drastically with a change in the deposition potential of selenium. The inlets still show heavier deposition as with the samples in the previous set of experiments. SEM images show that the morphology has different shaped clusters of material. There is a heavier density of growth at the outlets in figure 3.8 than shown in the previous experiment, figure 3.4. The EDS ratios are very constant for these thin films as seen in figure 3.9. For most samples, the inlet and outlet ratio is close to 1:1. This is very different from the previous data. This indicates that the deposition of the thin film relies more on

the deposition potential of Sn than the Se deposition potential. The Raman spectroscopy and XRD data in figures 3.10 and 3.11 show that the thin films have both SnSe and $SnSe_2$ present in the films.

The irregularity observed in the morphology and thickness of the films indicated that there was an issue in the method that the tin selenide films were growing. Not only were films inhomogeneous, but there was also the presence of SnSe and $SnSe_2$. This would cause issues in its performance in a device because SnSe and $SnSe_2$ exhibit different band gaps and are different n/p type materials. A known issue with this system was the tin solution. Precipitation occurred within less than 48 hours. The issue with this is that the tin concentration would constantly be changing based on the age of the solution. For this reason, a new precursor and electrolyte were selected for experimentation.

3.4.2 TIN SELENIDE THIN FILMS USING PERCHLORIC ACID ELECTROLYTE

Due to instability with the tin solution, other solutions were investigated. In the following section, perchloric acid was used as the electrolyte in both the Sn and Se solutions. Figure 3.12 shows a window opening of Sn in 0.1 M $HClO_4$ and figure 3.13 shows the window opening of Se 0.1 M $HClO_4$. Both solutions have a pH of 1.6 like previous solutions. The new Sn window opening has similar areas of deposition and oxidation when compared to the sulfuric acid CVs in figure 3.1. The UPD can be seen in the negative scan starting at -200 mV. It is much easier to identify where bulk deposition begins in perchloric acid solutions. Bulk deposition of Sn begins at -350 mV. In the reverse scans, oxidation of the bulk Sn happens between -350 mv and -200 mV. The UPD Sn strips from the substrate between -150 mV and 50 mV. The Se CVs in perchloric acid also shows similarities to the CVs in sulfuric acid seen in figure 3.2. The Se CVs

in perchloric acid seen in figure 3.13 show two surface limited deposition peaks at 400 mV and 200 mV. The reductive stripping of Se can be seen at -300 mV. Oxidation of bulk Se occurs between 700 mV and 850 mV and the oxidation of surface limited Se happens past that between 850 mV and 1100 mV. Peaks observed in the perchloric acid scans are much sharper than those in the sulfuric acid.

Because deposition ranges for Sn and Se remained the same in the new solutions, the previous E-ALD cycle developed was used for making thin films with the perchloric acid based solutions. Figure 3.14 shows the resulting film made using a deposition potential of -300 mV for Sn and -100 mV for Se as well as different characterization results of the film. Vast improvements can be seen when comparing this film and the -300mV Sn/-100 mV Se film deposited from sulfuric acid shown in figure 3.4. This thin film is more homogeneous across the substrate. Though improved, the thin film does not have complete uniformity across the surface and does not have the correct ratio of Sn:Se for SnSe or $SnSe_2$. The Raman and XRD data both confirm the presence of SnSe and $SnSe_2$. There is also a change in the Raman spectra taken from the inlet to the outlet, indicating differences in the film.

One of the changes made that helped improve the uniformity of the tin film was changing the flow rate used in the deposition cycle. Initially, 10 mL/min was selected as the flow rate of solutions. This was changed to 3 mL/min to lessen convection in the cell and promote epitaxial growth. The time for solution flow was increased to reflect the new flow rate and ensure that proper rinsing and solution replacement occurred. Figure 3.15 shows the subsequent thin film and its characterization. This film shows deposition completely across the surface of the exposed substrate and the Raman spectra are very comparable regardless of location on the film. The Raman and XRD data still exhibit the presence of SnSe and $SnSe_2$. Another issue was the ratio of

Sn:Se. The ratios for thin films made using perchloric acid were closer to 1:1 than 1:2 but not sufficiently so. Excess Se was observed in the thin films regardless of the Sn deposition potential used or the Se deposition potential. The concentration of the Sn solution used for E-ALD was increased from 0.2 mM to 2 mM to encourage tin deposition in the films. 0.5 M $HClO_4$ was required to dissolve the increased tin concentration. EDS results showed that the resulting thin films had a ratio closer to 1:1 however Raman spectroscopy and XRD data confirmed that both SnSe and $SnSe_2$ species were present in the film regardless of the improved Sn:Se ratio. The Sn solution was reevaluated as a possible cause for this occurrence since the solution still eventually precipitated, though at a slower rate than Sn in sulfuric acid.

3.4.3 TIN SELENIDE THIN FILMS USING HYDROCHLORIC ACID ELECTROLYTE

The final electrolyte investigated was hydrochloric acid. A solution with 2 mM Sn in 0.1 M HCl was used. This solution was at pH 1.6 as with the previous Sn solution. No change was made to the perchloric acid Se solution. A window opening of the new Sn solution is seen in figure 3.16. The major difference in this solution when compared to the others is the sharp reduction feature for bulk deposition just before -400 mV. The resulting oxidation is also much larger. This can be expected because of the increase in tin concentration. The regions where UPD and bulk deposit and strip from the surface occur at very similar to the other solutions and thus the same E-ALD cycle was used.

Figure 3.17 shows a comparison of the obtained thin films using the same parameters but different electrolytes. It should be noted that the sulfuric acid thin film was made using a 10 mL/ min flow rate whereas the $HClO_4$ and HCl electrolyte thin films both used 3 mL/min. The HCl electrolyte thin film exhibits the least flow patterns and shows high uniformity across the surface

when compared to the other two samples. SEM images and EDS data is shown in figure 3.18. The SEM image of the HCl electrolyte thin film closely resembles the morphology of a clean gold substrate indicating that the thin film grew layer by layer. The EDS data also shows that this thin film has the best 1:1 ratio, indicating the thin film is pure SnSe.

The Raman spectra of each film can be seen in figure 3.19. The HCl thin film has peaks for SnSe only. The sulfuric acid thin film shows the presence of SnSe and $SnSe_2$. It also shows large peaks for amorphous selenium at the center and outlet of the film. Though the $HClO_4$ thin film Raman spectra look the same across the surface, both SnSe and $SnSe_2$ are present. In the XRD data in figure 3.20, the same trends are observed. The HCl electrolyte sample is the only sample that has the presence of SnSe only. The presence of $SnSe_2$ is possibly related to the precipitation of Sn in the other two electrolytes. The presence of multiple Sn ions would allow both species of tin selenide to form. It is possible that the precipitated Sn had a different oxidation state and caused these issues. The results obtained from SnSe thin films deposited from HCl indicate the success of the optimized E-ALD cycle and solution makeups.

3.5 CONCLUSION

An E-ALD cycle for tin selenide deposition was successfully developed. Thin films were deposited using three different electrolytes. Sulfuric acid solutions were used to initially develop the E-ALD cycle. Perchloric acid solutions improved film quality using the same cycle. The thin films were further optimized by slowing the flow rate of solutions. Highest quality films were obtained with a higher concentration Sn solution and HCl electrolyte. Further studies should be done to evaluate the photoelectrochemical response of SnSe thin films. Additional investigations should also be done to see if $SnSe_2$ films can be obtained by changing deposition parameters

REFERENCES

1. Boscher, N. D.; Carmalt, C. J.; Palgrave, R. G.; Parkin, I. P. Atmospheric Pressure Chemical Vapour Deposition of SnSe and $SnSe_2$ Thin Films on Glass. *Thin Solid Films* **2008**, *516* (15), 4750–4757.
2. Pejjai, B.; Reddy, V.R.M.; Gedi, S.; Park, C. Status Review on earth-abundant and environmentally green Sn-X (X = Se, S) nanoparticle synthesis by solution methods for photovoltaic applications. *Int. J. Hydrogen Energy* **2016**, 1-42.
3. Im, H. S.; Lim, Y. R.; Cho, Y. J.; Park, J.; Cha, E. H.; Kang, H. S. Germanium and Tin Selenide Nanocrystals for High-Capacity Lithium Ion Batteries: Comparative Phase Conversion of Germanium and Tin. *The Journal of Physical Chemistry C* **2014**, *118*(38), 21884–21888.
4. Sharma, P.; Rangra, V. S.; Sharma, P.; Katyal, S. C. Effect of Antimony Addition on the Optical Behaviour of Germanium Selenide Thin Films. *Journal of Physics D: Applied Physics***2008**, *41*(22), 225307.
5. Pugh, J.R.; Mao, D.; Zhang, J; Heben, M.J.; Nelson, A.J.; Frank, A.J. A metal:p-n-CdTe Schottky-barrier solar cell: Photoelectrochemical generation of a shallow p-type region in n-CdTe. *J. Appl. Phys.* **1993**, *74,* 2619-2625.
6. Qiao, Z.; Shang, W.; Wang, C. Fabrication of Sn-Se compounds on a gold electrode by electrochemical atomic layer epitaxy. *J. Electroanal. Chem.* **2005**, *576,* 171-175.

7. Gregory, B. W.; Stickney, J. L. Electrochemical Atomic Layer Epitaxy (ECALE). *Journal of Electroanalytical Chemistry* **1991**, 300, 543561.
8. Villegas, I.; Stickney, J. L. Preliminary Studies of GaAs Deposition on Au(100), (110), and (111) Surfaces by Electrochemical Atomic Layer Epitaxy. *Journal of the Electrochemical Society* **1992**, 139, 686694.
9. Colletti, L. P.; Teklay, D.; Stickney, J. L. Thin-Layer Electrochemical Studies of the Oxidative Underpotential Deposition of Sulfur and Its Application to the Electrochemical Atomic Layer Epitaxy Deposition of CdS. *Journal of Electroanalytical Chemistry* **1994**, 369, 145152.
10. Colletti, L. P.; Stickney, J. L. Optimization of the growth of CdTe thin films formed by electrochemical atomic layer epitaxy in an automated deposition system. *Journal of the Electrochemical Society* **1998**, 145, 35943602.
11. Venkatasamy, V.; Jayaraju, N.; Cox, S. M.; Thambidurai, C.; Mathe, M.; Stickney, J. L. Deposition of HgTe by electrochemical atomic layer epitaxy (EC-ALE). *Journal of Electroanalytical Chemistry* **2006**, 589, 195202.
12. Venkatasamy, V.; Jayaraju, N.; Cox, S. M.; Thambidurai, C.; Stickney, J. L. Studies of Hg((1-x))Cd(x)Te formation by electrochemical atomic layer deposition and investigations into bandgap engineering. *Journal of the Electrochemical Society* **2007**, 154, H720H725.
13. Kim, J. Y.; Stickney, J. L. Ultrahigh vacuum surface studies of the electrochemical atomic layer deposition of indium telluride on n-type GaAs(100). *Journal of Physical Chemistry C* **2008**, 112, 59665971.

14. Gebregziabiher, D. K.; Kim, Y. G.; Thambidurai, C.; Ivanova, V.; Haumesser, P. H.; Stickney, J. L. Electrochemical atomic layer deposition of copper nanofilms on ruthenium. *Journal of Crystal Growth* **2010**, *312*, 12711276.

15. Lister, T. E. Electrochemical Formation of Se Atomic Layers on Au(100). *Journal of Vacuum Science & Technology B: Microelectronics and Nanometer Structures* **1995**, *13* (3), 1268.

16. Lister, T. E.; Stickney, J. L. Atomic Level Studies of Selenium Electrodeposition on Gold(111) and Gold(110). *The Journal of Physical Chemistry* **1996**, *100* (50), 19568–19576.

17. Sorenson, T. A. A Comparison of Atomic Layers Formed by Electrodeposition of Selenium and Tellurium Scanning Tunneling Microscopy Studies on Au(100) and Au(111). *Journal of The Electrochemical Society* **1999**, *146* (3), 1019.

18. Huang, B. M.; Lister, T. E.; Stickney, J. L. Se Adlattices Formed on Au(100), Studies by LEED, AES, STM and Electrochemistry. *Surface Science* **1997**, *392* (1-3), 27–43.

19. Ravindiran, M.; Praveenkumar, C. Status Review and the Future Prospects of CZTS Based Solar Cell – A Novel Approach on the Device Structure and Material Modeling for CZTS Based Photovoltaic Device. *Renewable and Sustainable Energy Reviews* **2018**, *94*, 317–329.

CHAPTER 3 FIGURES

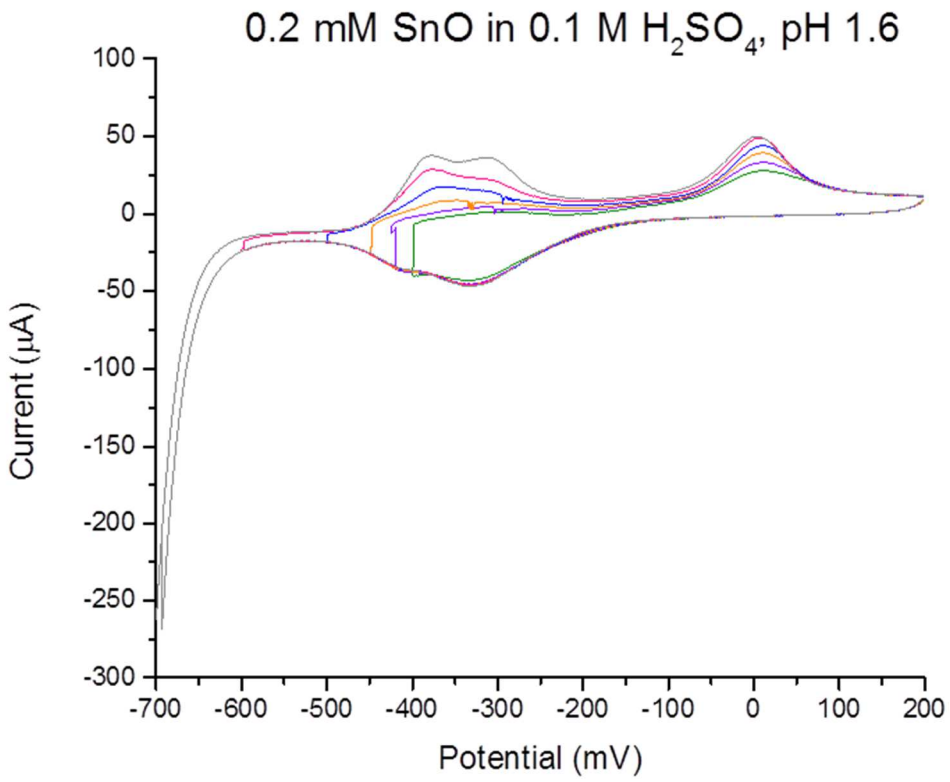

Figure 3.1 Window opening of cyclic voltammetry scans in a 0.2 mM Sn solution at pH 1.6 in 0.1 M H_2SO_4. Scans were held for 30 seconds at the negative turning potentials

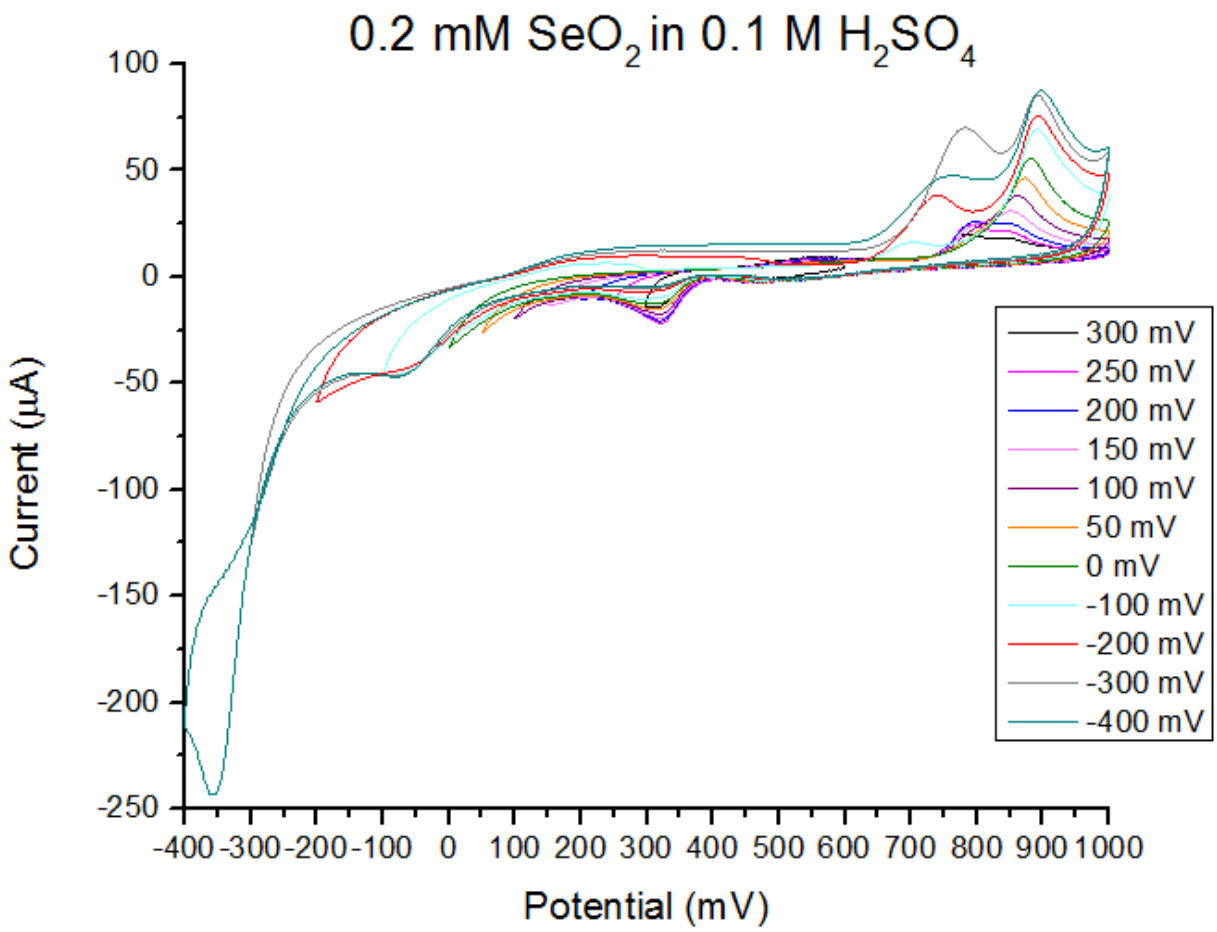

Figure 3.2 Window opening of CVs of a 0.2 mM Se solution at pH 1.6 in 0.1 M H_2SO_4.

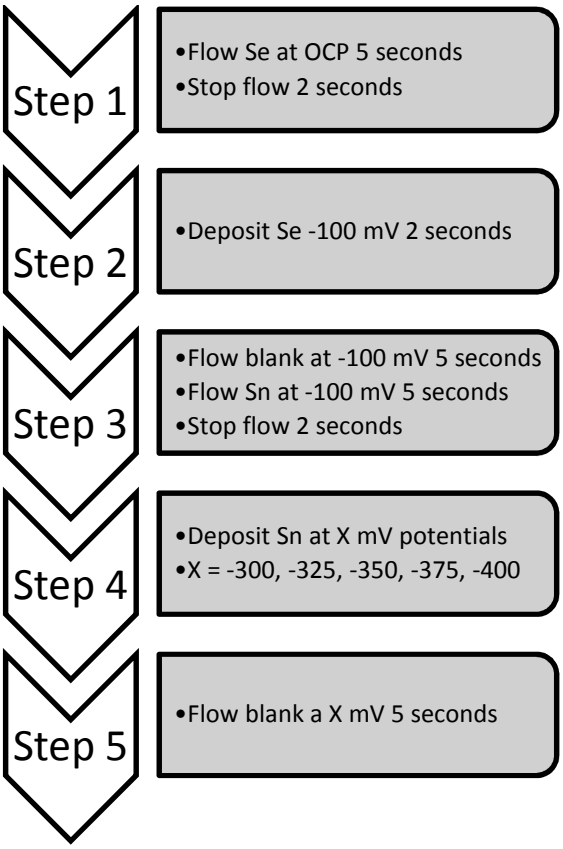

Figure 3.3 Example of E-ALD cycle used to deposit SnSe thin films. The flow rate used was 10 mL/min. Step length would be lengthened for 3 mL/min flow rate samples.

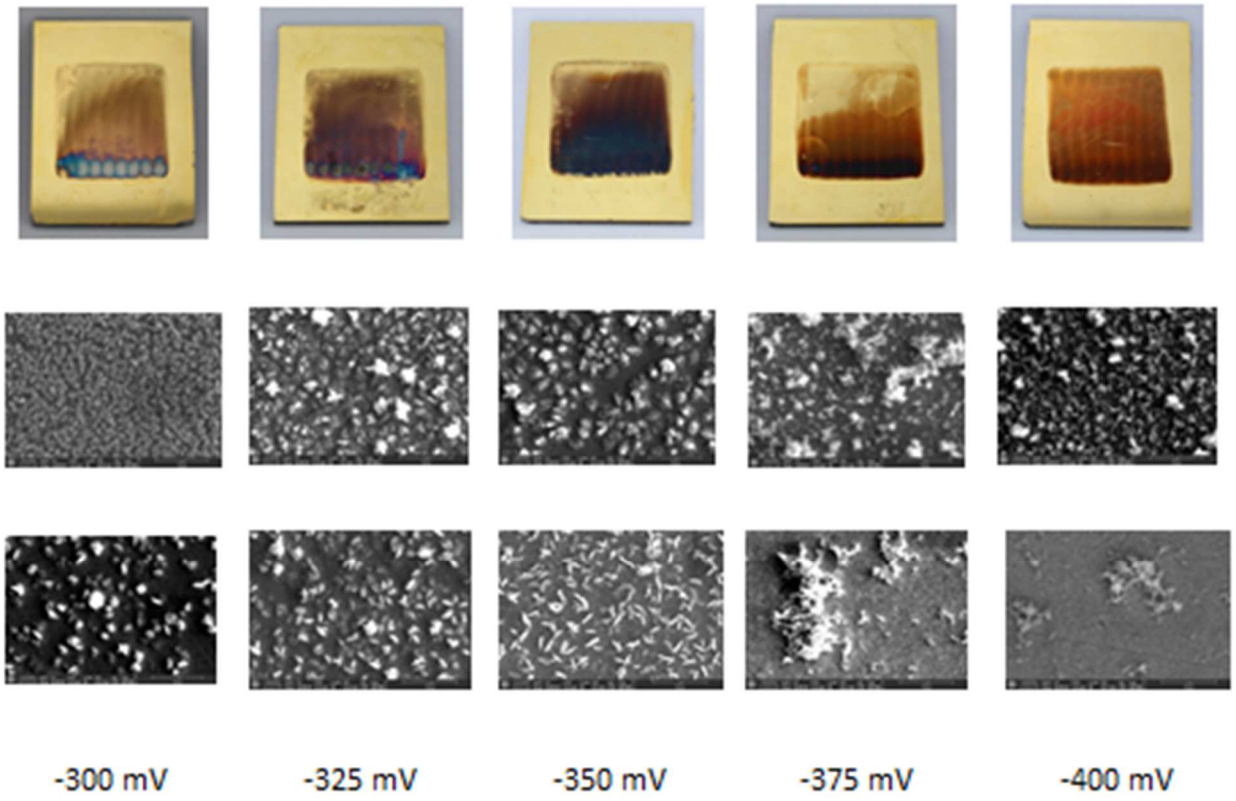

Figure 3.4 Pictures of tin selenide thin films with constant Se deposition of -100 mV and varied Sn deposition potential as listed. Optical images of thin films are all aligned so that the inlet of the flow cell is shown at the bottom and the outlet is at the top (top row). SEM images are 100,000x magnification with the inlet (middle row) and outlet (bottom row) pictured.

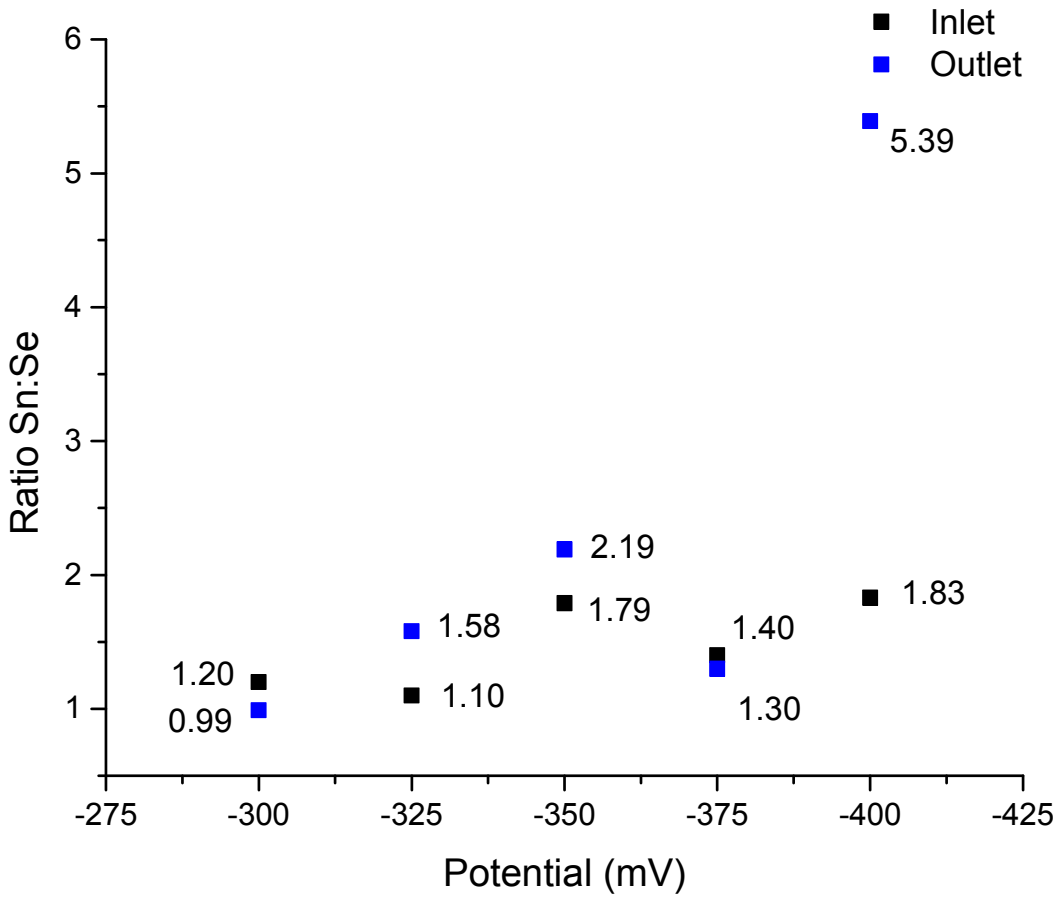

Figure 3.5 Ratio of Sn:Se listed as 1:X. Ratios listed for the inlet and the outlet of thin films deposited with a constant Se deposition potential of -100 mV and varying Sn deposition potentials as listed. Elemental data from EDS.

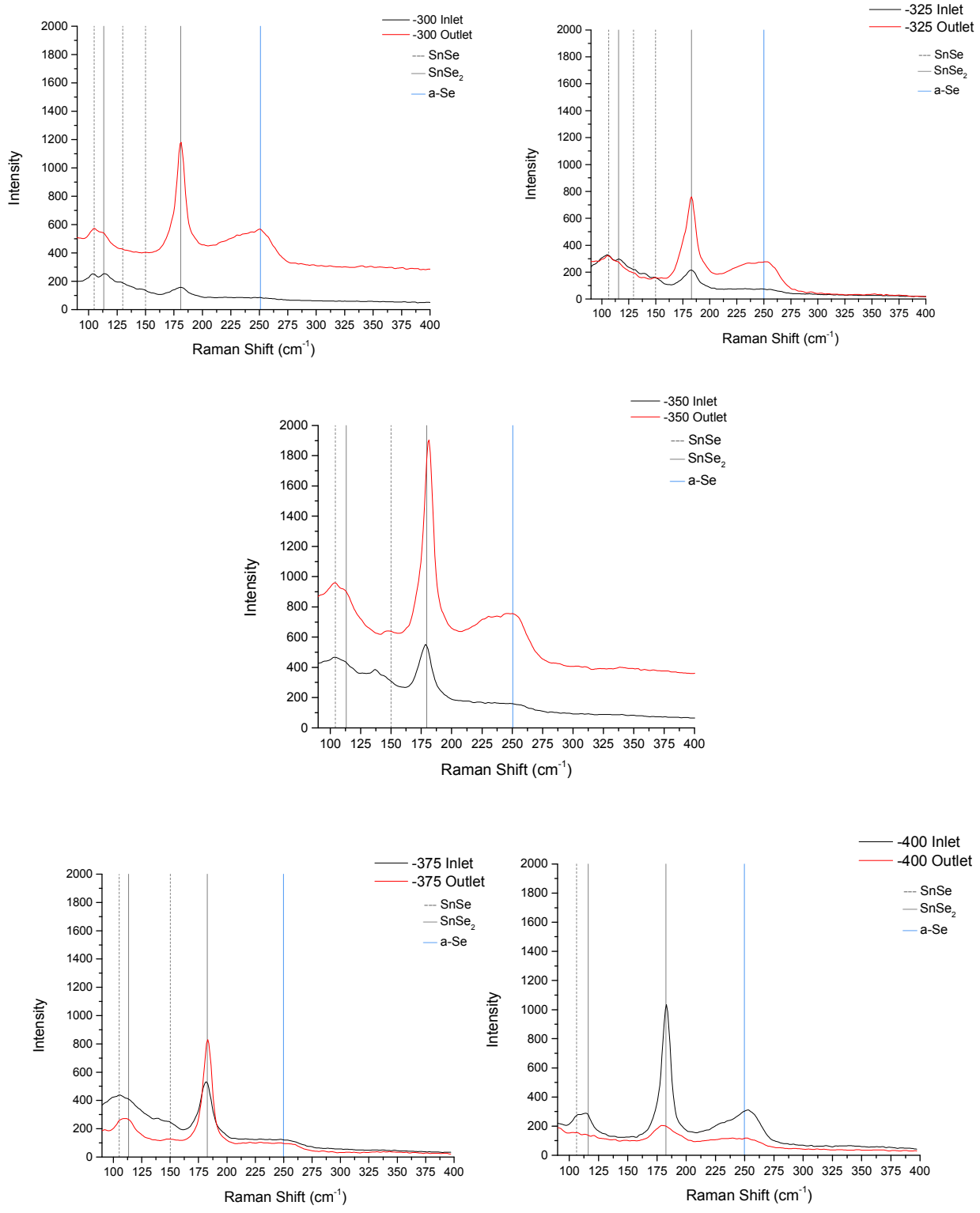

Figure 3.6 Raman spectra of tin selenide thin films deposited with a constant Se deposition potential of -100 mV and varying Sn deposition potentials as listed. A 532 nm laser was used to obtain data. Spectra taken at the inlet and outlet of the tin films and relevant peaks listed for identification.

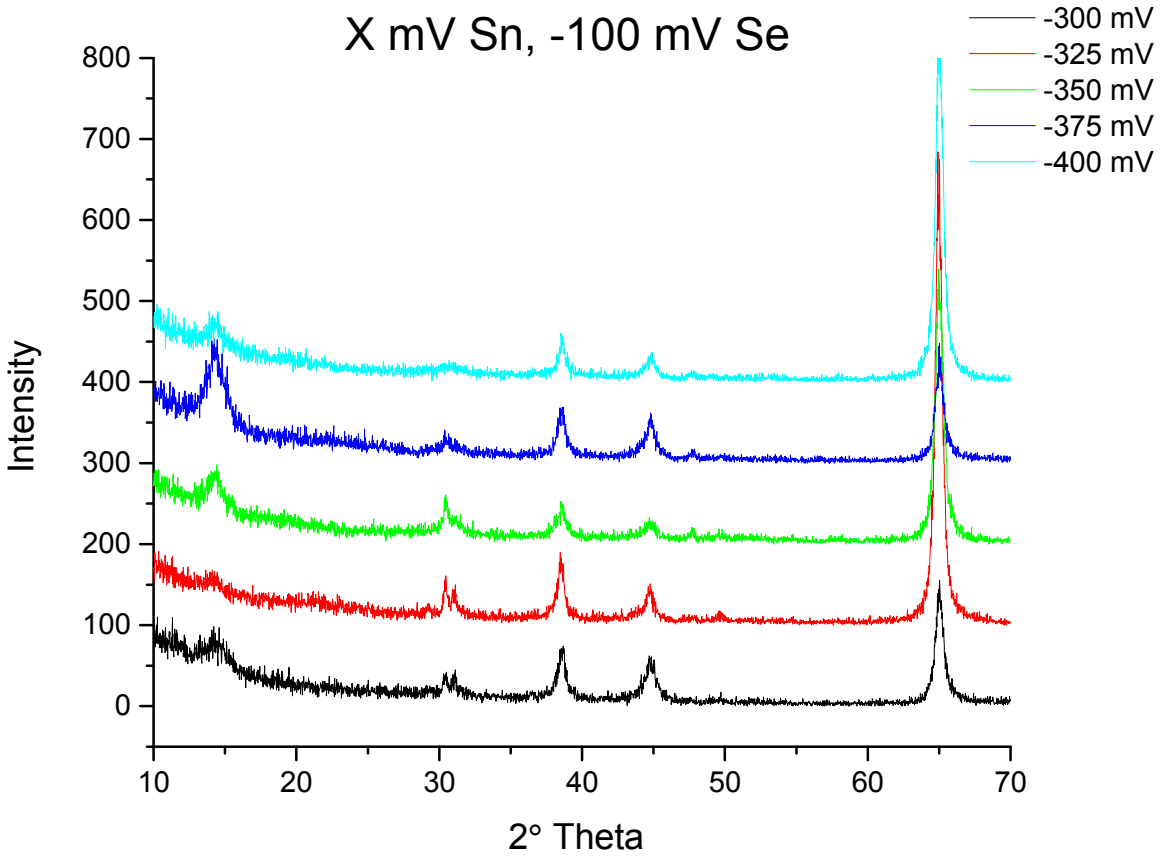

Figure 3.7 X-ray diffractograms of tin selenide thin films deposited with a constant Se deposition potential of -100 mV and varying Sn deposition potentials as listed. Glancing angle XRD was used with a Cu radiation source to obtain data. Relevant peaks listed for identification.

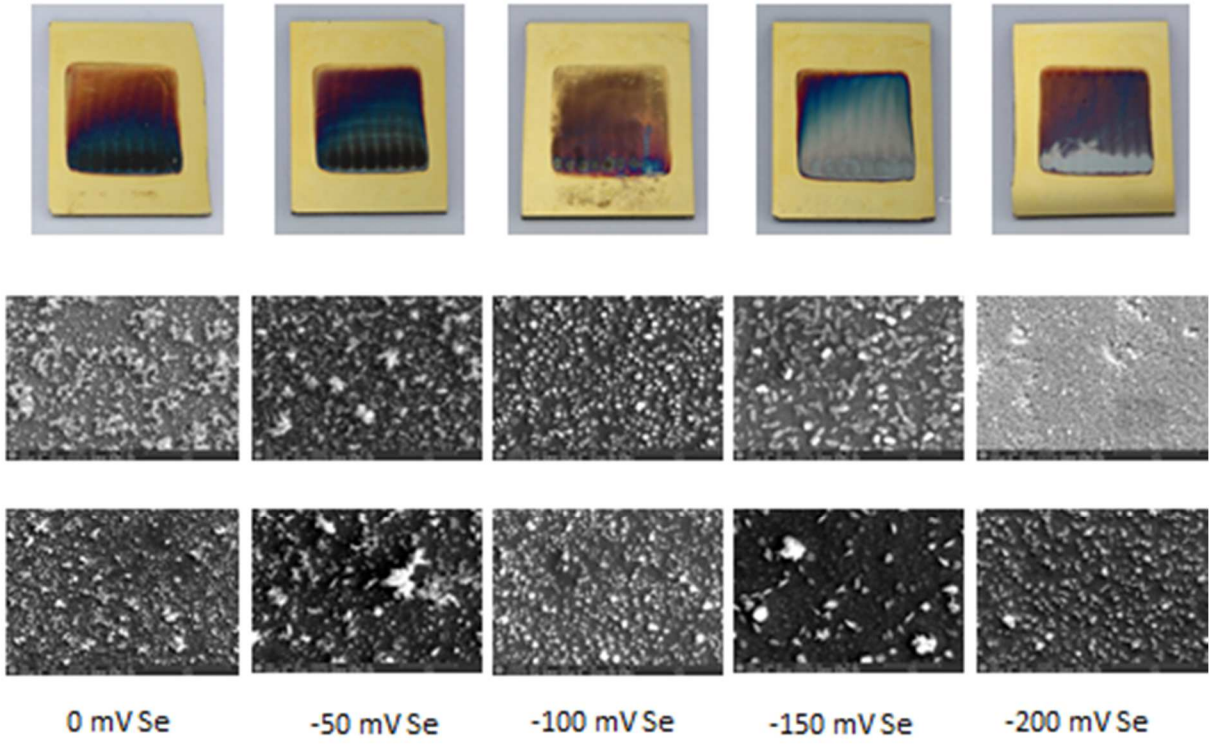

Figure 3.8 Pictures of tin selenide thin films with constant Sn deposition of -325 mV and varied Se deposition potential as listed. Optical images of thin films are all aligned so that the inlet of the flow cell is shown at the bottom and the outlet is at the top (top row). SEM images are 50,000x magnification with the inlet (middle row) and outlet (bottom row) pictured.

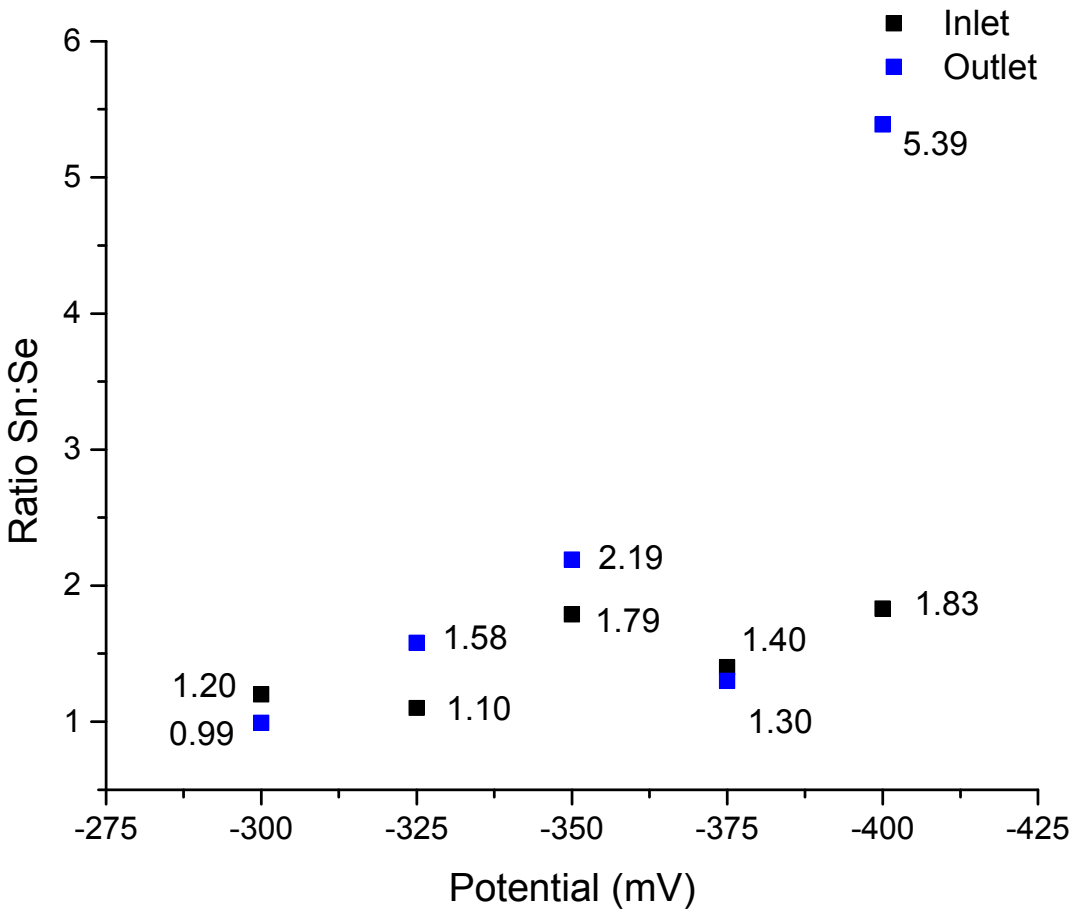

Figure 3.9 Ratio of Sn:Se listed as 1:X. Ratios listed for the inlet and the outlet of thin films deposited with a constant Sn deposition potential of -325 mV and varying Sn deposition potentials as listed. Elemental data from EDS.

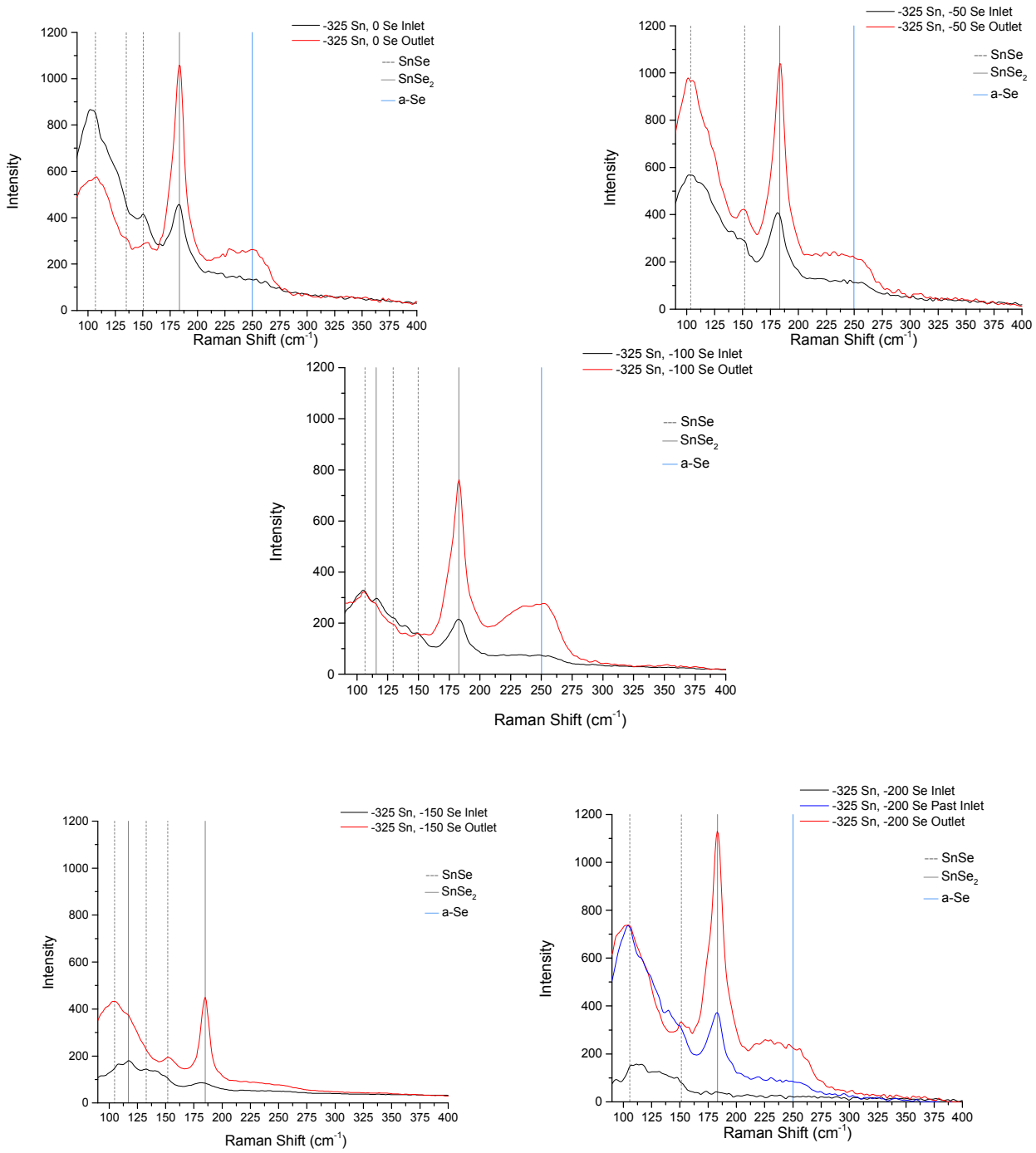

Figure 3.10 Raman spectra of tin selenide thin films deposited with a constant Sn deposition potential of -325 mV and varying Se deposition potentials as listed. A 532 nm laser was used to obtain data. Spectra taken at the inlet and outlet of the tin films and relevant peaks listed for identification.

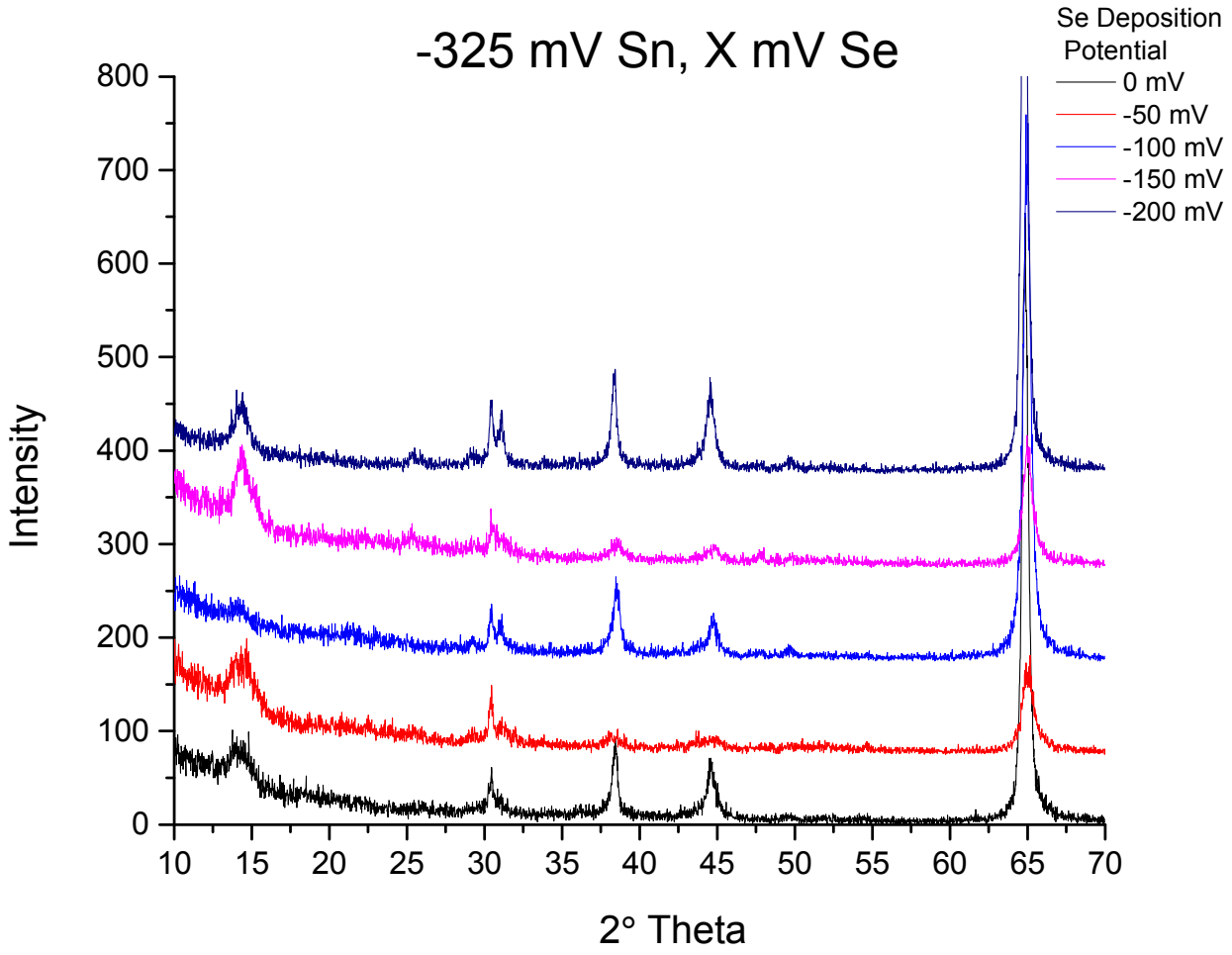

Figure 3.11 X-ray diffractograms of tin selenide thin films deposited with a constant Sn deposition potential of -325 mV and varying Se deposition potentials as listed. Glancing angle XRD was used with a Cu radiation source to obtain data. Relevant peaks listed for identification.

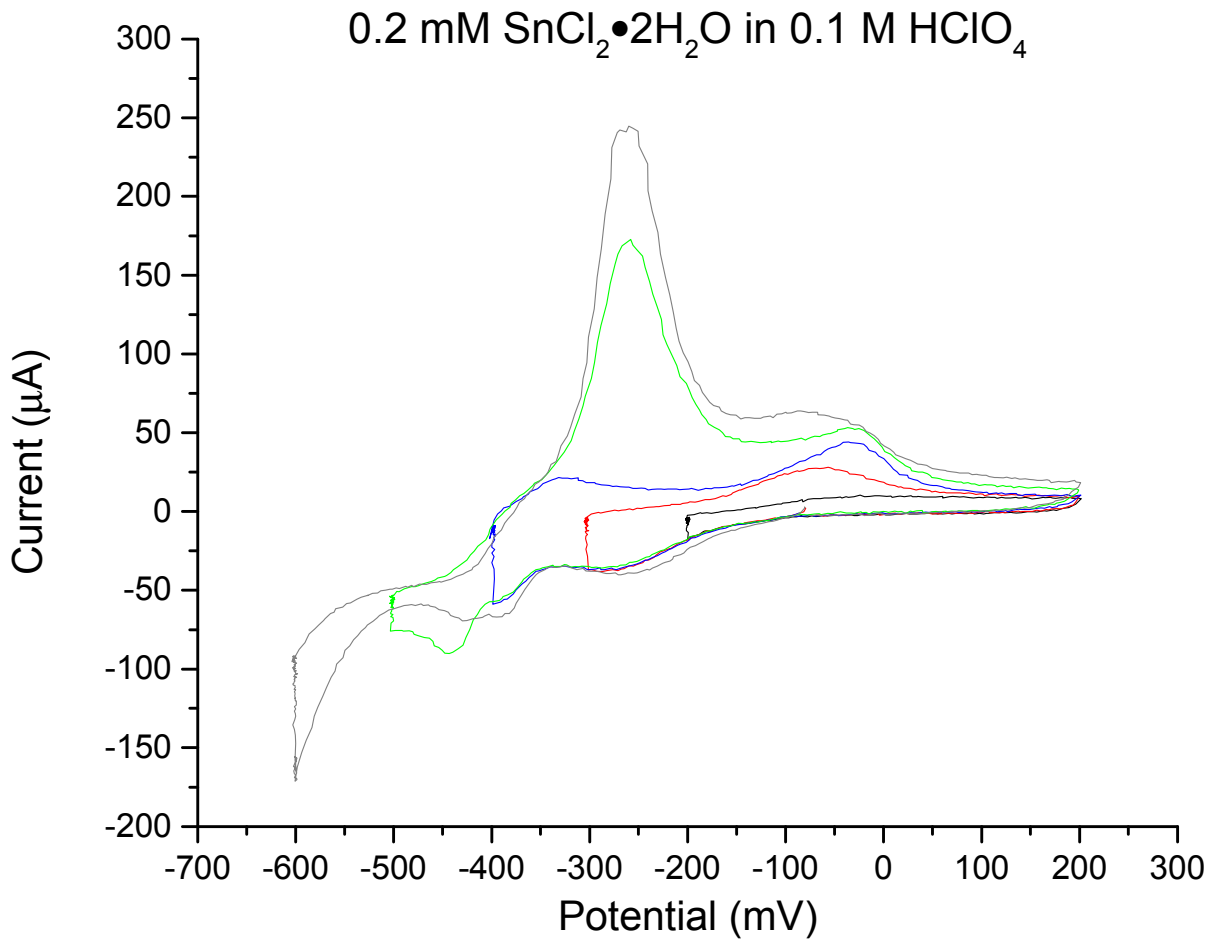

Figure 3.12 Window opening of cyclic voltammetry scans in a 0.2 mM Sn solution at pH 1.6 in 0.1 M $HClO_4$. Scans were held for 30 seconds at the negative turning potentials

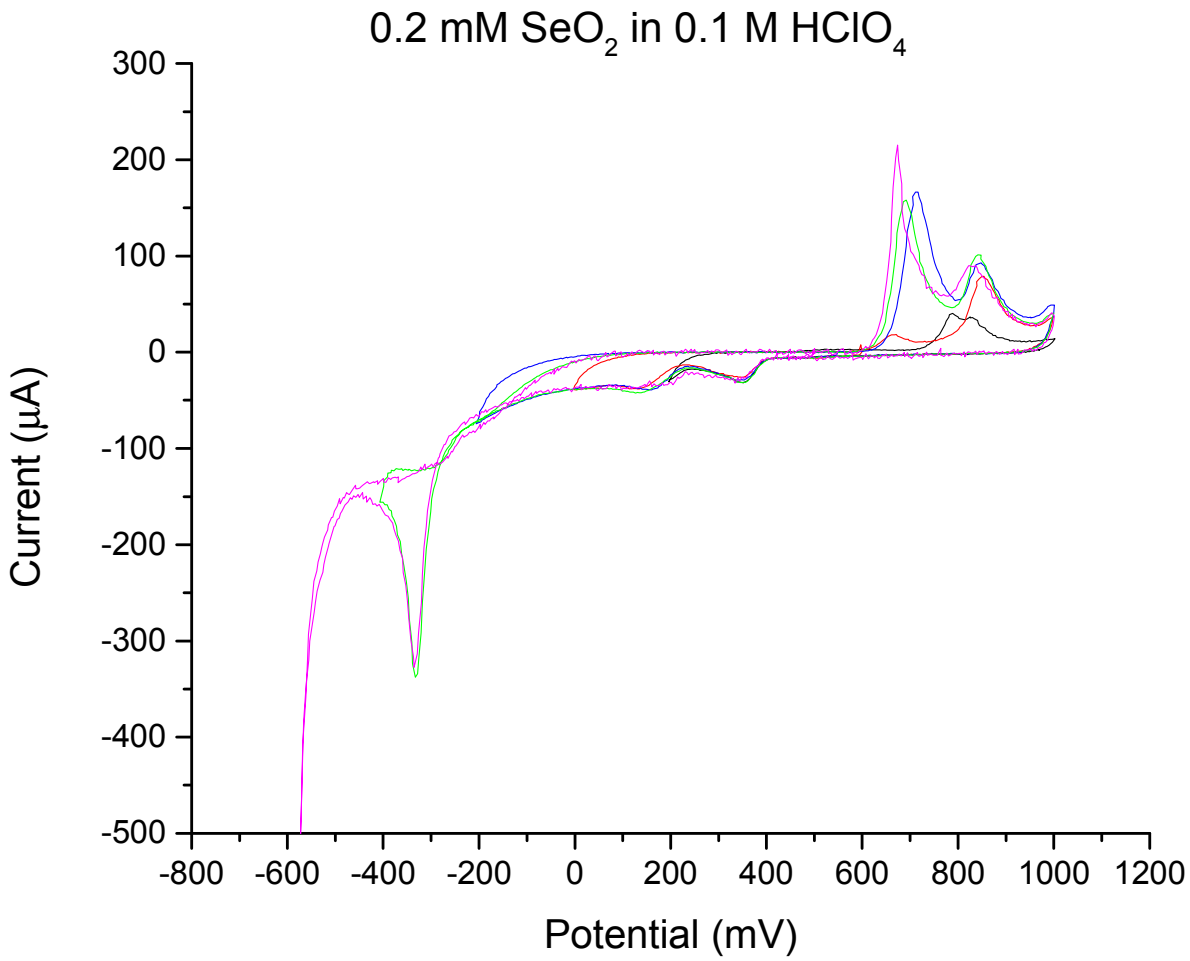

Figure 3.13 Window opening of CVs of a 0.2 mM Se solution at pH 1.6 in 0.1 M $HClO_4$.

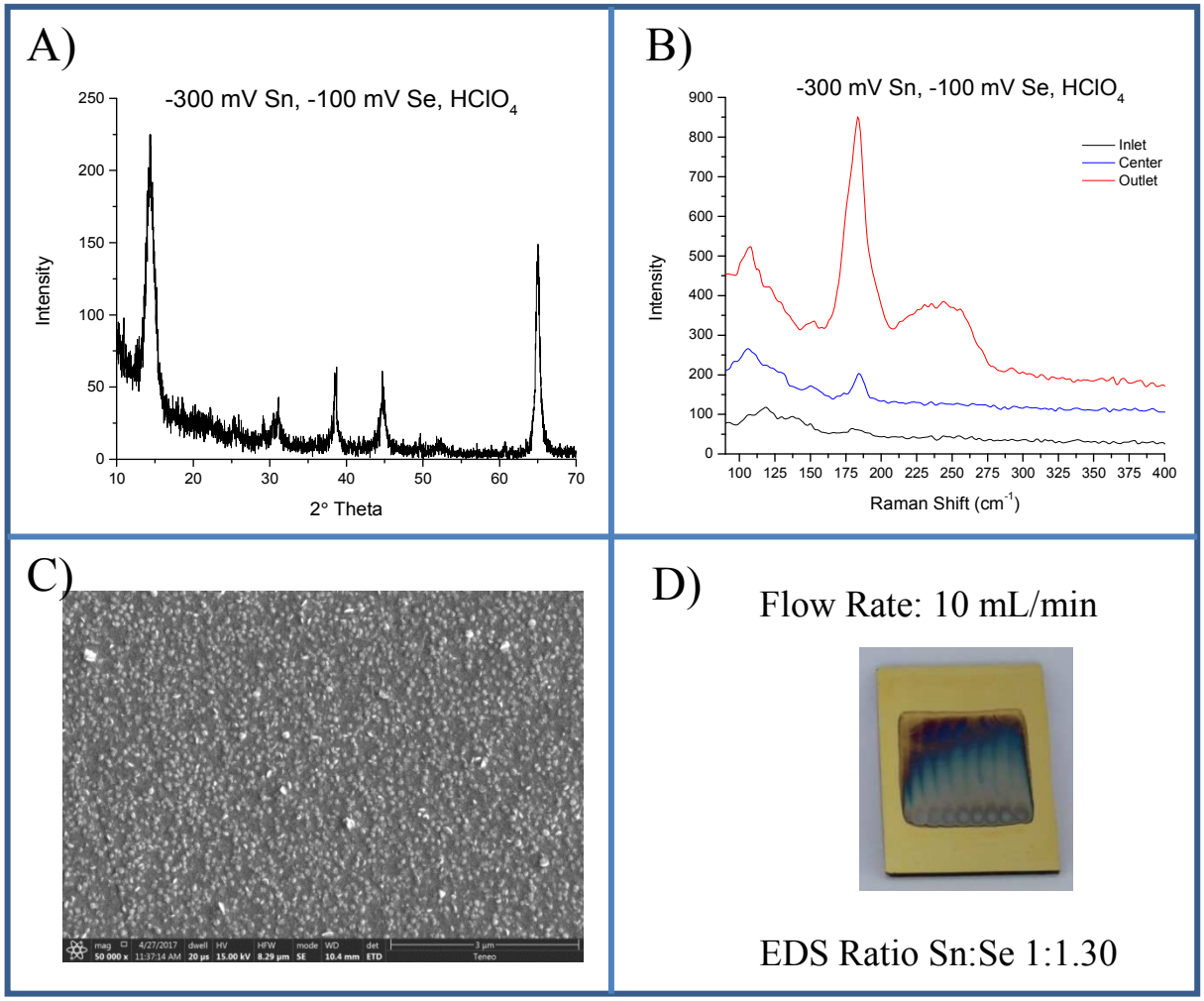

Figure 3.14 Characterization of a tin selenide thin film made using a 10 mL/minute flow rate. Sn deposition parameters were -300 mV and Se -100 mV. A) is the XRD data of the thin film. B) shows the Raman spectrum of the thin film using a 532 nm laser. C) is an SEM image of the thin film from the center of the deposit at 50,000 magnification. D) is an optical image of the thin film with the EDS ratio of Sn:Se.

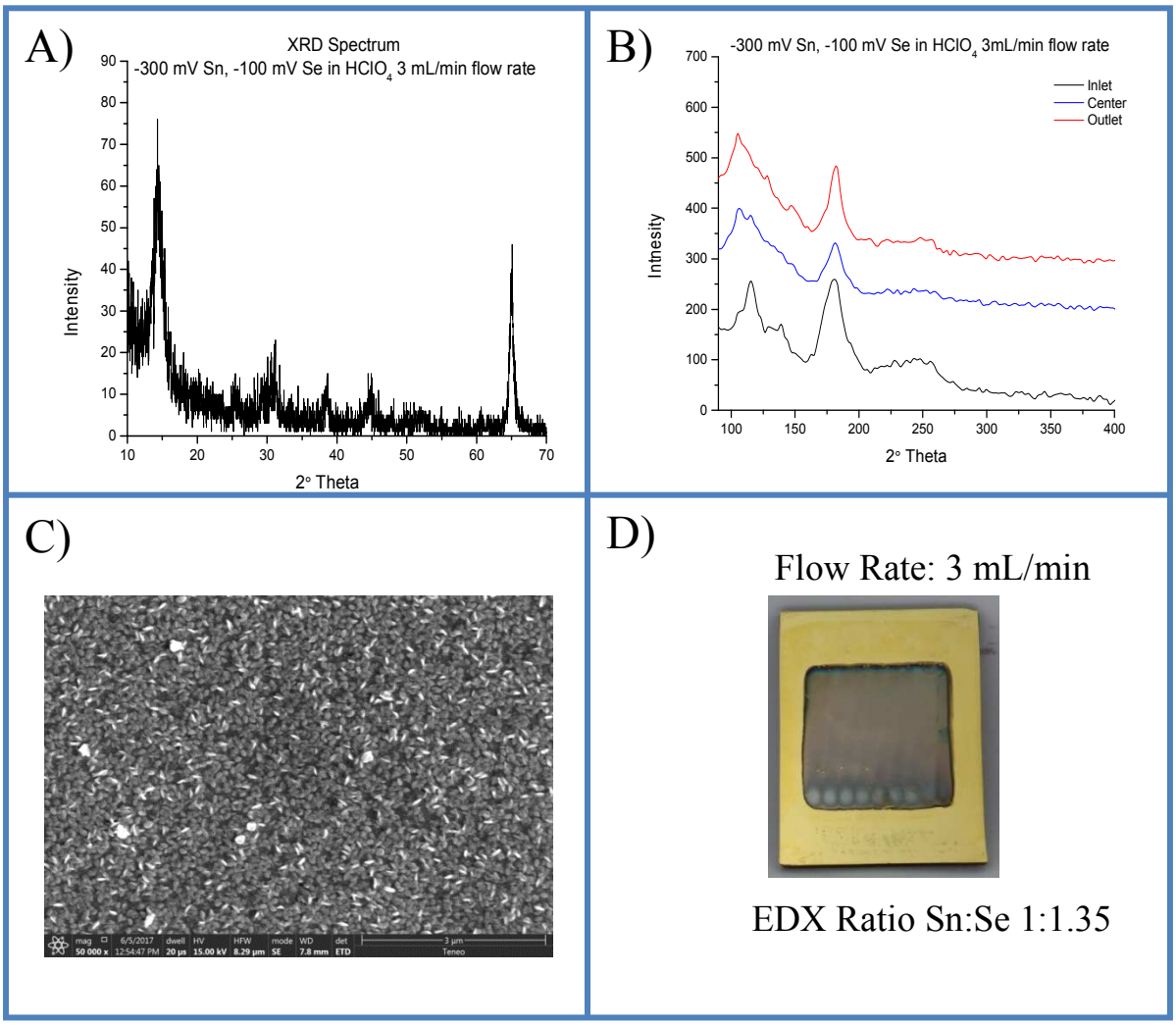

Figure 3.15 Characterization of a tin selenide thin film made using a 3 mL/minute flow rate. Sn deposition parameters were -300 mV and Se -100 mV. A) is the XRD data of the thin film. B) shows the Raman spectrum of the thin film using a 532 nm laser. C) is an SEM image of the thin film from the center of the deposit at 50,000 magnification. D) is an optical image of the thin film with the EDS ratio of Sn:Se.

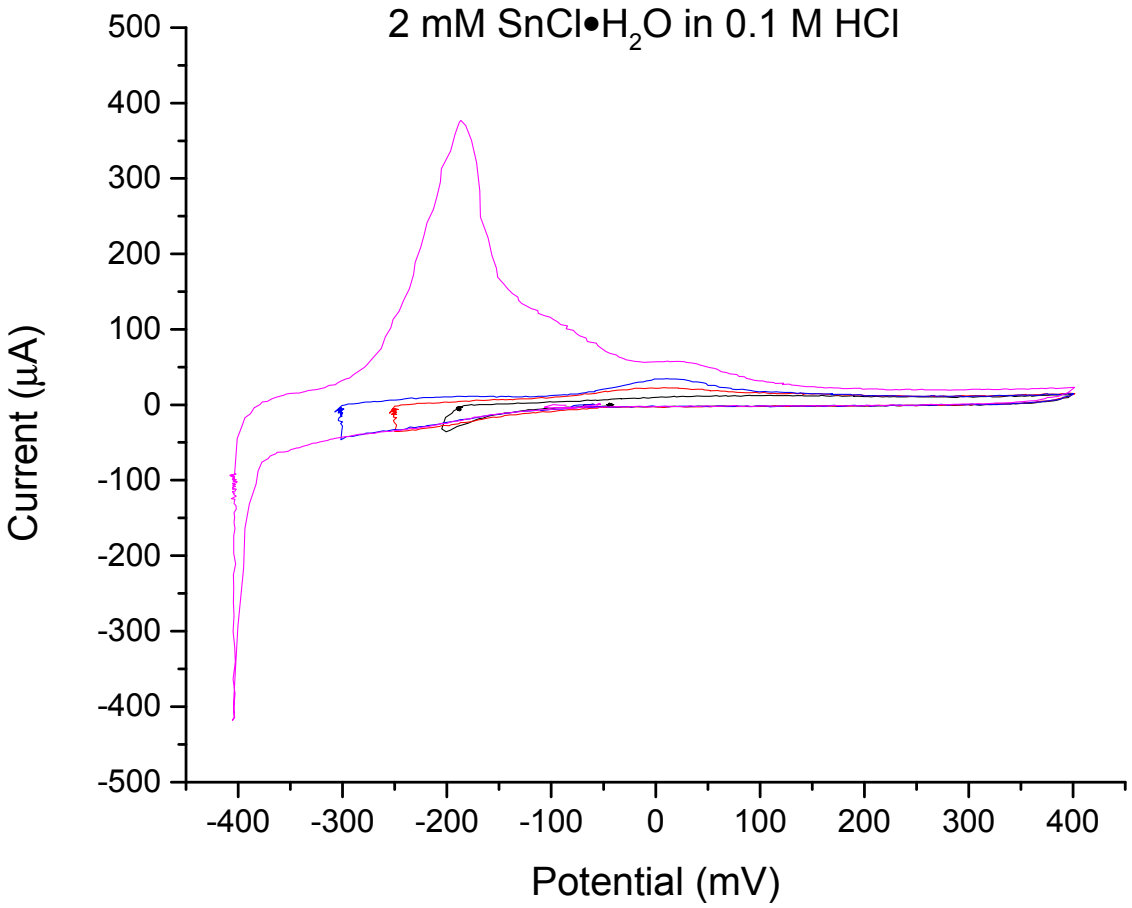

Figure 3.16 Window opening of cyclic voltammetry scans in a 2 mM Sn solution at pH 1.6 in 0.1 M HCl. Scans were held for 30 seconds at the negative turning potentials

0.2 mM SnO_2, 0.1 M H_2SO_4 0.2 mM SeO_2, 0.1 M H_2SO_4	0.2 mM $SnCl_2 \cdot 2H_2O$, 0.1 M $HClO_4$ 0.2 mM SeO_2, 0.1 M $HClO_4$	2 mM $SnCl_2 \cdot 2H_2O$, 0.1 M HCl 0.2 mM SeO_2, 0.1 M $HClO_4$

All solutions pH 1.6

Figure 3.17 Optical images of tin selenide thin films deposited using different electrolyte based solutions. The composition is as listed. The alignment of the thin films is all the same with the inlet at the bottom and outlet at the top.

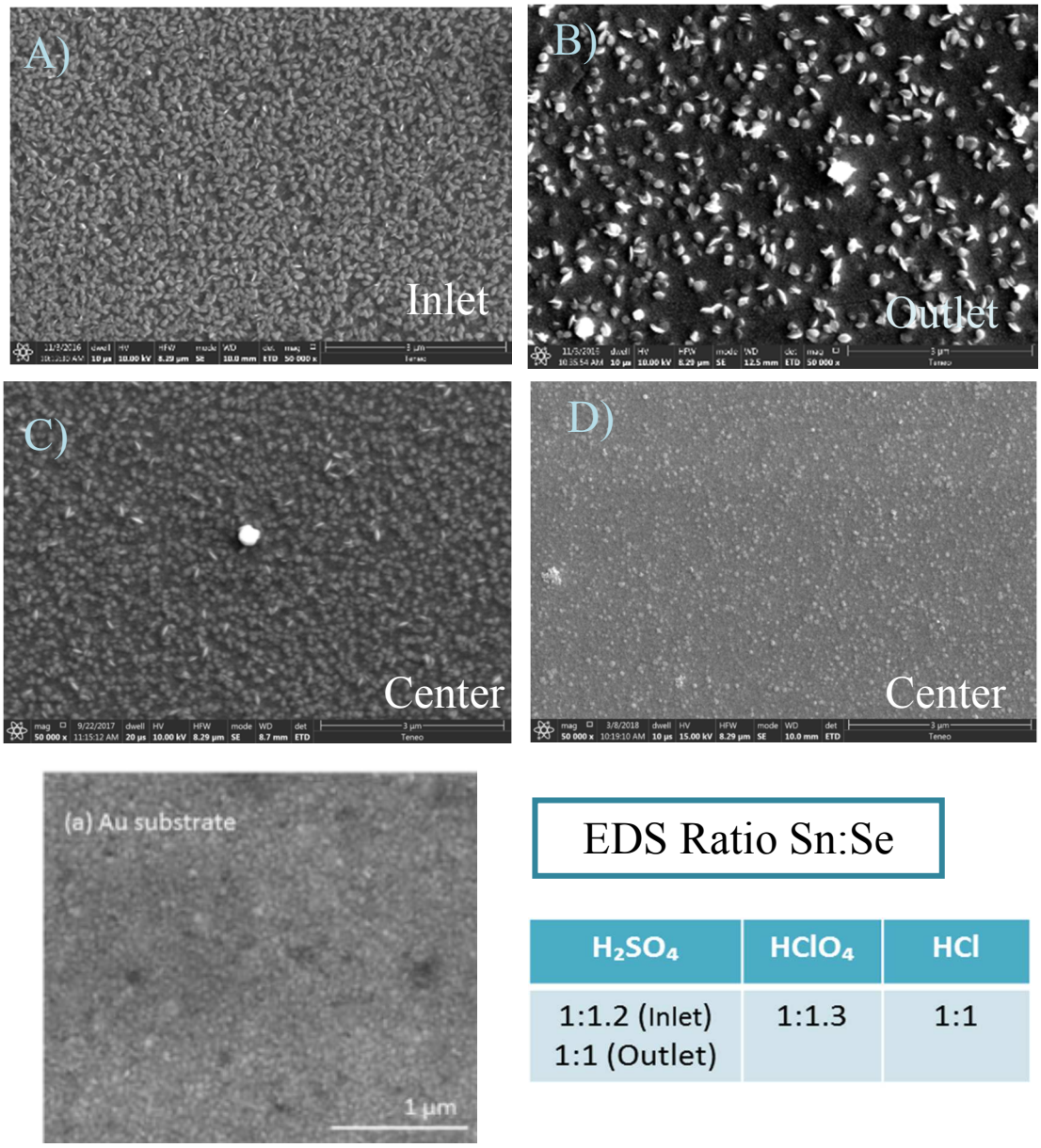

EDS Ratio Sn:Se

H_2SO_4	$HClO_4$	HCl
1:1.2 (Inlet) 1:1 (Outlet)	1:1.3	1:1

56

Figure 3.18 SEM images and EDS ratio of tin selenide thin films deposited using different electrolyte based solutions. The composition is as listed. A) corresponds to the sulfuric acid thin film inlet, B) corresponds to the sulfuric acid thin film outlet, C) the perchloric acid thin film center, and D) the HCl thin film center. All images are shown at 50,000 magnification. Below in a) is an example of the polycrystalline Au substrate.

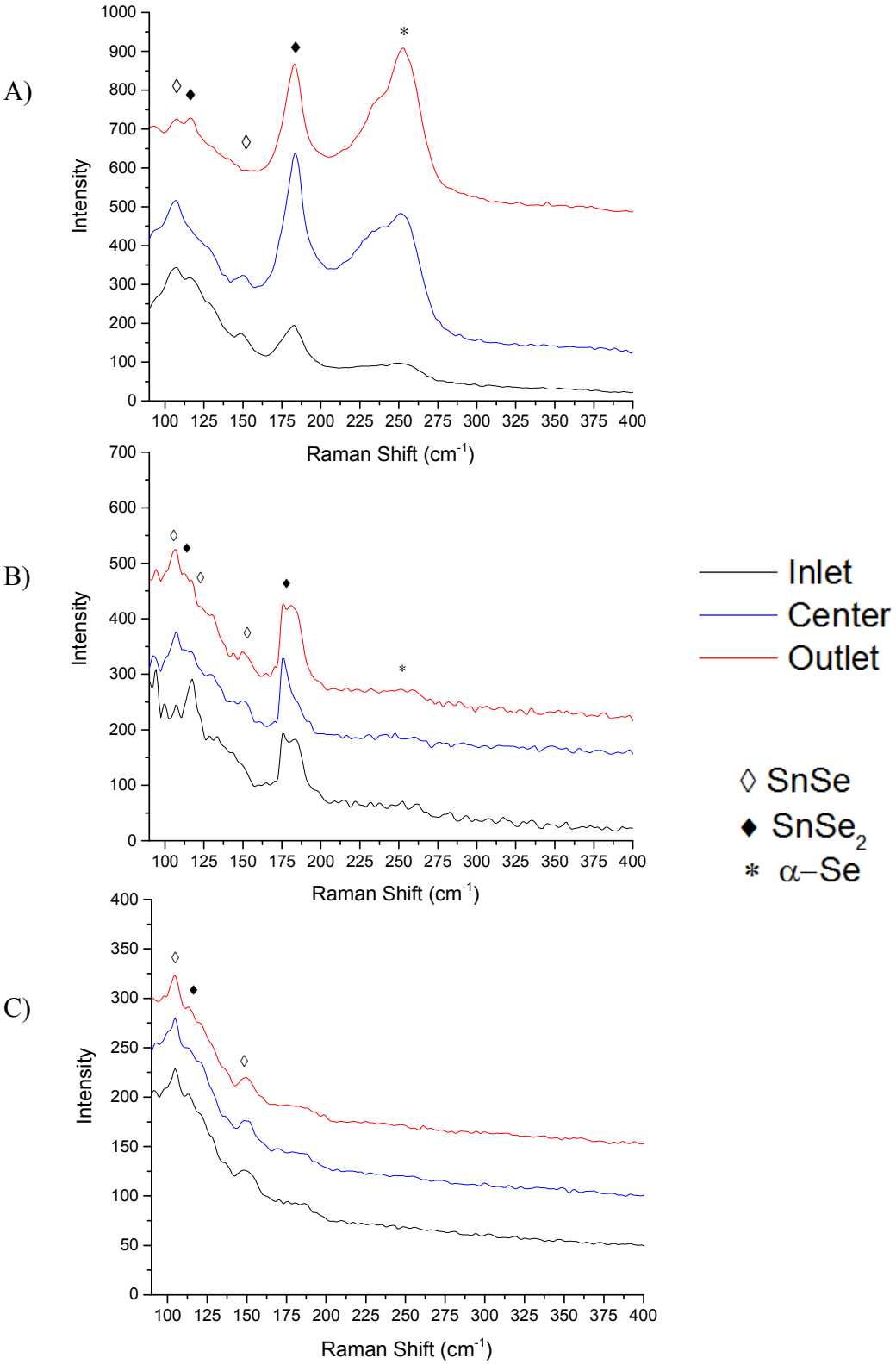

Figure 3.19 Raman spectra of tin selenide thin films made from different electrolyte based solutions. 532 nm laser was used for the acquisition of the spectra. A) corresponds to the sulfuric acid thin film, B) the perchloric acid thin film, and C) the HCl thin film.

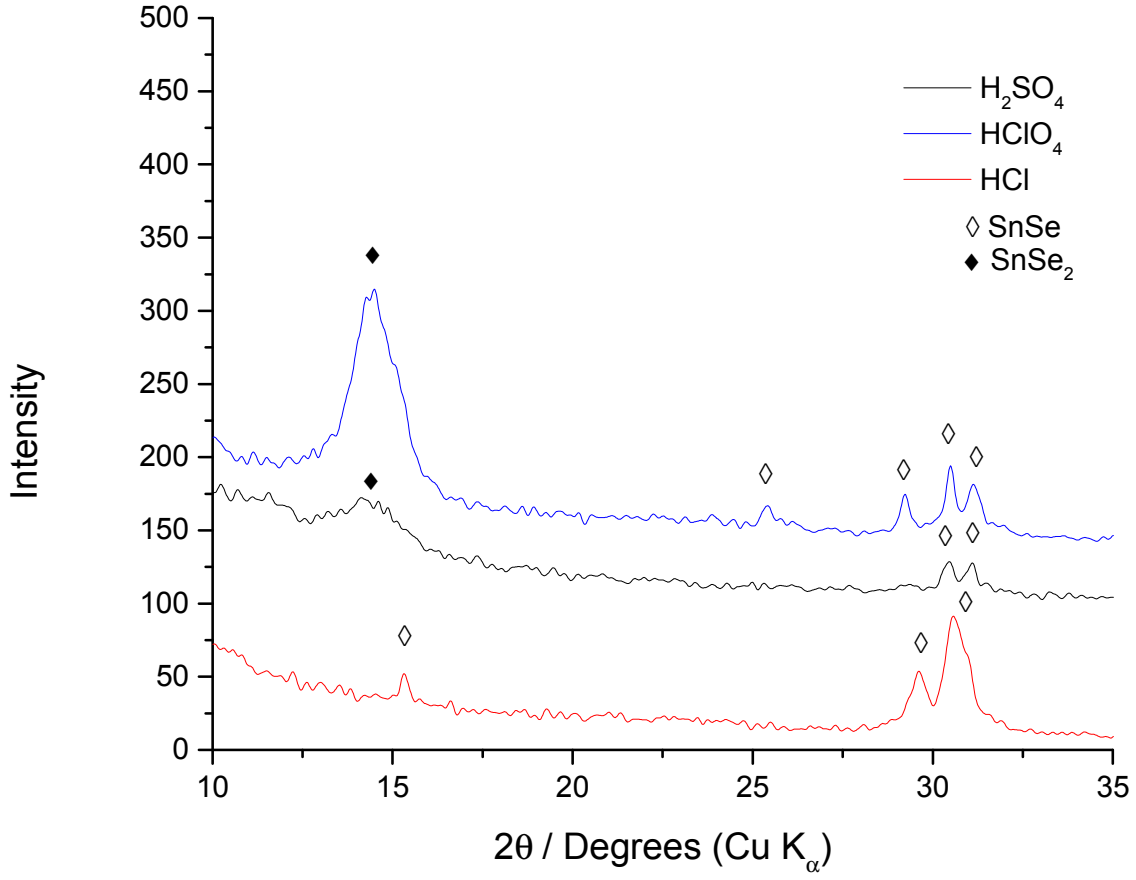

Figure 3.20 X-ray diffractograms of tin selenide thin films deposited from different electrolyte based solutions. Relevant peaks have been labeled. Glancing angle XRD with a Cu radiation source was used.

CHAPTER 4

ANTIMONY SELENIDE[3]

[3] Howell, P.; Sisk, P.; Stickney, J. To be submitted to the ECS Journal

4.1 ABSTRACT

The electrochemistry of Sb and Se were studied to develop an E-ALD cycle for Sb_2Se_3. First, multiple Sb solutions were made using different electrolytes. Antimony solutions were made using sulfuric acid, perchloric acid, and hydrochloric acid. Cyclic voltammetry was used to discern the best choice of electrolyte. Perchloric acid was selected as the electrolyte for both Sb and Se. pH 1.6 and pH 3 solutions were compared to determine the best scenario for eventually developing an E-ALD cycle. Selenium can reductively strip so it is ideal that Sb would be deposited at a potential where the Se is stable. When designing an E-ALD cycle, each parameter needs to be carefully chosen. Some of the parameters that need to be examined are the deposition time and potential for each element, the potential for rinsing with a blank solution, and the potential for flowing in the precursor solutions. Sb stability was analyzed by depositing Sb on the Au substrate and then flowing in a blank solution at different potentials to determine the maximum potential that could be used without oxidizing Sb. Deposition time studies were done with the Sb and Se solutions to determine the necessary time needed for deposition during the E-ALD cycle. An E-ALD cycle was created that successfully deposited Sb and Se for 2 cycles. Further studies are needed to determine whether the as developed cycle works to deposit a thin film.

4.2 INTRODUCTION

Interest in Sb_2Se_3 has grown in recent years as a viable material for photovoltaics.[1-7] It is a p-type material with an indirect band gap between 1.0-1.2 eV making it suitable as an absorber layer in solar cells.[1] It is also a good replacement for CIGS absorber layers because it makes use of low cost and low toxicity materials.[2] As described in chapter 2, CZTS is one option for CIGS replacement. An issue with CZTS is the complexity in controlling the composition and phases of the material. Sb_2Se_3 is a possible replacement that eliminates the complexity in synthesis because it is a binary material that exhibits one singular crystal structure.[2,3] Sb_2Se_3 has been synthesized using several methods including chemical bath deposition, spray pyrolysis, and pulsed layer deposition.[10-12] Though many techniques have been used, electrodeposition is one of the most popular choices for making Sb_2Se_3 thin films.[4,5,8,9] These electrodeposition methods typically involve using a bath that has Se and Sb in the solution. In addition to the precursor elements electrolytes, additives, and buffers may also be added to the deposition bath. A single deposition potential is applied to deposit the thin film. The issue with this method of thin film growth is the lack of control over the deposition of Sb_2Se_3 and the possibility of impurities in the thin film from the additives. E-ALD is a viable option to improve the growth of the thin film via electrodeposition. At present, no reports have been published using E-ALD to form Sb_2Se_3 thin films.

E-ALD is an electrodeposition method pioneered by the Stickney group 30 years ago that utilizes multiple individualized solutions to deposit thin films layer by layer. Control over this deposition method is possible due to the mechanical setup that is used. A computer program controls the flow of solutions through a valve block and into a flow cell. This ensures that cross-contamination does not occur between the solutions without physically switching the substrate

between deposition baths. By depositing one element at a time, the deposition potential can be selected for each element's needs. The growth can be limited to a monolayer (ML) or less per cycle by using surface limited deposition like underpotential deposition (UPD). UPD only allows the deposition of the element on the substrate, not on itself, thus limiting the deposition to a maximum of 1 ML.

The electrochemistry of selenium has been well documented by the Stickney group.[21-24] Based on their research and the research described in chapters 2 and 3, it is known that selenium exhibits regions of surface limited deposition, bulk deposition, and reductive stripping. Also, it's acknowledged that selenium electrodeposits best from acidic conditions. Sb_2Te_3 and $Ge_xSb_yTe_z$ thin films have been grown by the Stickney group.[25,26] The Sb_2Te_3 thin films were deposited from an acid Sb solution with a pH of 1.4 and Na_2SO_4 supporting electrolyte. [25] $Ge_xSb_yTe_z$ deposition used an Sb solution with a basic pH of 9.4 and Na_2SO_4 supporting electrolyte.[26] Based on this research, Sb can electrodeposit from a range of pHs. To develop an E-ALD cycle for Sb_2Se_3, acidic solutions will be investigated.

4.3 EXPERIMENTAL

0.1 mM Sb_2O_3 solutions were made using three different electrolytes at pH 1.6. The electrolytes used were 0.5 M $HClO_4$ (GFS Chemicals, Inc.), 0.1 M HCl (JT Baker), and 0.5 M H_2SO_4 (Fisher Chemical). A higher concentration of electrolyte was required to fully dissolve the Sb than previous solutions needed. A 0.1 M HCl concentration was sufficient for dissolving Sb and ensured the safety of the Plexiglas cell. The perchloric acid Sb solution was also made at pH 3. The solution makeup was of 0.2 mM SeO_2 (Alfa Æsar 99.999% pure) in 0.1 M $HClO_4$ (GFS Chemicals, Inc.). The pH used for Se solutions was 1.6 and 3. All pH 3 solutions were adjusted

using NaOH (Fisher Chemical). Blank solutions used were 0.1 M $HClO_4$ (GFS Chemicals, Inc.) at pH 1.6 and 3.

The solution bottles used to store and connect solutions to the electrochemical flow cell were first cleaned by soaking them in a Nochromix (Godax Labratories) bath for a minimum of one hour. They were then rinsed sufficiently with 18 MΩ water (Millipore Advantage 10). All solutions are purged with N_2 gas to remove any oxygen for at least one hour before the experiments. The electrochemical flow cell (Electrochemical ALD L.C.) has a three-electrode setup. The auxiliary electrode is an inlaid Au wire in the shape of an "S." The reference electrode was Ag/AgCl in 3 M NaCl (Bioanalytical Systems, Inc.). When not in use the reference electrode was stored in a supersaturated NaCl solution. The working electrode is the substrate that will be deposited on. All experiments in this chapter use polycrystalline Au (Evaporated Metal Films) as the substrate. The polycrystalline Au is comprised of 100 nm of Au on top of 5 nm Ti on a glass slide, with the Ti used as an adhesion layer. The resulting working area of the cell is 2.2 cm^2. The Au slides are cleaned before putting them into the cell. This process includes rinsing the slide with acetone (Fisher Chemical), then rinsing with nanopure water, and drying it in N_2 gas. Next, the slide soaks in concentrated nitric acid (JT Baker) for at least 30 seconds. An additional rinse with nanopure water and N_2 drying precedes the immediate placement of the slide inside the cell.

The slide is additionally cleaned electrochemically before starting experimentation. A 0.1 M H_2SO_4 (Fisher Chemical) solution is used to clean the slide. This solution is flown into the cell at open circuit potential (OCP) and then a cleaning program is used to oxidize and reduce contaminants off the Au surface. The cleaning program pulses the potential to -200 mV and 1400 mV multiple times and then performs two CVs between -200 mV and 1400 mV. These potentials

are chosen based on the electrochemistry of Au in sulfuric acid. This method has been recognized in the Stickney group as a sufficient method of cleaning before experimentation. Depending on the type of experiment performed, Au slides can sometimes be reused by simply employing an electrochemical cleaning cycle after the experiment.

Solutions flow through a valve block (Neptune Research & Development, Inc.) before entering the flow cell. The valve block allows for multiple solutions to be flown through the cell without contamination or manual solution switching. The solution flow and potential control are automated using an in-house Labview program, Sequencer, that previous group members developed. The potentiostat (Electrochemical ALD L.C.) allows potential control of the cell at any given time.

4.4 RESULTS AND DISCUSSION

4.4.1 CYCLIC VOLTAMMTERY OF ANTIMONY

Before starting antimony selenide research, the electrochemistry of Sb needed to be inspected. Three different solutions of 0.1 mM Sb were made at pH 1.6 using different electrolytes. The three electrolytes used were sulfuric acid, perchloric acid, and hydrochloric acid. A CV for each solution can be seen in figure 4.1. In these scans, the lower potentials were all the same at -400 mV. Similar trends can be seen in the scans with slight differences in peak locations. The major difference between the three solutions is the large oxidation peak seen in the perchloric acid Sb solution at -50 mV. HCl exhibits a peak in the same location that is less than a third of the size in the perchloric based solution. One of the issues observed with making Sb solutions was getting the solid precursor to dissolve into solution. It is believed that perchloric

acid was more successful in getting the solid Sb to fully dissolve into solution when compared to the other electrolytes.

A window opening of CVs for 0.1 mM Sb in 0.5 M $HClO_4$ is shown in figure 4.2. This is at a pH of 1.6. In the scan towards negative potentials, the first reductive features can be seen starting just past 100 mV. These two reductive features correlate to surface limited structures. In the -100 mV scan, only two oxidative features are observed and strip off of the gold surface at 50 mV and 200 mV. When the scan is increased to more negative potentials, a third reductive peak starts at -150 mV. This peak turns into more of a plateau than the other observed peaks. This peak is related to bulk deposition and can be seen stripping at a peak that eventually centers around -25 mV. In the -200 mV scan, the bulk peak is small and strips around -75 mV. As the potential is scanned to a negative potential of -250 mV, the bulk Sb is now larger and strips at -50 mV. This trend increases as the scan is pushed to -300 mV where now the bulk peak strips at -25 mV and continues increasing in size. The peak location does not change from -25 mV as the potential scanned to increases to -400 m V but the peak does continue to grow in size. The shift in peak location indicates that as additional Sb is deposited at more negative locations, the Sb stability is increased as well.

Solutions of 0.1 mM Sb in 0.5 M $HClO_4$ were also made at pH 3 to evaluate the best situation for depositing Sb_2Se_3. E-ALD cycles for SnSe and GeSe described in chapters 2 and 3 used pH 1.6 and pH 3 Se solutions with success. Figure 4.3 shows the window openings for pH 3 Sb. Figure 4.3.A has window openings with negative limits between -200 mV and -600 mV. The first reductive feature observed in the CV appears at -125 mV. The resulting oxidative peak for this feature is a low broad peak between -50 mV and 300 mV. As the scan goes to further negative potentials, a second reductive feature is observed starting at -350 mV. Two additional

oxidative features can now be seen in the oxidative scan at -150 mV and -75 mV. At this point, it is believed that they both correspond to bulk features. Figure 4.3.B shows the window openings for more negative potentials including scans between -500 mV and -1000 mV. Three peaks can be observed for oxidative stripping in the -500 mV CV. There is a peak at -175 mV that corresponds to a bulk feature and a second bulk peak at -25 mV that is growing in as well. The surface limited peak at 75 mV sits in the background of the -25 mV bulk peak. As the potential is increased to -600 mV, the -175 mV peak shrinks and the -25 mV peak grows. This indicates that the bulk regime is changing from one less stable structure to a more stable structure related to the -25 mV peak. By the -800 mV scan, the -25 mV peak now centers at 75 mV and is so large that the surface limited peak is no longer visible. This trend continues for the -1000 mV scan.

Figure 4.4 shows a window opening of Se at pH 1.6 and figure 4.5 shows a window opening for Se at pH 3. The oxidative stripping potentials of Se at pHs 1.6 and 3 are much higher than any Sb deposition potential and thus will not be a concern when developing an E-ALD cycle for Sb_2Se_3. At pH 1.6, Sb oxidative stripping begins at -100 mV. This establishes the upper limit for Se deposition as -100 mV. Se reductively strips at -275 mV meaning that Sb deposition potentials should ideally be positive of this potential. These limitations create a workable deposition window of 175 mV. When looking at pH 3 Sb and Se, reductive stripping of Se occurs at -430 mV and oxidative stripping of Sb begins at -150 mV. This window of deposition allows for more potentials of deposition than the window of available deposition at pH 1.6 for Sb and Se. Based on this fact, pH 3 will be investigated further for a successful deposition.

4.4.2 PULSE DEPOSITION STUDIES OF ANTIMONY

It is important to evaluate the parameters of even simple experiments to ensure that the results seen come from a selected isolated change. Figure 4.6 shows an example of how improper parameters can skew results. In these experiments, pH 3 Sb was first deposited at -500 mV for 5 seconds. After that, a blank solution was flown into the cell before oxidatively stripping the Sb to determine how much was left. The original purpose of this experiment was to determine the cutoff potential at which blank could be introduced to the cell without losing any of the Sb. In figure 4.6.A, the blank was introduced at the chosen stripping potential for 30 seconds before stripping. In figure 4.6.B, a blank was introduced at -500 mV for 15 seconds before pulsing to the starting oxidation potential, holding for 30 seconds, the performing an oxidative scan. Based on figure 4.6.A, the difference in choice of potential shows a large change in the resulting CVs and indicates that the potential choice is very important. The -250 mV scan in figure 4.6.A exhibits almost a complete loss of bulk Sb at -150 mV. When the experiment was stabilized with the 15 seconds at -500 mV, there is still a difference in choice of potential but it is much less drastic. The issue that was occurring was that Sb was still depositing during the blank flow at different rates based off of potential choice in figure 4.6.A. This factor was eliminated by allowing the excess Sb deposition during flow time of blank to be the same by having the blank flown in at -500 mV before starting the changed parameters. As seen from the data in figure 4.6, the potential selection can alter the Sb if not properly selected.

Figure 4.7 has a series of pulse deposition experiments where the potential was pulsed down to a deposition potential in Sb and held for 5 seconds. Then a blank was introduced to the cell for 30 seconds at -300 mV before oxidatively stripping to determine the amount of Sb deposited at each potential. Potentials between -200 mV and -450 mV were selected based on Sb

and Se CVs in figures 4.3 and 4.6. In an E-ALD cycle, -200 mV would be the most positive deposition potential that could be used for Sb deposition that would not interfere with previously deposited Sb and -450 mV is the most negative Sb deposition potential that could be chosen without fully reducing Se. The coverages of deposition in figure 4.7 range between 0.44 MLs and 0.92 MLs which are satisfactory for an E-ALD cycle. This is promising for the development of an Sb_2Se_3 E-ALD cycle.

Another set of experiments that were done investigated the effect of time on Sb deposition. Figure 4.8 shows Sb pulse deposition experiments at -300 mV where Sb was deposited at this potential for different amounts of time. Figure 4.9 shows Sb pulse deposition experiments at -350 mV and -400mV for different amounts of time. At -300 mV, the amount of Sb that is oxidized off of the Au substrate is very close regardless of time. This is to be expected because -300 mV is in a surface limited deposition area for Sb and should not be changed very much with an increase of time due to the nature of surface limited deposition. At -350 mV, as the deposition time is increased the bulk peak at -125 mV grows larger. This phenomenon is more radical at -400 mV and by 30 seconds the amount of Sb deposited has doubled from the starting amount. These experiments show multiple ways to deposit Sb at different coverages. This information will help when developing an E-ALD cycle.

4.4.3 PULSE DEPOSITION STUDIES OF SELENIUM

Similar studies were done with selenium to evaluate appropriate deposition conditions for developing an E-ALD cycle for Sb_2Se_3. Figure 4.11 shows a pulse deposition study of Se on clean Au. First Se was deposited for 5 seconds at the listed potential. Blank was then flown in at -200 mV for 30 seconds before performing an oxidative strip scan in a blank. For potentials prior

to -430 mV, the location for reductive stripping, both bulk and surface limited peaks are present. The surface limited peak is fully formed. For potentials between -500 mv and -1100 mV, the bulk peak becomes smaller with increasingly negative potential choices. The surface limited peak at 700 mV is present at all chosen deposition potentials. A sufficient amount of Se is deposited for an E-ALD cycle even by using the most aggressive deposition of -1100 mV.

Time dependence studies were also performed to evaluate the proper amount of deposition time required to deposit Se. Figure 4.12 shows the variance in Se deposition at -200 mV for different amounts of holding time. -200 mV is at a potential before reductive stripping so increasing the amount of time should increase the amount of Se deposited. That is not the observed result. By 5 seconds of deposition, the amount of Se has already over a ML of material. The maximum amount of Se was deposited by holding for 15 seconds. However, at 30 seconds the deposition is close to that at 5 seconds. The deposition for Se happens rapidly as seen at 5 seconds and a monolayer may be all that can be deposited at -200 mV. A cross-comparison study was done at varying potentials by holding for 5 seconds versus 15 seconds in figure 4.13. These potentials are all more negative than the start of reductive stripping. In this scenario, the amount of time held does not drastically change the amount of Se that can be deposited. Less Se is deposited by holding for 15 seconds because it is in a region where Se can reductively strip. There are still Se ions present in this scenario so there would be both the deposition of Se on the surface and the reduction of Se off of the surface occurring simultaneously. The experiments prove that a 5 second deposition time would be sufficient for an E-ALD cycle at a variety of potentials using this deposition method. These studies use the Case 1 method of Se deposition described in chapter 2.

The Case 3 method of Se deposition described in chapter 2 utilizes reductive stripping of Se to tailor the amount of Se to the desired amount. Figures 4.14, 4.15, and 4.16 show how variations of time and reduction potential affect Se when using case 3 deposition. In all experiments, Se was first deposited at -200 mV for 5 seconds. In figure 4.14, a reductive stripping potential of -500 mV was used for varying amounts of time. Figure 4.15 uses -700 mV for reductive stripping and figure 4.16 uses -900 mV to reductively strip Se. The original Se -200 mV with no reductive stripping has been included in the figures for comparison. All reductive potentials exhibit a larger loss of Se as the potential is held for longer amounts of time. There are not any Se ions present during the reductive holding times causing this situation to differ from the experiments in figures 4.12 and 4.13. The most Se is lost when using a more negative stripping potential like -900 mV, as is expected. Based on this data, a variety of Se coverages can be achieved by manipulating the deposition parameters which is ideal for attaining the desired ratio of a binary compound.

4.4.4 DEPOSITION OF Sb_2Se_3

To begin developing an E-ALD cycle for antimony selenide, conditions for depositing Se on Sb were first examined. Figure 4.17 shows the effect of depositing Se on Sb for different potentials. Sb was initially deposited for 5 seconds at -300 mV for all experiments. Afterward, a blank was rinsed through the cell to remove Sb and then Se was introduced to the cell and deposited. The most positive Se deposition potential chosen was -300 mV to ensure that no Sb was lost through this process. The most negative potential used was -700 mV. The maximum amount of Se was deposited by using -300 mV or -400 mV as expected because these potentials are before reductive Se stripping. Potentials -600 mV and -700 mV show a large decrease in the resulting Se. The Sb remains stable throughout almost all experiments though some is lost by

depositing Se at -300 mV. An interesting observation in the peak shapes observed in the CVs is that the Sb changes shape, as Ge did in chapter 2, based on the amount of Se deposited. As more Se is deposited on Sb, the Sb oxidation occurs at a more positive potential and the peaks form one conglomerate peak. This indicates that the Sb is being stabilized and either forming an Sb-Se compound or being lifted from the Au surface. Figure 4.18 shows initial studies that were done to form two complete cycles of Sb-Se. These studies show that Sb remains stable through the process though some Se is lost when Sb is deposited in step 3. Parameters for deposition need to be reevaluated to obtain the desired 2:3 Sb:Se ratio but show promise for the ability to deposit Se on Sb and vice versa.

CONCLUSION

Early investigations of the Sb-Se system showed promise for depositing Sb_2Se_3 thin films. Cyclic voltammetry studies of different Sb solutions showed that using perchloric acid as an electrolyte allowed maximum Sb deposition. Time studies were performed and proved that in bulk deposition regions longer holding times deposited more Sb. Similar time studies in Se solutions indicated that Se had a much faster deposition process than Sb. An E-ALD cycle for deposition was successfully created for depositing Sb_2Se_3, as proved by the resulting CVs. Further optimization is required to correct the stoichiometry. Future studies should attempt depositing a thin film using updated parameters.

REFERENCES

1. Carey, J. J.; Allen, J. P.; Scanlon, D. O.; Watson, G. W. The Electronic Structure of the Antimony Chalcogenide Series: Prospects for Optoelectronic Applications. *Journal of Solid State Chemistry* **2014**, *213*, 116–125.
2. Zeng, K.; Xue, D.-J.; Tang, J. Antimony Selenide Thin-Film Solar Cells. *Semiconductor Science and Technology* **2016**, *31* (6), 063001.
3. Chen, C.; Bobela, D. C.; Yang, Y.; Lu, S.; Zeng, K.; Ge, C.; Yang, B.; Gao, L.; Zhao, Y.; Beard, M. C.; Tang, J. Characterization of Basic Physical Properties of Sb2Se3 and Its Relevance for Photovoltaics. *Frontiers of Optoelectronics* **2017**, *10* (1), 18–30.
4. Ngo, T. T.; Chavhan, S.; Kosta, I.; Miguel, O.; Grande, H.-J.; Tena-Zaera, R. Electrodeposition of Antimony Selenide Thin Films and Application in Semiconductor Sensitized Solar Cells. *ACS Applied Materials & Interfaces* **2014**, *6* (4), 2836–2841.
5. Lai, Y.; Chen, Z.; Han, C.; Jiang, L.; Liu, F.; Li, J.; Liu, Y. Preparation and Characterization of Sb2Se3 Thin Films by Electrodeposition and Annealing Treatment. *Applied Surface Science* **2012**, *261*, 510–514.
6. Radaf, I. M. E. Structural, Optical, Optoelectrical and Photovoltaic Properties of the Thermally Evaporated Sb2Se3 Thin Films. *Applied Physics A* **2019**, *125* (12).
7. Maghraoui-Meherzi, H.; Nasr, T. B.; Dachraoui, M. Synthesis, Structure and Optical Properties of Sb2Se3. *Materials Science in Semiconductor Processing* **2013**, *16* (1), 179–184.

8. Lai, Y.; Han, C.; Lv, X.; Yang, J.; Liu, F.; Li, J.; Liu, Y. Electrodeposition of Antimony Selenide Thin Films from Aqueous Acid Solutions. *Journal of Electroanalytical Chemistry* **2012**, *671*, 73–79.
9. Barcelos Costa, M.; Lucas, F.W.S.; Mascaro, L.H. Electrodeposition Conditions Effect Sb2Se3 Thin-Film Properties. *Chem. Electro.Chem.* **2019**, *6*, 2937–2944
10. Rodríguez-Lazcano, Y.; Peña, Y.; Nair, M.; Nair, P. Polycrystalline Thin Films of Antimony Selenide via Chemical Bath Deposition and Post Deposition Treatments. *Thin Solid Films* **2005**, *493* (1-2), 77–82.
11. Rajpure, K.; Bhosale, C. Effect of Se Source on Properties of Spray Deposited Sb2Se3 Thin Films. *Materials Chemistry and Physics* **2000**, *62* (2), 169–174.
12. Tian, Y.; Sun, Z.; Zhao, Y.; Tan, T.; Liu, H.; Chen, Z. One-Dimensional Sb2Se3 Nanorods Synthesized through a Simple Polyol Process for High-Performance Lithium-Ion Batteries. *Journal of Nanomaterials* **2018**, *2018*, 1–9.
13. Gregory, B. W.; Stickney, J. L. Electrochemical Atomic Layer Epitaxy (ECALE). *Journal of Electroanalytical Chemistry* **1991**, 300, 543561.
14. Villegas, I.; Stickney, J. L. Preliminary Studies of GaAs Deposition on Au(100), (110), and (111) Surfaces by Electrochemical Atomic Layer Epitaxy. *Journal of the Electrochemical Society* **1992**, 139, 686694.
15. Colletti, L. P.; Teklay, D.; Stickney, J. L. Thin-Layer Electrochemical Studies of the Oxidative Underpotential Deposition of Sulfur and Its Application to the Electrochemical Atomic Layer Epitaxy Deposition of CdS. *Journal of Electroanalytical Chemistry* **1994**, 369, 145152.

16. Colletti, L. P.; Stickney, J. L. Optimization of the growth of CdTe thin films formed by electrochemical atomic layer epitaxy in an automated deposition system. *Journal of the Electrochemical Society* **1998**, 145, 35943602.

17. Venkatasamy, V.; Jayaraju, N.; Cox, S. M.; Thambidurai, C.; Mathe, M.; Stickney, J. L. Deposition of HgTe by electrochemical atomic layer epitaxy (EC-ALE). *Journal of Electroanalytical Chemistry* **2006**, 589, 195202.

18. Venkatasamy, V.; Jayaraju, N.; Cox, S. M.; Thambidurai, C.; Stickney, J. L. Studies of Hg((1-x))Cd(x)Te formation by electrochemical atomic layer deposition and investigations into bandgap engineering. *Journal of the Electrochemical Society* **2007**, 154, H720H725.

19. Kim, J. Y.; Stickney, J. L. Ultrahigh vacuum surface studies of the electrochemical atomic layer deposition of indium telluride on n-type GaAs(100). *Journal of Physical Chemistry C* **2008**, 112, 59665971.

20. Gebregziabiher, D. K.; Kim, Y. G.; Thambidurai, C.; Ivanova, V.; Haumesser, P. H.; Stickney, J. L. Electrochemical atomic layer deposition of copper nanofilms on ruthenium. *Journal of Crystal Growth* **2010**, *312*, 12711276.

21. Lister, T. E.; Stickney, J. L. Atomic Level Studies of Selenium Electrodeposition on Gold(111) and Gold(110). *The Journal of Physical Chemistry* **1996**, *100* (50), 19568–19576.

22. Sorenson, T. A. A Comparison of Atomic Layers Formed by Electrodeposition of Selenium and Tellurium Scanning Tunneling Microscopy Studies on Au(100) and Au(111). *Journal of The Electrochemical Society* **1999**, *146* (3), 1019.

23. Huang, B. M.; Lister, T. E.; Stickney, J. L. Se Adlattices Formed on Au(100), Studies by LEED, AES, STM and Electrochemistry. *Surface Science* **1997**, *392* (1-3), 27–43.

24. Venkatasamy, V.; Shao, I.; Huang, Q.; Stickney, J. L. ALD Approach toward Electrodeposition of Sb_2Te_3 for Phase-Change Memory Applications. *Journal of The Electrochemical Society* **2008**, *155* (11).

25. Liang, X.; Jayaraju, N.; Thambidurai, C.; Zhang, Q.; Stickney, J. L. Controlled Electrochemical Formation of Ge x Sb y Te z using Atomic Layer Deposition (ALD). *Chemistry of Materials* **2011**, *23*(7), 1742–1752.

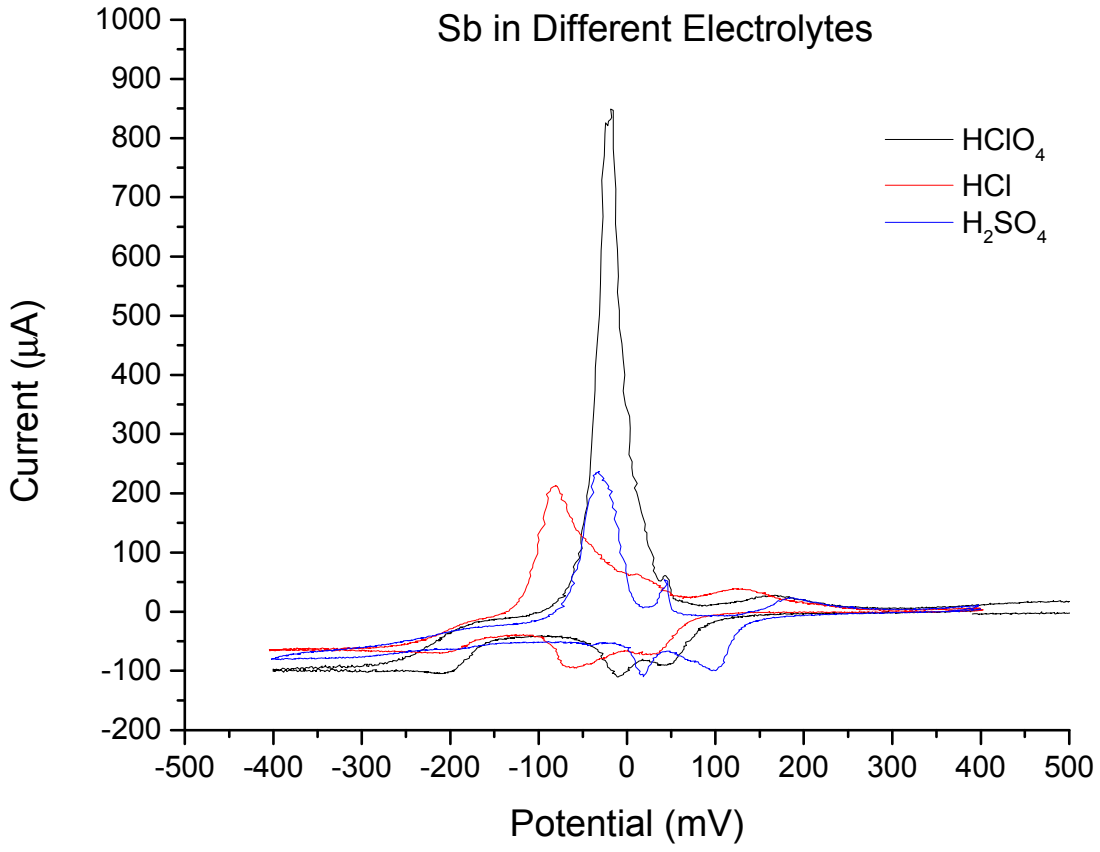

Figure 4.1 Cyclic voltammetry of 0.1 mM Sb in different electrolytes. Concentrations of the electrolyte are as follows: 0.5 M $HClO_4$, 0.1 M HCl, and 0.5 M H_2SO_4. All solutions have a pH of 1.6.

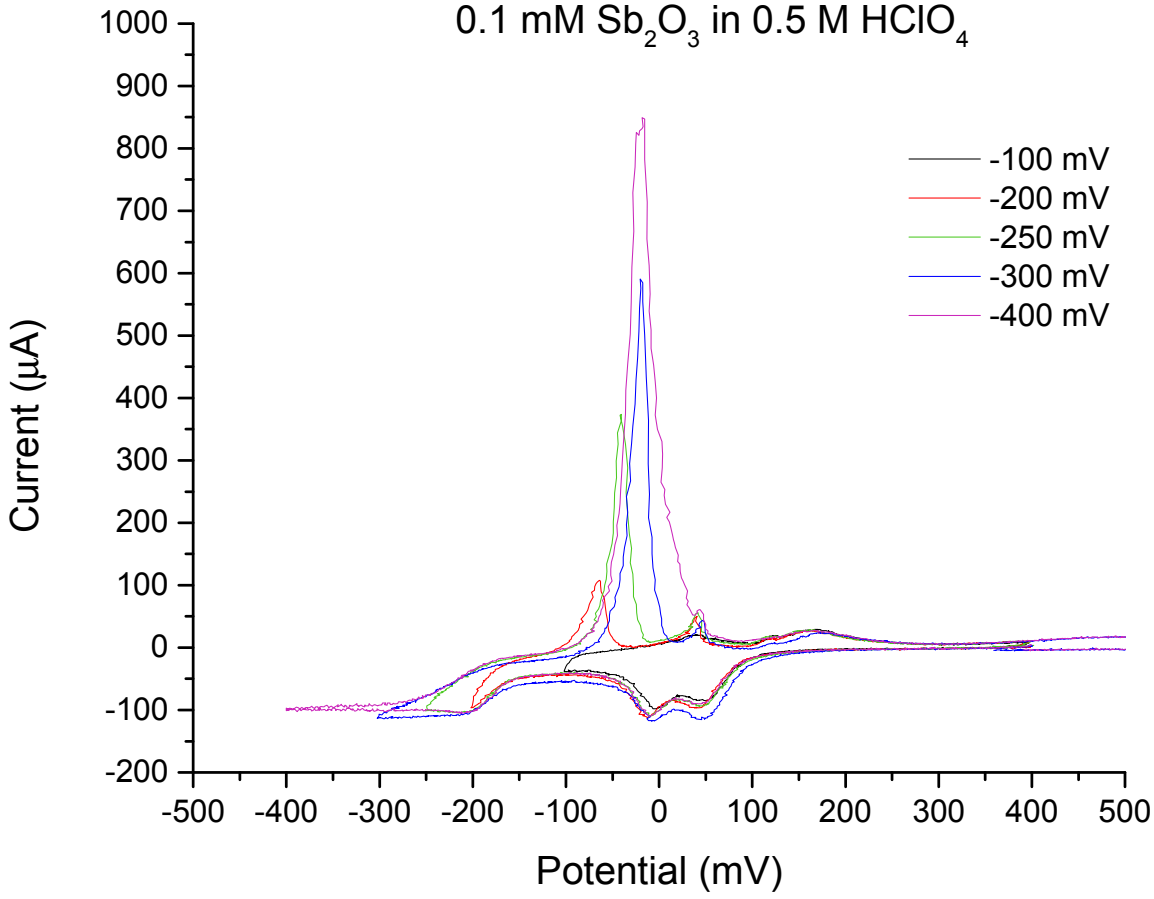

Figure 4.2 Window opening of CVs using a 0.1 M Sb solution in 0.5 M $HClO_4$. The pH of the Sb solution was 1.6.

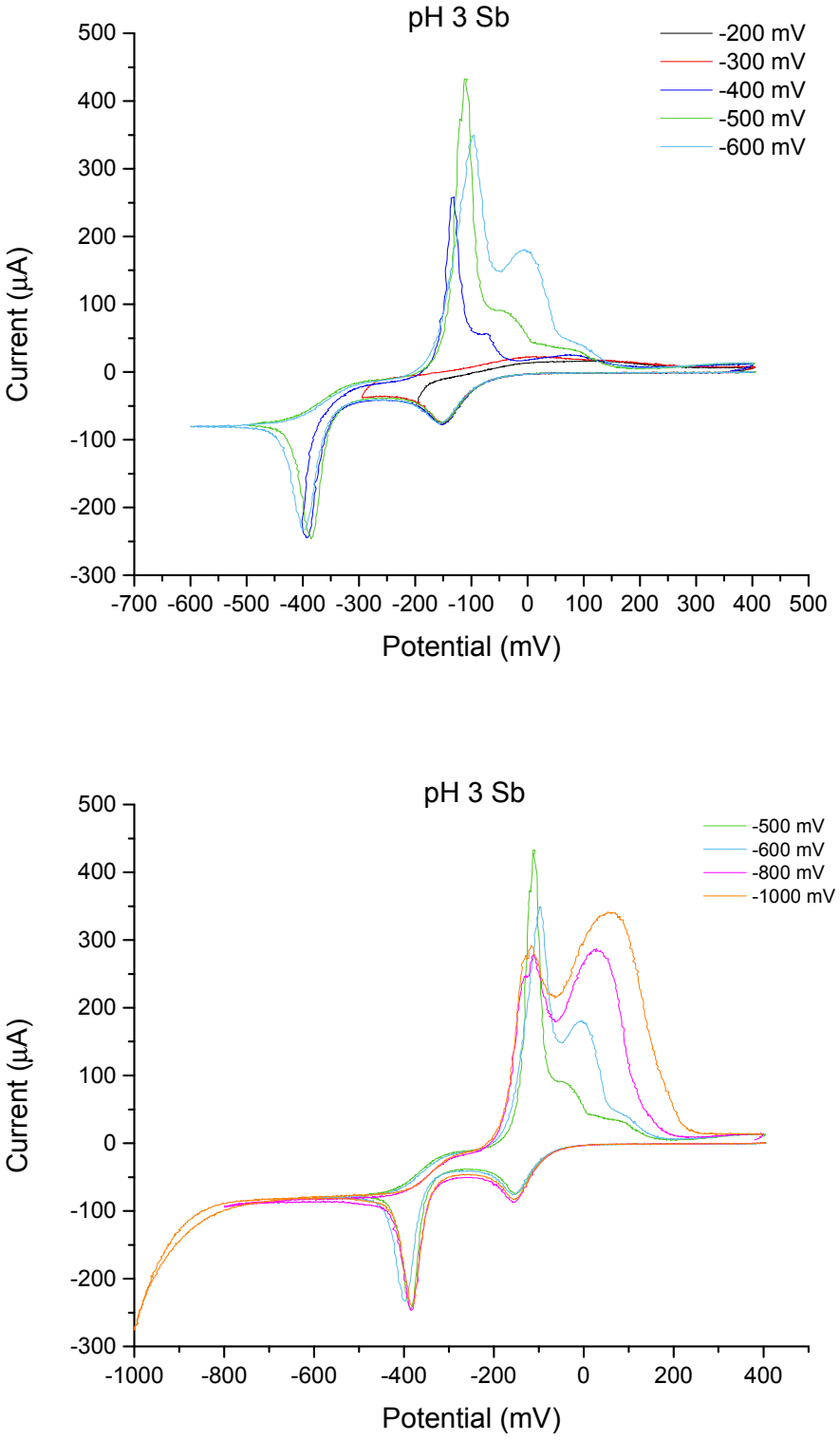

Figure 4.3 Window opening of CVs using a 0.1 M Sb solution in 0.5 M $HClO_4$. The pH of the Sb solution was 3. Negative limits between -200 mV and -600 mV are shown in the top figure and -500 mV to -1000 mV is shown in the bottom.

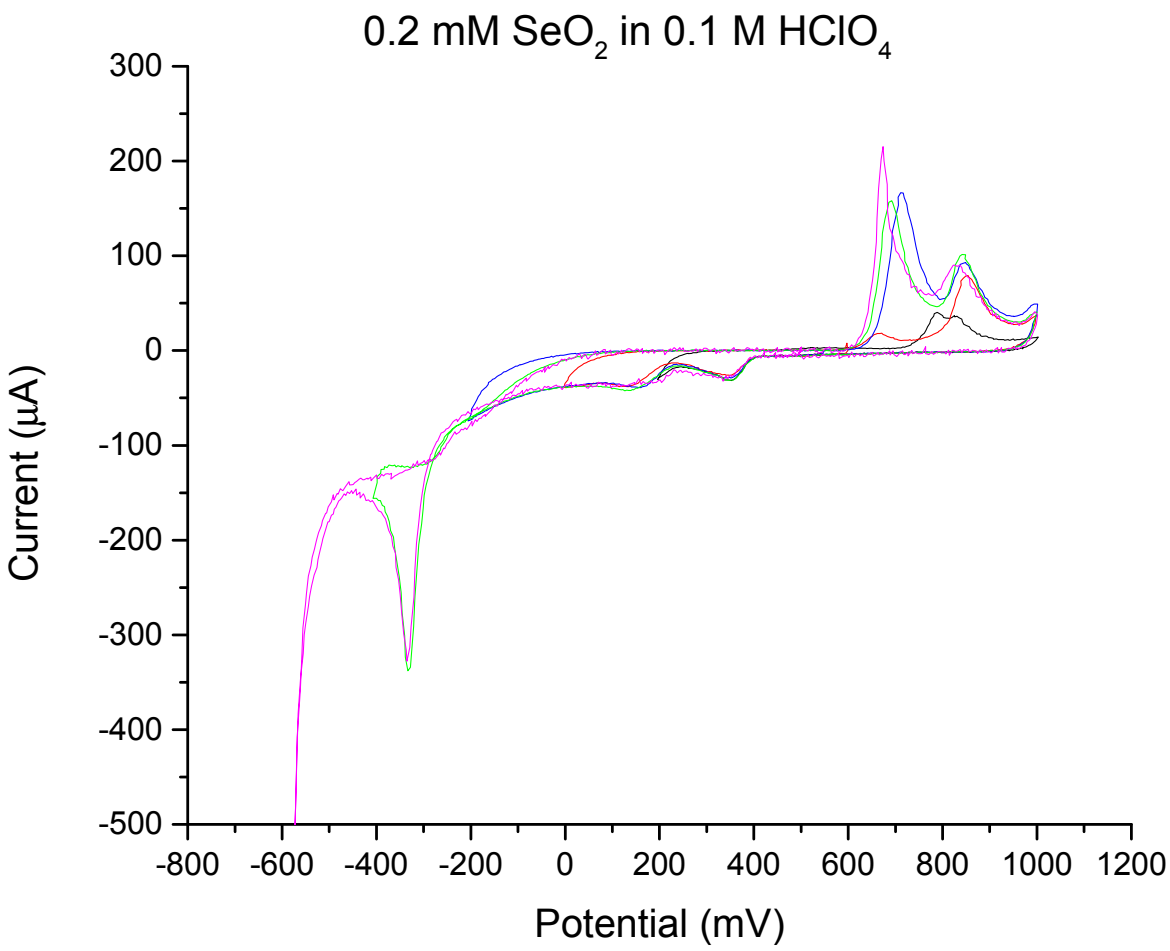

Figure 4.4 Window opening of CVs showing pH 1.6 Se. The solution was comprised of 0.2 mM Se with a 0.1 M $HClO_4$.

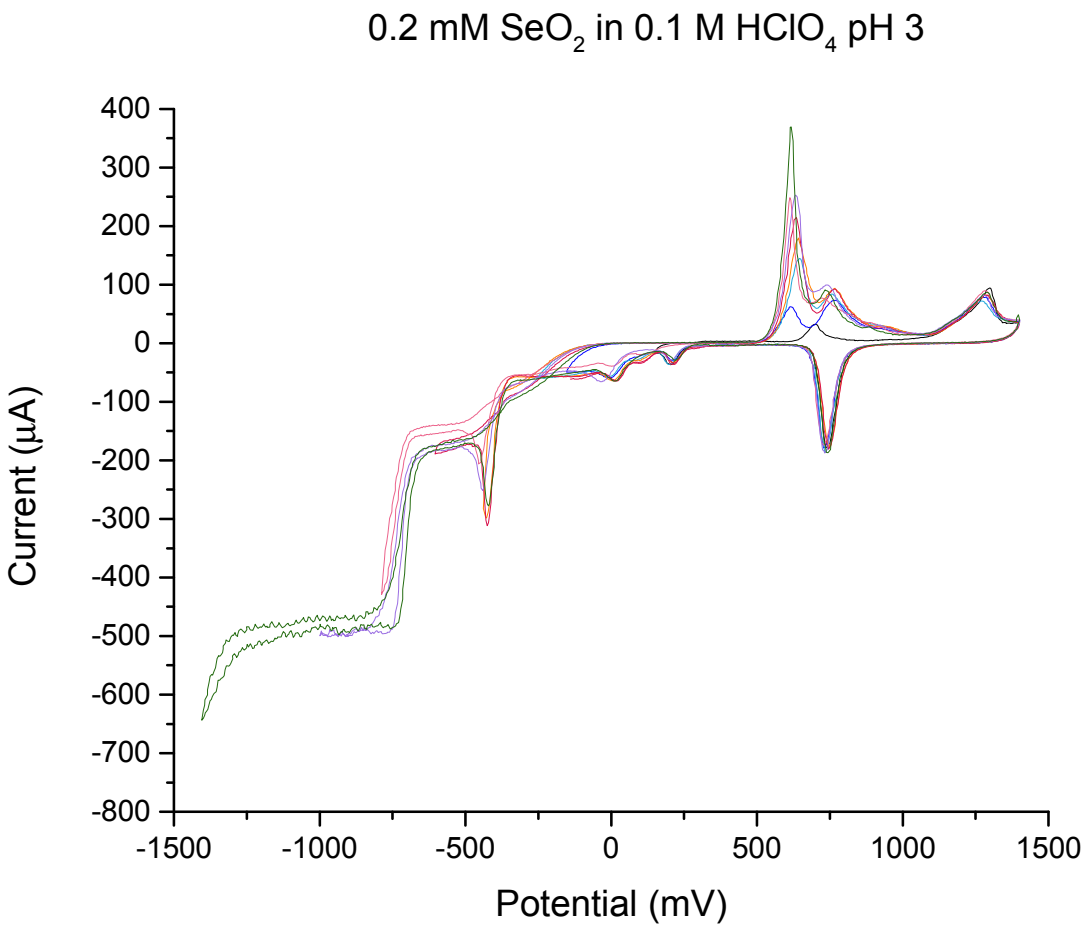

Figure 4.5 Window opening of CVs with 0.2 mM Se in 0.1 M $HClO_4$. The pH of the solution was 3.

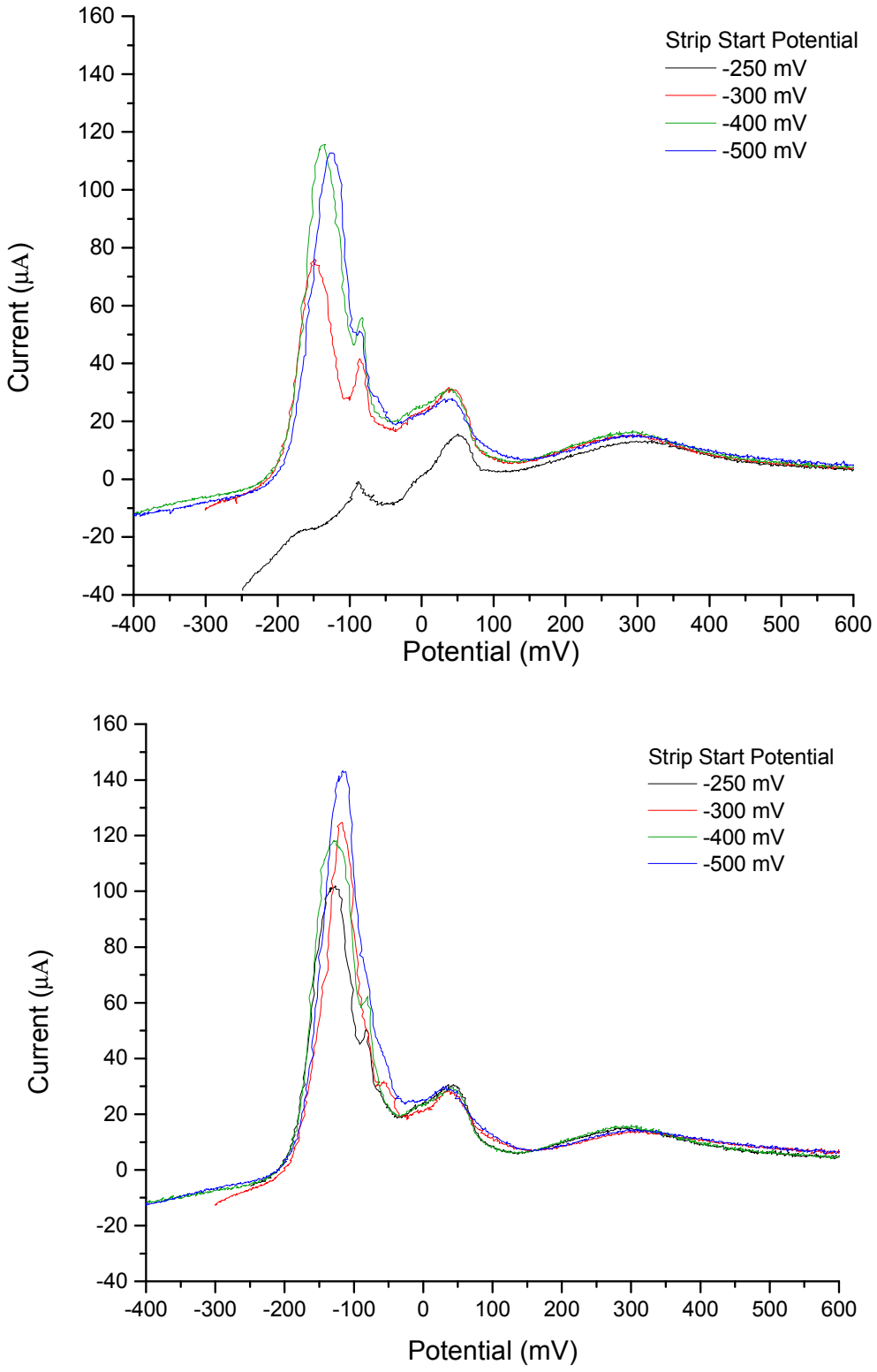

Figure 4.6 Oxidative CVs in blank following the pulse deposition of Sb. Sb was first deposited at -500 mV and then stripped from various starting potentials as listed. Top shows the scans with blank flown at the listed potential directly after deposition. The bottom shows the scans with an additional 15 seconds flowing blank at -500 mV before stepping to the starting strip potential.

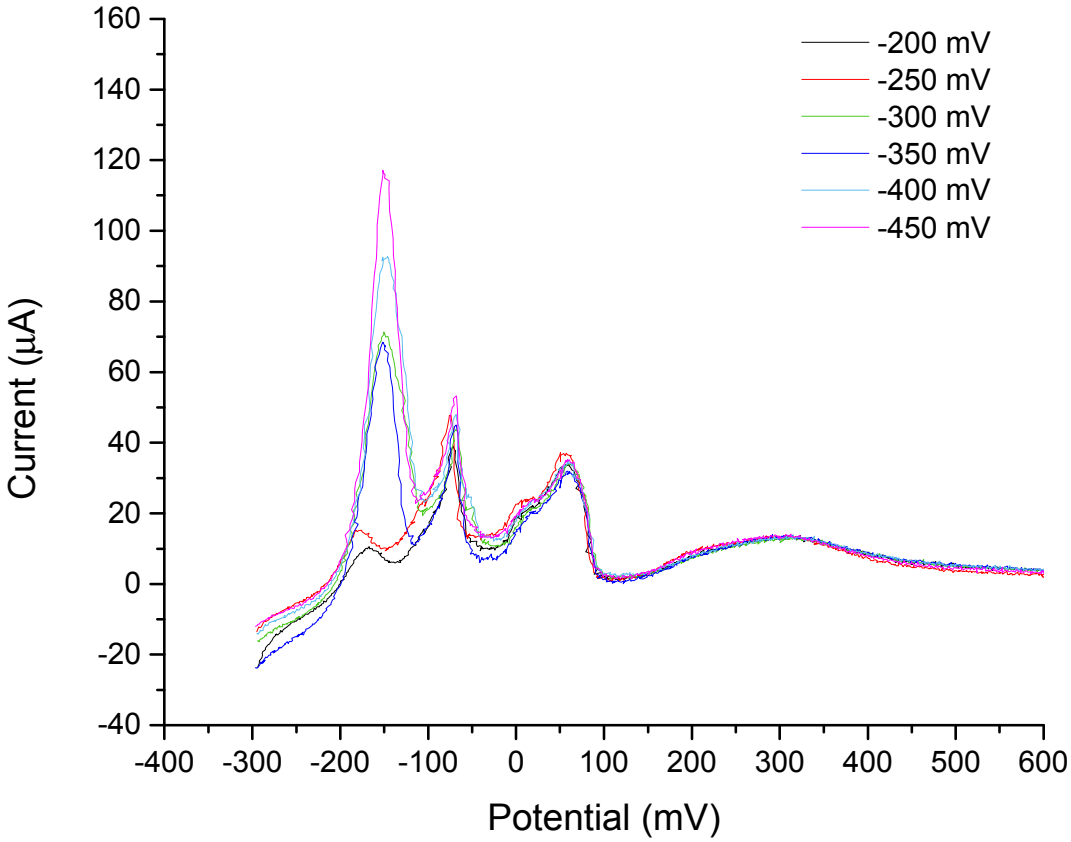

Potential (mV)	Coverage (MLs)
-200	0.44
-250	0.61
-300	0.76
-350	0.81
-400	0.89
-450	0.92

Figure 4.7 Oxidative CVs following deposition of pH 3 Sb for 5 seconds at various potentials. All scans were stripped from -300 mV after a blank rinse at -300 mV for 30 seconds.

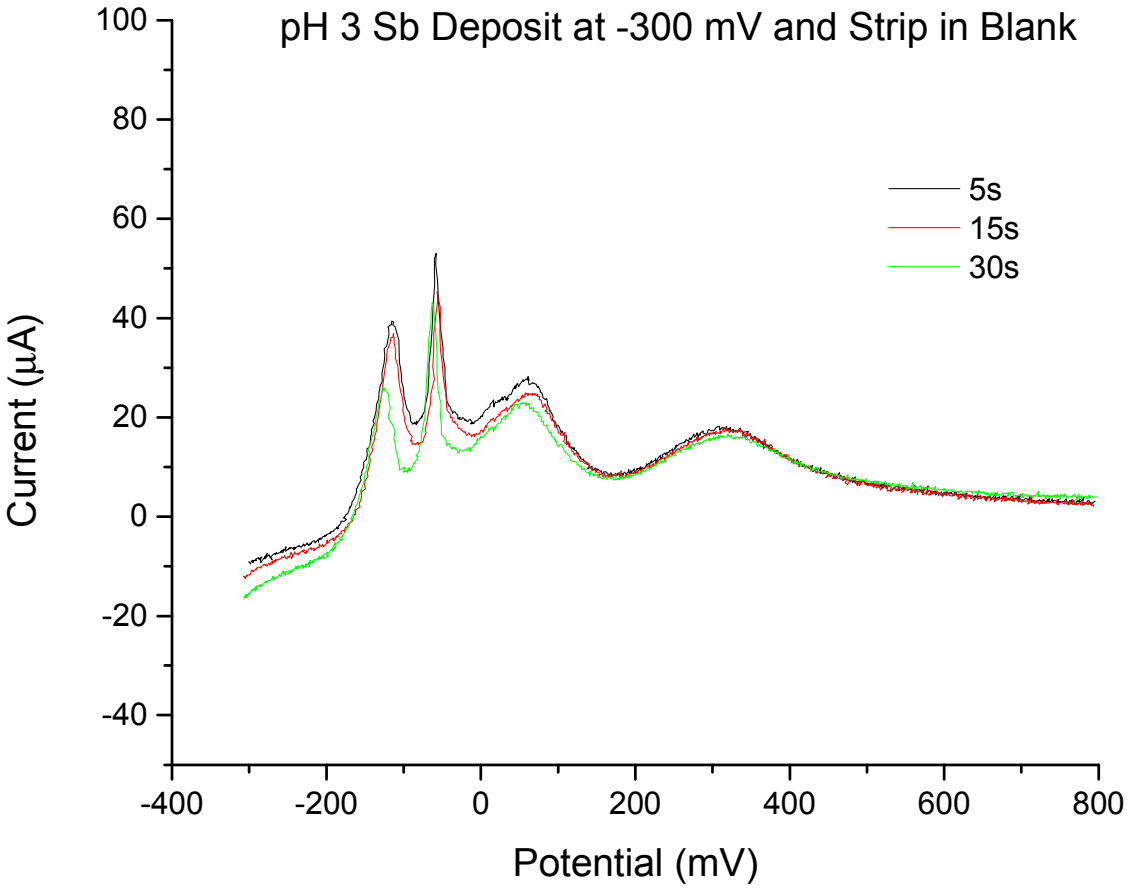

Time (sec)	Coverage (MLs)
5	0.70
15	0.69
30	0.63

Figure 4.8 Oxidative CVs showing the difference in depositing Sb at -300 mV for different amounts of time before stripping the deposit off of Au.

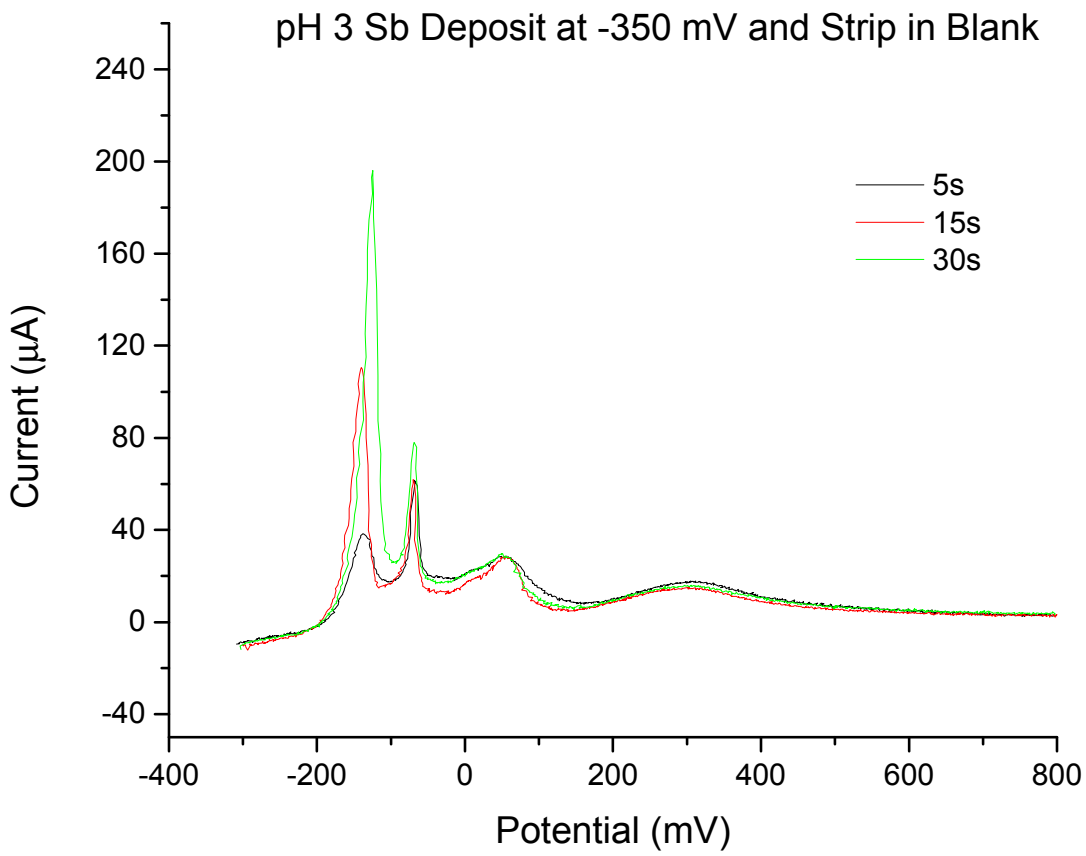

Time (sec)	Coverage (MLs)
5	0.62
15	0.79
30	0.99

Figure 4.9 Oxidative CVs showing the difference in depositing Sb at -350 mV for different amounts of time before stripping the deposit off of Au.

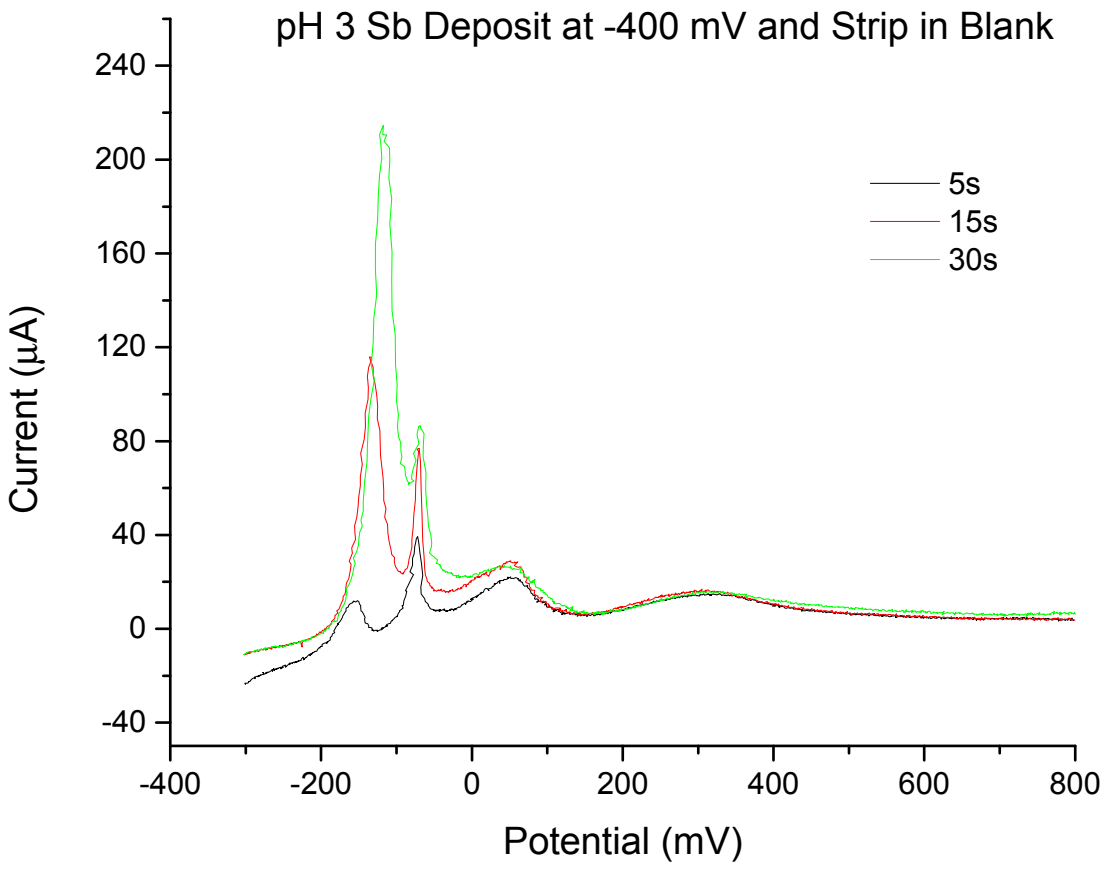

Time (sec)	Coverage (MLs)
5	0.63
15	0.91
30	1.26

Figure 4.10 Oxidative CVs showing the difference in depositing Sb at -400 mV for different amounts of time before stripping the deposit off of Au.

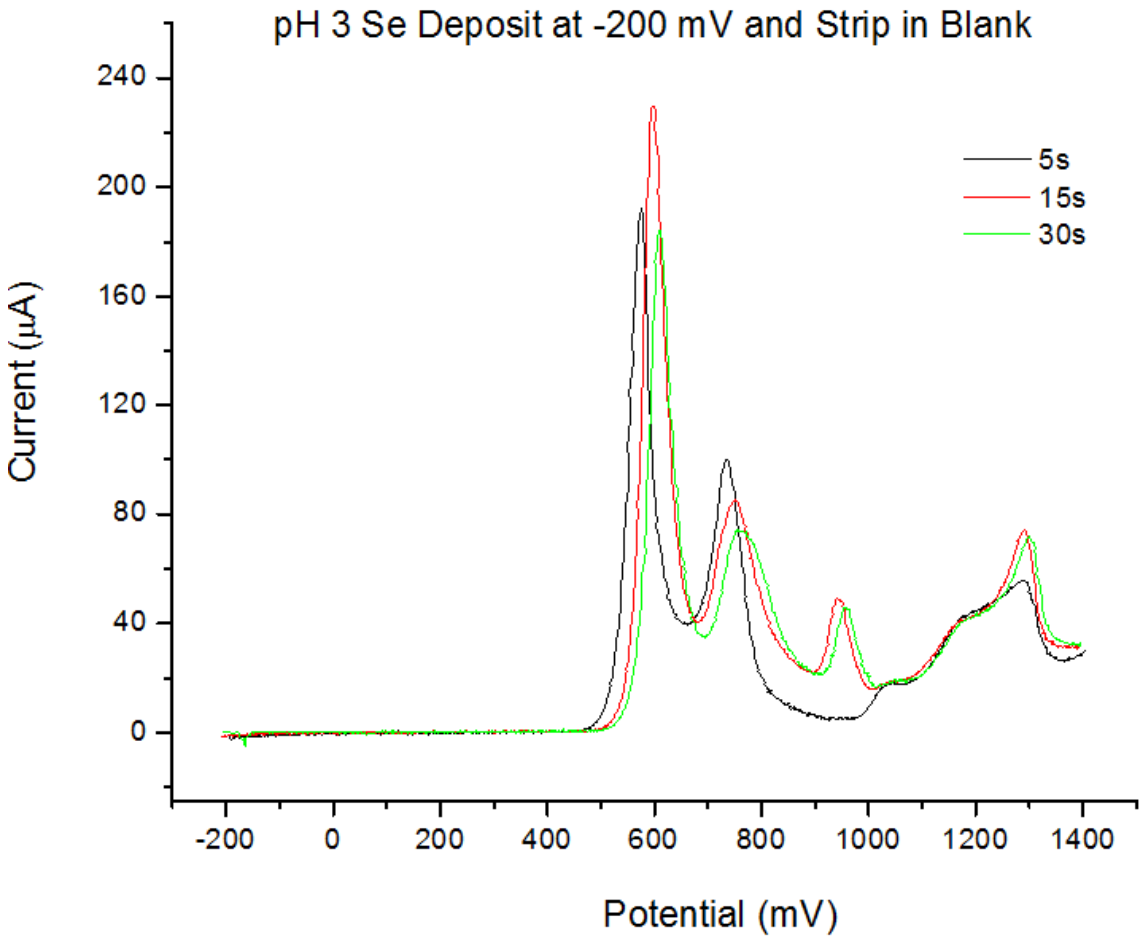

Time (sec)	Coverage (MLs)
5	1.10
15	1.24
30	1.12

Figure 4.11 CVs resulting from depositing pH 3 Se at different potentials for 5 seconds. Blank was flown through the cell at -200 mV before starting the oxidative scan.

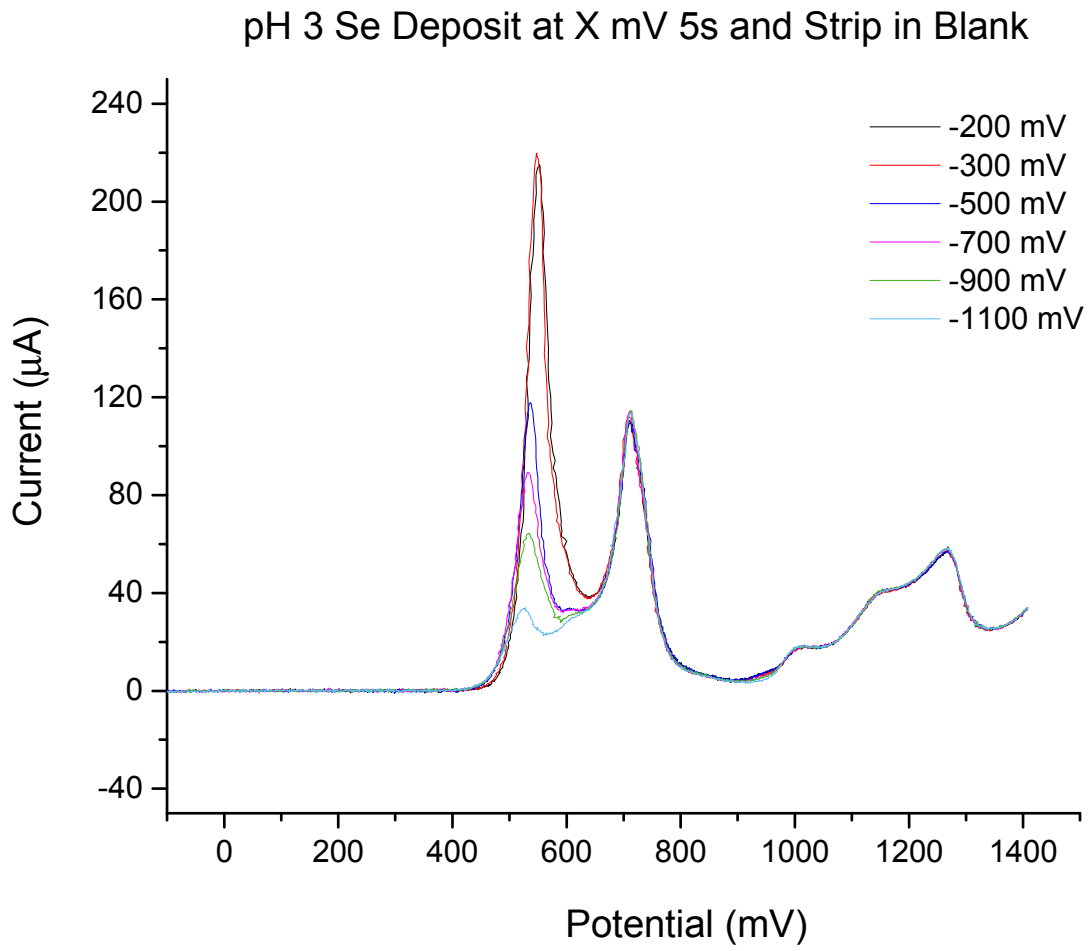

Potential (mV)	Coverage (MLs)
-200	1.14
-300	1.14
-500	0.88
-700	0.85
-900	0.78
-1100	0.69

Figure 4.12 Stripping CVs of pH 3 Se deposited at -200 mV for different amounts of time stripped in pH 3 blank.

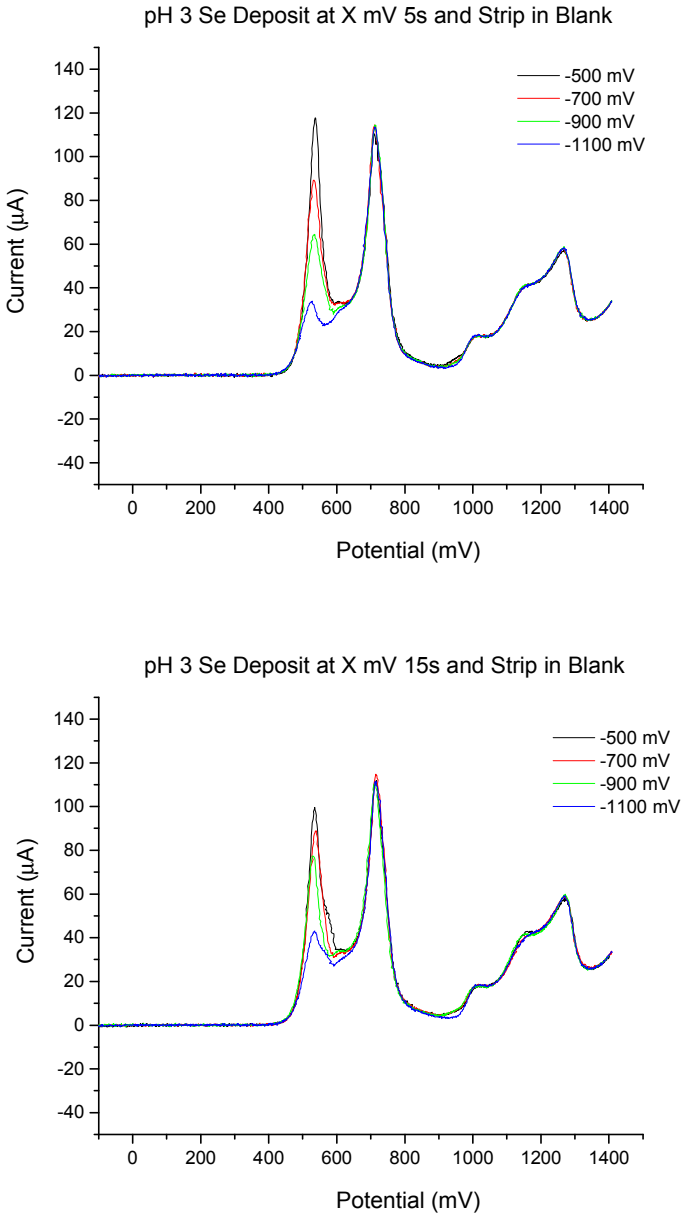

Figure 4.13 Comparison of CVs in blank of Se deposited at different potentials for 5 seconds (top) and 15 seconds (bottom).

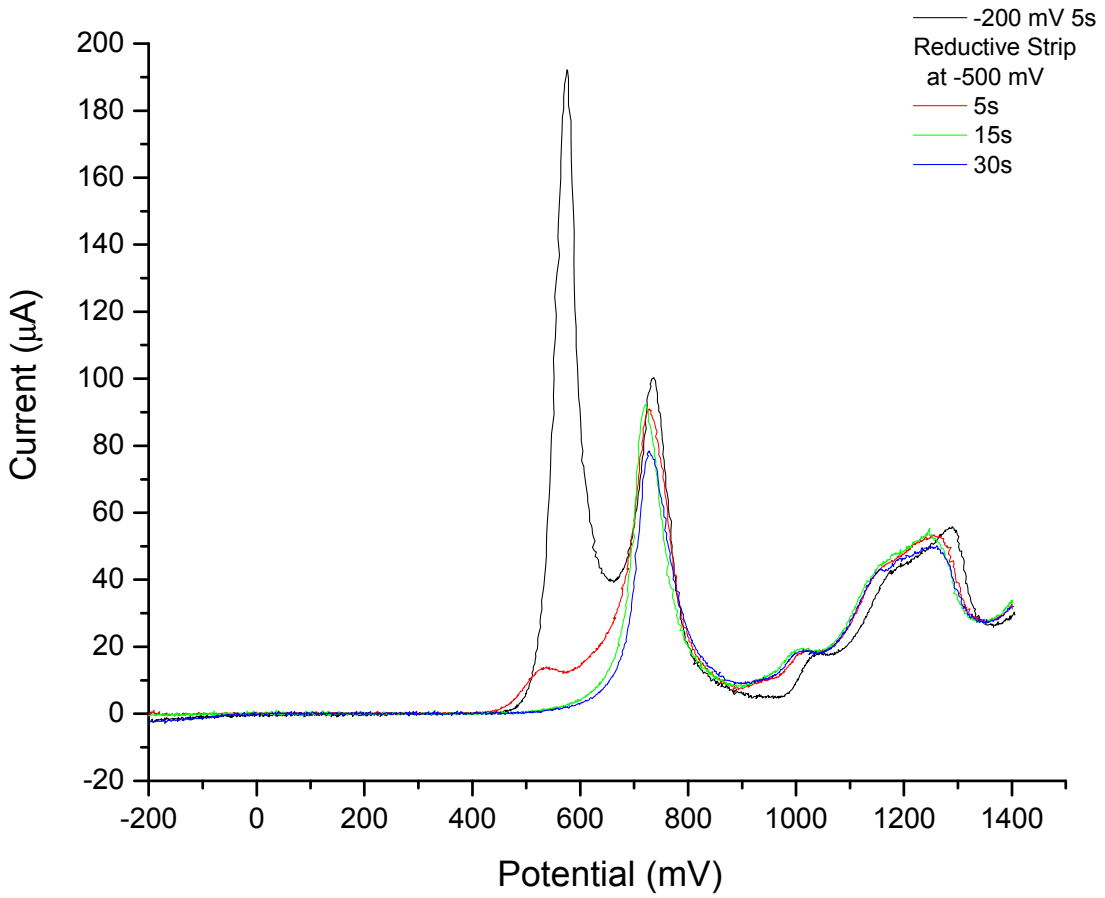

Time (sec)	Coverage (MLs)
5	0.52
15	0.37
30	0.34

Figure 4.14 CVs showing the change in Se after reductive stripping at -500 mV for different lengths of time. Se was first deposited for 5 seconds at -200 mV before a blank solution was introduced and the potential was pulsed to -500 mV.

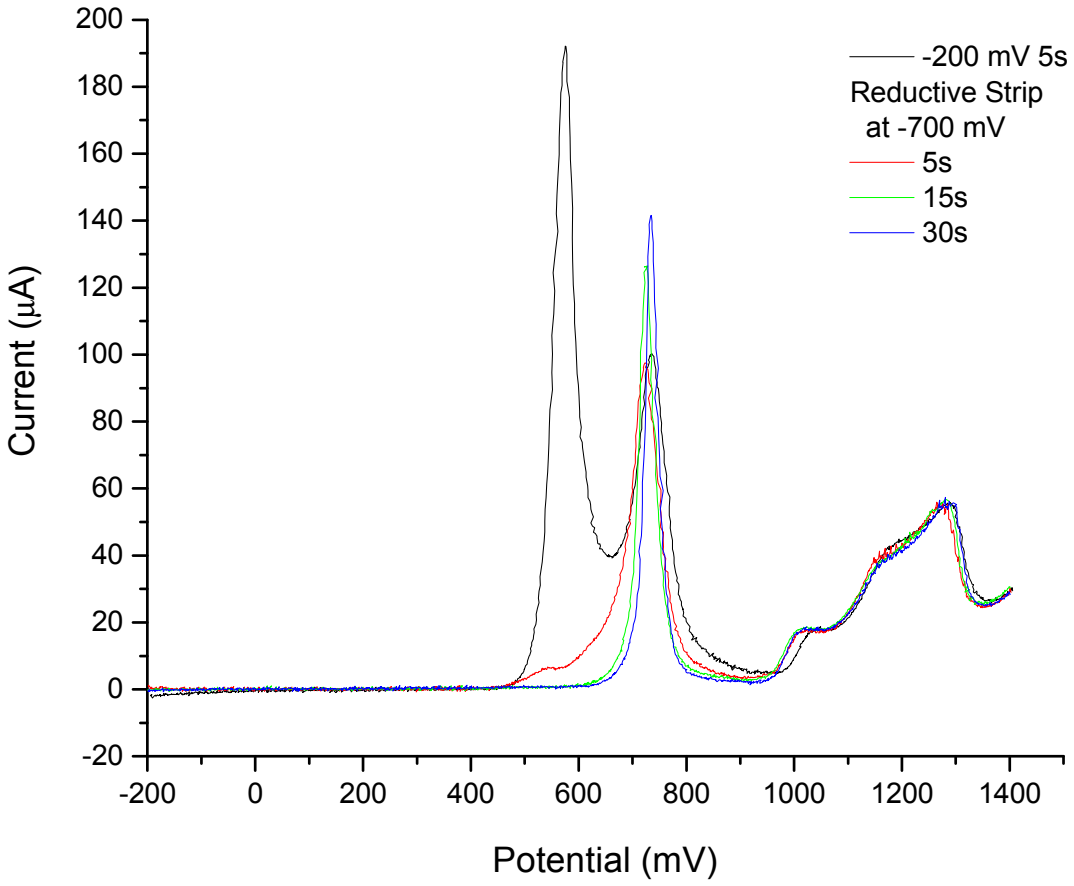

Time (sec)	Coverage (MLs)
5	0.43
15	0.30
30	0.28

Figure 4.15 CVs showing the change in Se after reductive stripping at -700 mV for different lengths of time. Se was first deposited for 5 seconds at -200 mV before a blank solution was introduced and the potential was pulsed to -700 mV.

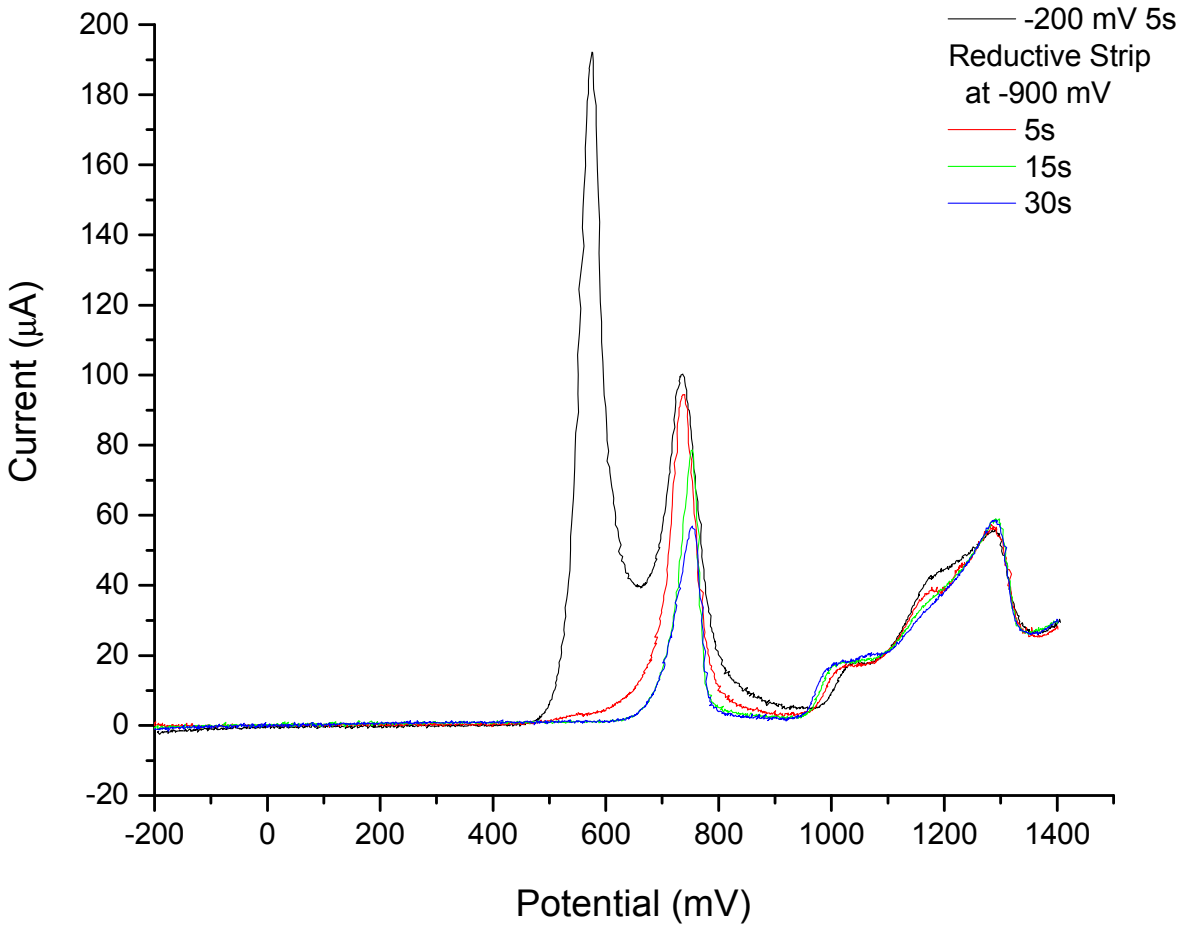

Time (sec)	Coverage (MLs)
5	0.34
15	0.20
30	0.18

Figure 4.16 CVs showing the change in Se after reductive stripping at -900 mV for different lengths of time. Se was first deposited for 5 seconds at -200 mV before a blank solution was introduced and the potential was pulsed to -900 mV.

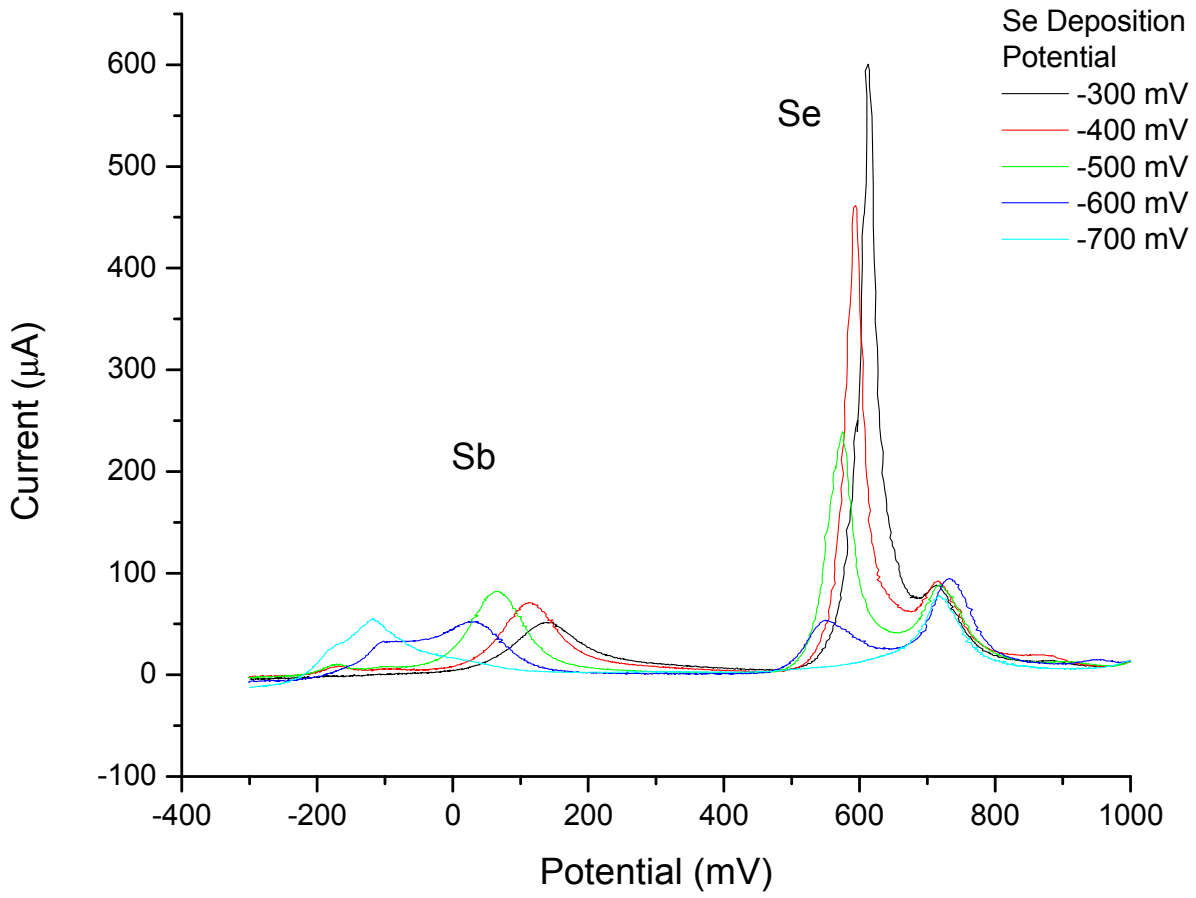

Potential (mV)	Sb Coverage (MLs)	Se Coverage (MLs)
-300	0.56	1.59
-400	0.65	1.43
-500	0.70	1.08
-600	0.77	0.60
-700	0.64	0.35

Figure 4.17 CVs in blank of the resulting oxidative scan after Se was deposited on Sb at different potentials. Sb was first deposited at -300 mV for 5 seconds before a blank rinse was done. Se deposition followed.

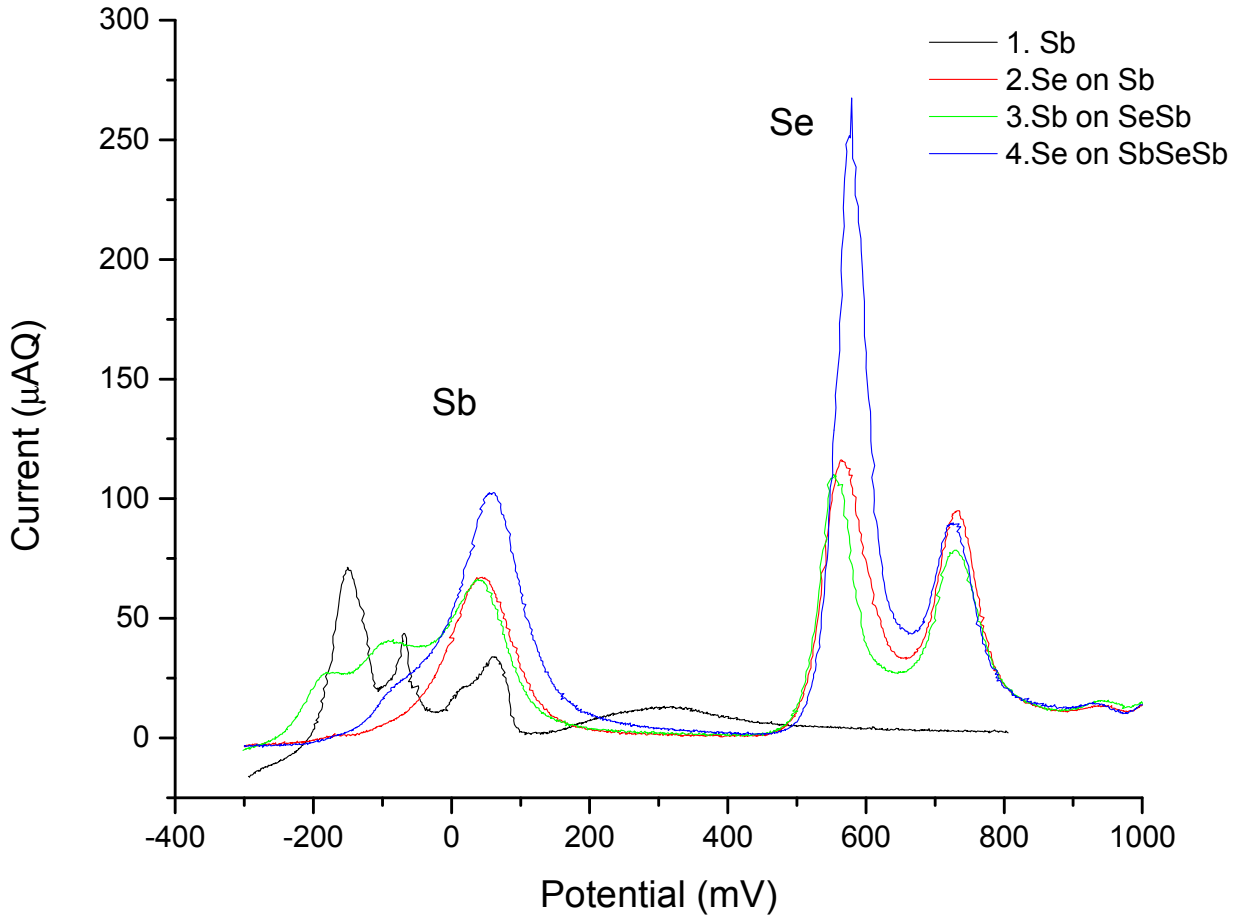

Step #	Sb Coverage (MLs)	Se Coverage (MLs)
	0.71	n/a
2	0.68	0.91
3	1.02	0.75
4	1.13	1.25

Figure 4.18 CVs showing the oxidative scans of Sb-Se deposits for two complete E-ALD cycles.

CHAPTER 5

CONCLUSION AND OUTLOOK

The focus of this dissertation was to develop methods to deposit selenium-based chalcogenides using E-ALD. The compounds investigated were GeSe, SnSe, and Sb_2Se_3. Chapter 1 introduced the importance of these materials as components in alternative energy devices like photovoltaic cells, solar cells, and photoelectrochemical cells.[1,2] The motivation to research these binary compounds is prompted by the need to replace high-cost and toxic components that are currently used in these devices. For the materials to function in a device they must be high quality. Chapter 1 gives a brief introduction on E-ALD and why this method is ideal for growing thin films with control and precision in a low-cost way.[3-10] Years of research in the Stickney lab has fostered the ability to do this methodically. Much more detailed electrochemical studies can be done due to the flow cell setup that has been designed and optimized over time. Methods of thin film characterization are also presented in chapter 1. *In situ* methods include cyclic voltammetry studies of each element as well as combinations of different elements. This information allows for the identification of different deposition regimes occurring, as well as how an element's electrodeposition is affected by the presence or deposition of another. *Ex situ* methods of characterization include optical microscopy, XRD, Raman spectroscopy, EPMA, and SEM/EDS. These methods of characterization aid in determining the homogeneity of a thin film's morphology, compound phases present, and the elemental stoichiometry.

Chapter 2 presented research investigating the electrochemical deposition of GeSe. In-depth studies were performed examining the electrochemistry of Se and Ge at multiple pHs. Solutions at pH 3 and pH 9 were chosen as the best options for deposition based on cyclic voltammetry studies. Three scenarios were selected to study: pH 9 Ge and pH 9 Se, pH 9 Ge and pH 3 Se, as well as pH 3 Ge and pH 3 Se. Germanium showed the ability to deposit the maximum amount possible at higher pHs like pH 9. However, selenium was unable to successfully deposit at that pH. Studies of Se showed that it was able to deposit best in acidic conditions like pH 3 or below. It was proved that though Se is unable to deposit from a pH 9 solution it was stable in a pH 9 blank after depositing from an acidic solution. Careful investigation of the stability of Se and Ge at both pH 3 and pH 9 was done to ensure the results of deposition were not affected by changing the pH. CV studies were performed examining the ability to deposit both Se and Ge on gold, as well as on each other. This allowed for ranges of stability to be determined and to see how peaks changed when a second element was deposited. For example, the deposition of Se on Ge caused the oxidation peaks of Ge to change from two surface limited peaks to one peak located near the location of the germanene peak.

The latter two scenarios, pH 9 Ge/pH 3 Se and pH 3 Ge/pH 3 Se, both allowed the deposition of GeSe at low coverages. Further investigation needs to be done on thicker thin films. Initial attempts to deposit thicker thin films led to Se-rich deposits. Studies would need to focus on determining whether the Ge is no longer depositing at the chosen potential or if Se is replacing the previously deposited Ge. This could be accomplished by studying the progression of the current-time traces and making changes to the deposition parameters as the thin films grow. During the deposition process, the substrate changes from a predominantly Au surface to the compound itself. The deposition of Ge or Se on GeSe will most definitely be different than

depositing Ge or Se on Au. Typically it is harder to deposit an element on these types of semiconductor compounds than on clean Au and deposition potentials may need to be altered to reflect that. Previous research has used a staggering potential where the potential for deposition is changed to a more negative potential every 5-10 cycles to increased deposition.[11] This would help combat lower coverages in later cycles and help maintain Ge growth. Another method for investigating how the deposition process changes over time would be using *in situ* Raman spectroscopy. A modified flow cell was developed by a previous group member that was able to fit into a Raman spectrometer, allowing for spectra to be obtained during the deposition process.[12] Doing this would allow for the identification of the materials present throughout the growth of the thin film. Using a SERS substrate would allow even sub-monolayer materials to be observed. The observed peaks would help determine at which point GeSe stops successfully depositing and allow the E-ALD cycle to be optimized. The detailed CV studies performed to investigate the first few layers Se and Ge at multiple pHs allowed for the identification of two circumstances where GeSe could be deposited. From this data, further studies would be able to produce GeSe films using E-ALD.

Chapter 3 highlighted the use of E-ALD to deposit tin selenide thin films. Initial studies were performed using sulfuric acid as the electrolyte for Sn and Se. Tin solutions were not only hard to make but also precipitated within 48 hours. Due to this, Sn solutions were made every 2 days. Window openings allowed the identification of areas where Sn and Se should be deposited. Potentials between -300 mV and -400 mV were suitable to deposit Sn and potentials between 0 mV and -200 mV for Se. The selection of these ranges was based on the ability to deposit a surface limited amount of the element while also ensuring the stability of the other element in successive cycles. Many E-ALD cycles were tried before finding a cycle that successfully

deposited any material on the substrate at all. The effect of potential choice was investigated by depositing thin films using the previously described cycle and repeating it 100 times. The potential of one element was kept constant while the other was varied in its potential range. The thin films were then evaluated using XRD, Raman spectroscopy, and SEM/EDS. The morphology and ratio of Sn:Se changed as the deposition potentials were altered. However, no potential combination produced a thin film that had high quality or the correct stoichiometry.

Based on this fact, it was decided to try seeing if changing the electrolyte had an effect. By using perchloric acid as the electrolyte, the tin solution stability increased and better thin films were successfully deposited using the previously developed E-ALD cycle. The morphology of the perchloric thin films were more homogeneous and the thin film deposited across the entire exposed substrate uniformly in comparison to thin films deposited from the sulfuric acid electrolyte. Reducing the flow rate from 10 mL/minute to 3 mL/minute further improved the quality of the thin film deposited at a microscopic and macroscopic view. SEM images showed a more ideal morphology. The remaining issue that needed resolution was the presence of SnSe and $SnSe_2$ in the deposited films, as seen in XRD and Raman spectroscopy data. Since SnSe is a p-type material and $SnSe_2$ is an n-type material, the presence of both species in the film would reduce its performance in a device.[13-15] The presence of both species also indicates that a cohesive compound is not being formed. Changes to the cycle did not change the presence of these species in resulting thin films so the electrolyte for Sn was changed again. The third solution researched was Sn in HCl. In addition to changing the electrolyte, the concentration of Sn was also increased to promote its deposition. This change finally produced a thin film that exhibited high uniformity and smooth morphology. These thin films presented only SnSe when characterized.

These final films were characterized by collaborators to evaluate the photoelectrochemical performance of the thin films. The thin films were p-type as is expected for SnSe. However, these films had low current density and only lasted 1-2 cycles in an electrolyte. Further investigations should be performed to evaluate the cause of this degradation and how to prevent this from happening. A protective layer deposited on top of the SnSe thin film may increase stability. One way of increasing the current density could be by doping it with another element. Doping can increase a variety of characteristics and has been successful for SnSe thin films using other methods of deposition.[16,17] Several dopants could be easily tried because of the nature of E-ALD. The choice of dopant and the amount of dopant used would be investigated.

Other future studies to perform would be tailoring the selected deposition potentials to see if the deposition of a $SnSe_2$ film is achievable using E-ALD. If possible, a solar cell could be easily developed by first depositing SnSe via E-ALD onto an appropriate back contact then depositing $SnSe_2$. A front contact could then be deposited onto the $SnSe_2$, allowing for a complete solar cell to be created without ever exposing it to air.

Chapter 4 describes early research on Sb_2Se_3. Based on the knowledge gained from the research described in chapters 2 and 3, the solution makeup of Sb was tested before starting further studies. Chapter 2 detailed the effect pH can have on deposition and chapter 3 showed the effect of electrolyte. The electrolyte choice was evaluated by making three different solutions and comparing the CVs. Perchloric acid was selected as the best choice from this data. Sb was deposited by other group members at both acidic and basic conditions with success.[18,19] Based on the inability to deposit Se at basic conditions, Sb solutions were made at pH 1.6 and pH 3. When comparing the deposition and oxidation ranges of Se and Sb at these pHs, pH 3 offered the widest range of stability. Sb deposition was examined by using pulse deposition studies. The

effects of changing the potential of deposition and the time for deposition were researched. By changing either parameter, varying amounts of Sb could be deposited on Au with control. Similar studies were done to examine the effect of time on Se deposition. Additionally, reductive stripping studies were done where the potential for reductive stripping and the time for reductive stripping was changed to see how the previously deposited Se coverage could be manipulated. These experiments laid the groundwork for future work by creating several ways to deposit different amounts of both Sb and Se.

Sb-Se was successfully deposited on Au using the developed E-ALD cycle. The presence of Sb and Se was confirmed through oxidative stripping scans after deposition. Deposition potentials still need adjusting to achieve the desired 2:3 ratio. After fine-tuning the E-ALD cycle, thin films can be deposited by repeating the cycle until the desired thickness. Systematic investigations should be done where the cycle is repeated a different number of times to grow films with different thicknesses. After depositing these thin films, characterization should be done to determine the stoichiometry and morphology of the thin films. If the E-ALD cycle is successful, all thin films should exhibit a 2:3 stoichiometry and a smooth surface. This will prove that the cycle is complete.

REFERENCES

1. Armaroli, N; Balzani, V. Solar Electricity and Solar Fuels: Status and Perspectives in the Context of the Energy Transition. *Chem. Eur. J*. **2016**, *22*, 32 – 57
2. Archer, M. Photovoltaics and photoelectrochemistry: similarities and differences. *Physica E.* **2002,** *22,* 61-64.
3. Gregory, B. W.; Stickney, J. L. Electrochemical Atomic Layer Epitaxy (ECALE). *Journal of Electroanalytical Chemistry* **1991**, 300, 543561.
4. Villegas, I.; Stickney, J. L. Preliminary Studies of GaAs Deposition on Au(100), (110), and (111) Surfaces by Electrochemical Atomic Layer Epitaxy. *Journal of the Electrochemical Society* **1992**, 139, 686694.
5. Colletti, L. P.; Teklay, D.; Stickney, J. L. Thin-Layer Electrochemical Studies of the Oxidative Underpotential Deposition of Sulfur and Its Application to the Electrochemical Atomic Layer Epitaxy Deposition of Cds. *Journal of Electroanalytical Chemistry* **1994**, 369, 145152.
6. Colletti, L. P.; Stickney, J. L. Optimization of the growth of CdTe thin films formed by electrochemical atomic layer epitaxy in an automated deposition system. *Journal of the Electrochemical Society* **1998**, 145, 35943602.
7. Venkatasamy, V.; Jayaraju, N.; Cox, S. M.; Thambidurai, C.; Mathe, M.; Stickney, J. L. Deposition of HgTe by electrochemical atomic layer epitaxy (EC-ALE). *Journal of Electroanalytical Chemistry* **2006**, 589, 195202.

8. Venkatasamy, V.; Jayaraju, N.; Cox, S. M.; Thambidurai, C.; Stickney, J. L. Studies of Hg((1-x))Cd(x)Te formation by electrochemical atomic layer deposition and investigations into bandgap engineering. *Journal of the Electrochemical Society* **2007**, 154, H720H725.
9. Kim, J. Y.; Stickney, J. L. Ultrahigh vacuum surface studies of the electrochemical atomic layer deposition of indium telluride on n-type GaAs(100). *Journal of Physical Chemistry C* **2008**, 112, 59665971.
10. Gebregziabiher, D. K.; Kim, Y. G.; Thambidurai, C.; Ivanova, V.; Haumesser, P. H.; Stickney, J. L. Electrochemical atomic layer deposition of copper nanofilms on ruthenium. *Journal of Crystal Growth* **2010**, 312, 12711276.
11. Wade, T. L.; Vaidyanathan, R.; Happek, U.; Stickney, J. L. Electrochemical Formation of a III–V Compound Semiconductor Superlattice: InAs/InSb. *Journal of Electroanalytical Chemistry* **2001**, *500* (1-2), 322–332.
12. Jung, J.; Bui, N. N.; Shen, S.; Reber, T. J.; Brezner, J. M.; Mubeen, S.; Stickney, J. L. In Situ Surface-Enhanced Raman Spectroscopic Studies of Electrochemically Formed Germanene. *The Journal of Physical Chemistry C* **2018**, *122* (27), 15696–15705.
13. Boscher, N. D.; Carmalt, C. J.; Palgrave, R. G.; Parkin, I. P. Atmospheric Pressure Chemical Vapour Deposition of SnSe and $SnSe_2$ Thin Films on Glass. *Thin Solid Films* **2008**, *516* (15), 4750–4757.
14. Pejjai, B.; Reddy, V.R.M.; Gedi, S.; Park, C. Status Review on earth-abundant and environmentally green Sn-X (X = Se, S) nanoparticle synthesis by solution methods for photovoltaic applications. *Int. J. Hydrogen Energy* **2016**, 1-42.

15. Im, H. S.; Lim, Y. R.; Cho, Y. J.; Park, J.; Cha, E. H.; Kang, H. S. Germanium and Tin Selenide Nanocrystals for High-Capacity Lithium Ion Batteries: Comparative Phase Conversion of Germanium and Tin. *The Journal of Physical Chemistry C* **2014**, *118*(38), 21884–21888.
16. Solanki, G.; Chauhan, I.; Patel, K. Study of Structural, Electrical, and Optical Properties of Nickel-Doped Tin Selenide Crystals. *Canadian Journal of Physics* **2016**, *94* (2), 212–217.
17. Singh, N. K.; Bathula, S.; Gahtori, B.; Tyagi, K.; Haranath, D.; Dhar, A. The Effect of Doping on Thermoelectric Performance of p-Type SnSe: Promising Thermoelectric Material. *Journal of Alloys and Compounds* **2016**, *668*, 152–158.
18. Venkatasamy, V.; Shao, I.; Huang, Q.; Stickney, J. L. ALD Approach toward Electrodeposition of Sb_2Te_3 for Phase-Change Memory Applications. *Journal of The Electrochemical Society* **2008**, *155* (11).
19. Liang, X.; Jayaraju, N.; Thambidurai, C.; Zhang, Q.; Stickney, J. L. Controlled Electrochemical Formation of Ge x Sb y Te z using Atomic Layer Deposition (ALD). *Chemistry of Materials* **2011**, *23*(7), 1742–1752.